Title
Hot and heterogenous high-3He/4He components: New constraints from proto-Iceland plume lavas from Baffin Island

Author
Willhite, Lori Nicole

Publication Date
2019

Peer reviewed|Thesis/dissertation

UNIVERSITY OF CALIFORNIA

Santa Barbara

Hot and heterogenous high-$^{3}He/^{4}He$ components:

New constraints from proto-Iceland plume lavas from Baffin Island

A Thesis submitted in partial satisfaction of the

requirements for the degree Master of Science

in Earth Science

by

Lori Nicole Willhite

Committee in charge:

Professor Matthew G. Jackson, Chair

Professor Roberta L. Rudnick

Dr. Matthew E. Rioux, Lecturer

September 2019

The thesis of Lori Nicole Willhite is approved.

Roberta L. Rudnick

Matthew E. Rioux

Matthew G. Jackson, Committee Chair

July 2019

ACKNOWLEDGEMENTS

This thesis is dedicated to Roxanne, for her love and friendship, and for her curious and playful spirit; and to Devin, for the honesty, and special times. I would like to thank my family for their constant support. I acknowledge support from NSF EAR-1624840 and NSF EAR-1900652. I would especially like to thank my advisor, Matthew Jackson, for always believing in me and for guiding me to become a confident and capable scientist. Roberta Rudnick and Matthew Rioux, my exceptional committee members, have not only made this work better, but also more fun. I am grateful to Janne Blichert-Toft, Ilya Bindeman, Mark Kurz, Sæmundur A. Halldórsson, Sunna Harðardóttir, Esteban Gazel, Ellie Price, and Ben Byerly for their intellectual and analytical contributions to this work. I thank Don Francis for generously providing access to his collection of Baffin Island lavas. I appreciate Douglas Wilson for constructive discussion and feedback. I thank Keith Putirka for sharing his MORB database, and Jonathan Pinko for helping with sample preparation. Rick Carlson's continued generosity with ideas is gratefully acknowledged. I thank Lotte Larsen and Asger Pedersen for advice and discussion regarding West Greenland samples.

ABSTRACT

Hot and heterogenous high-$^{3}He/^{4}He$ components:

New constraints from proto-Iceland plume lavas from Baffin Island

by

Lori Nicole Willhite

The Icelandic hotspot has erupted the highest terrestrial mantle-derived $^{3}He/^{4}He$ over a period spanning much of the Cenozoic, from the early-Cenozoic Baffin Island-West Greenland flood basalt province (49.8 R_A), to the mid-Miocene lavas in northwest Iceland (40.2 to 47.5 R_A), to Pleistocene lavas in Iceland's neovolcanic zone (34.3 R_A). This study provides a detailed geochemical data set—He-O-Sr-Nd-Hf-Pb isotopic compositions, as well as whole rock major and trace element concentrations—for a suite of 18 Baffin Island lavas. The Baffin Island lavas transited through and potentially assimilated variable degrees of Precambrian continental basement. We therefore use geochemical indicators sensitive to continental crust assimilation (whole rock Nb/Th, Ce/Pb, MgO) to identify the least crustally-contaminated lavas in the suite. Four lavas, identified as "least crustally-contaminated", have high MgO (>15 wt.%) and Nb/Th and Ce/Pb ratios that fall within the mantle range (Nb/Th=15.6±2.6, Ce/Pb=24.3±4.3). These four lavas have $^{3}He/^{4}He$ up to 39.9 R_A and mantle-like $\delta^{18}O$ of 5.03 to 5.21‰, $^{87}Sr/^{86}Sr$ = 0.703008–0.703021, $^{143}Nd/^{144}Nd$ = 0.513094–0.513128, $^{176}Hf/^{177}Hf$ = 0.283265–0.283284, $^{206}Pb/^{204}Pb$ = 17.7560–17.9375, and are located on or near the 4.5 Ga Pb isotope geochron. The radiogenic isotopic compositions of the least crustally-contaminated Baffin Island lavas

are offset to more geochemically depleted compositions compared to high-$^{3}He/^{4}He$ lavas from Iceland, a shift that cannot be explained by continental crust assimilation in the Baffin suite. While Sr-Nd-Pb isotopic heterogeneity among high-$^{3}He/^{4}He$ localities has been previously observed, this is an important observation of geochemically distinct high-$^{3}He/^{4}He$ endmembers within a single hotspot. Additionally, the least crustally-contaminated primary melts from Baffin Island-West Greenland have higher mantle potential temperatures (1510 to 1630 °C) than global MORB primary magmas located far from hotspots (1320 to 1480 °C), which supports a hot, buoyant plume origin for these early Iceland plume lavas. These observations support the contention that the geochemically heterogeneous high-$^{3}He/^{4}He$ domain is dense, located in the deep mantle, and sampled by only the hottest plumes.

TABLE OF CONTENTS

List of Figures

Figure 3. Histogram of calculated primary melt compositions for high-MgO (> 10 wt. %) MORB (blue) located far (>500 km) from hotspots from **Putirka (2007)** and primary melt compositions for Baffin Island (BI) and West Greenland (WG) lavas (red). The data in the histograms are consistent with hotter, deeper melting at BI-WG compared to MORB. BI-WG samples have been filtered for crustal assimilation so that all lavas plotted have Nb/Th > 13, Ce/Pb > 20, and MgO > 10 wt. %; high-Ba/Th (>100) samples from West Greenland are not considered as they are considered altered by mantle metasomatism. Primary melts are calculated using PRIMELT3 from **Herzberg and Asimow (2015)** using Fe_2O_3/TiO_2 = 0.5 and accumulated fractional melting. Mantle potential temperatures calculated with PRIMELT3 software are also shown. The number of samples for BI-WG (N=9) is greater here than in isotope plots because isotopes are not required for petrologic analyses.

Figure 4. Olivine CaO composition compared to forsterite content of olivines in all 18 samples examined in this study. Color coding reflects maximum forsterite content: red reflects samples with highest maximum forsterite. The CaO at a given forsterite value is distinctly higher in Baffin Island lava olivines compared to olivines found in global mantle xenoliths (from **Hervig et al., 1986**) and local mantle xenoliths from Ubkendt Ejland, West Greenland (**Bernstein et al., 2006**). Higher CaO in the picrite olivines demonstrates that these olivines were not mechanically entrained from the lithospheric mantle during magma ascent.

Figure 5. Primitive mantle (**McDonough and Sun, 1995**) normalized trace element patterns for Baffin Island lavas examined in this study plotted with an average N-MORB composition from **Gale et al. (2013)** (using the MORB average that excludes back arc basins and lavas located <500 km from known hotspots). For elements that have both XRF and ICP-MS analyses, ICP-MS data is plotted here.

Figure 6. Nb/Th and Ce/Pb plotted against Nb and Ce concentrations, respectively. The least contaminated lavas from this study (*N*=4) are denoted by a small black circle within the red square symbol. Continental crust rocks from West Greenland (WG, **Larsen and Pedersen, 2009**) have low Nb/Th and Ce/Pb. Low Nb/Th and Ce/Pb in Baffin Island and West Greenland lavas therefore are associated with higher degrees of crustal assimilation. Baffin Island (BI) and West Greenland samples considered to be crustally contaminated have Nb/Th < 13 and/or Ce/Pb < 20 (and/or MgO < 10 wt.%, not shown). These threshold values are the lower limit of the "mantle composition" defined by the MORB database of **Jenner and O'Neill (2012)**, which is shown as a dashed line and grey field (±1 SD) in both panels. The North Atlantic MORB field is **from Gale et al. (2013)** and only includes lavas from 50 to 80 °N that are > 500 km from known hotspots.

Figure 7. Sr, Nd, and Pb isotope compositions of Baffin Island (BI) and West Greenland (WG) lavas plotted as a function of the three geochemical indicators for crustal assimilation used here: Nb/Th, MgO, and Ce/Pb. Greater degrees of crustal assimilation are associated with lower Nb/Th, Ce/Pb, and MgO; Baffin and West Greenland lavas with evidence for

crustal contamination also have higher $^{87}Sr/^{86}Sr$, lower $^{143}Nd/^{144}Nd$, and generally lower $^{206}Pb/^{204}Pb$. Lavas (*N*=4) identified as the least crustally-contaminated using these criteria are marked with a black dot within the red square and outlined with a dashed box. Baffin Island and West Greenland lavas from a metasomatized source (Ba/Th>100) are marked with a black "X" over the red diamonds. In the bottom panel, five samples (shown with red arrows) with Ba/Th>100 plot outside the panel. The North Atlantic (50 to 80 °N) and global MORB fields are from **Gale et al. (2013)** and only include lavas located > 500 km from known hotspots (**King and Adam, 2014).**

Figure 8. Sr, Nd, and Hf isotopic compositions of Baffin Island (BI) lavas from this study (red squares) shown together with previously published data from Baffin Island and West Greenland (WG) (both as red diamonds) (**Jackson et al., 2010; Starkey et al., 2009; Larsen and Pedersen, 2009; Kent et al., 2004; Larsen and Pedersen, 2009**). Both crustally contaminated and least crustally-contaminated Baffin Island-West Greenland lavas are show in the left-hand side panels, whereas only the least crustally-contaminated lavas (Nb/Th > 13, Ce/Pb > 20, MgO wt. % > 10) are shown in the right-hand side panels. Paired Hf and Nd isotopic compositions are available from only two studies—this study (red squares) and **Jackson et al. (2010)** (red diamonds). Mid-Miocene Iceland (orange field), modern Iceland (yellow field), North Atlantic MORB (50° to 80° N) (blue field), and global MORB (light grey field) fields are shown for perspective (Iceland data from GEOROC; MORB data from **Gale et al. [2013]**); MORB fields exclude back arc basin lavas and MORB samples < 500

km from nearby hotspots (**Kind and Adam, 2014**). Data points shown are the measured isotopic compositions, and white and dark grey fields reflect age-corrected and calculated present-day mantle source compositions, respectively (see **Section 3.3 and Supplementary Figure 2)**. Age correction of the mid-Miocene and modern Iceland lavas is negligible (offset is less than the size of the Baffin Island lava symbols; **Supplementary Figure 3**). Lavas with the highest $^{3}He/^{4}He$ compositions from Iceland, Galápagos, Hawaii, and Samoa are indicated by the black circles with the letters I, G, H, and S, respectively (**see Jackson et al. [2008]**).

Figure 9. Sr, Nd, and Pb isotope compositions of Baffin Island (BI) lavas from this study (red squares) shown together with previously published data from Baffin Island and West Greenland (WG) (both red diamonds) (**Jackson et al., 2010; Starkey et al., 2009; Larsen and Pedersen, 2009; Kent et al., 2004**). Crustally-contaminated and least crustally-contaminated Baffin Island-West Greenland lavas are show in the left-hand side panels, whereas only the least crustally-contaminated lavas (Nb/Th > 13, Ce/Pb > 20, MgO wt. % > 10) are shown in the right-hand side panels. Mid-Miocene Iceland (orange field), modern Iceland (yellow field), and North Atlantic MORB (50° to 80° N) (blue field) and global MORB (light grey field) fields are shown for perspective (Iceland data from Georoc; MORB data from **Gale et al. [2013])**; MORB fields exclude back arc basin lavas and MORB samples < 500 km from nearby hotspots (**Kind and Adam, 2014**). For all plots that include Pb isotopes, fields for mid-Miocene and modern Iceland are defined using high-precision MC-ICP-MS data only, while MORB fields also include unspiked Pb isotopic data acquired by TIMS. For Pb isotopic data obtained on Baffin Island and West Greenland, both MC-ICP-MS and unspiked TIMS Pb isotopic data are included in the “global plots” (i.e., left-hand

side panels), whereas only samples with MC-ICP-MS Pb isotopic data are shown in the right-hand side panels. Data points shown are the measured isotopic compositions, while white and dark grey fields reflect age-corrected and calculated present-day mantle source compositions, respectively (see **Section 3.3 and Supplementary Figure 2)**. Age correction of the mid-Miocene and modern Iceland lavas is negligible (offset is less than the size of the Baffin Island lava symbols; **Supplementary Figure 3**) and the respective fields represent measured isotopic ratios; in the Sr-Pb panel, mid-Miocene Iceland has a narrower range than other panels because the highest and lowest $^{206}Pb/^{204}Pb$ samples lack Sr isotopic analyses. Lavas with the highest $^{3}He/^{4}He$ compositions from Iceland, Galápagos, Hawaii, and Samoa are indicated by the black circles with the letters I, G, H, and S, respectively (**see Jackson et al. [2008]**).

Figure 10. $\delta^{18}O$ compositions of Baffin Island olivines from this study (red squares) and **Kent et al. (2004)** (red diamonds) compared with olivine forsterite and Nb/Th. The range of $\delta^{18}O$ in MORB olivine is from **Eiler (2001).** The range of Nb/Th in MORB is from **Jenner and O'Neil (2012)** and includes 1σ variation. Low Nb/Th, which is associated with higher degrees of crustal assimilation, may relate to somewhat higher $\delta^{18}O$. The four Baffin Island lavas that are "least crustally-contaminated" (based on having high Nb/Th, Ce/Pb, and MgO) also have MORB-like $\delta^{18}O$.

Figure 11. Helium isotopic compositions compared to ^{4}He concentrations for Baffin Island and West Greenland magmatic olivines. Samples with lower helium concentrations tend to

have lower $^{3}He/^{4}He$, possibly due to greater sensitivity to post-eruptive radiogenic ingrowth of ^{4}He. The dashed lines connect the olivine crush experiment data to the respective fusion results for two different samples. For the highest $^{3}He/^{4}He$ crush experiment in this study (AK-9, 56.6 R_A), the fusion experiment resulted in a high $^{3}He/^{4}He$ (36.3 R_A), but the helium concentration is low and $^{3}He/^{4}He$ data for this sample is not further discussed here. The solid line connects a crush experiment on a single olivine megacryst (denoted by an "M" in the symbol) to the crush experiment for muliple olivine phenocrysts from the same lavas (AK-13). CC signifies crustal contamination.

Figure 12. Helium isotopic compositions for several hotspots shown as a function of whole rock $^{87}Sr/^{86}Sr$, $^{143}Nd/^{144}Nd$, and $^{206}Pb/^{204}Pb$. Data points shown are the measured isotopic compositions, and white and dark grey fields reflect age-corrected and calculated present-day mantle source compositions, respectively; $^{3}He/^{4}He$ data are not age corrected. Lavas with the highest $^{3}He/^{4}He$ in Iceland (yellow field and symbols) and the least crustally-contaminated Baffin Island lavas (red squares) exhibit different Sr, Nd, and Pb isotopic compositions (the comparisons rely on measured isotopic data [red squares] and calculated present-day isotopic compositions of the mantle source of the Baffin Island lavas; see **Section 3.3**). The least crustally-contaminated lavas from Baffin Island have lower $^{87}Sr/^{86}Sr$ and $^{206}Pb/^{204}Pb$ and higher $^{143}Nd/^{144}Nd$ than the highest $^{3}He/^{4}He$ Iceland lavas, suggesting a different high-$^{3}He/^{4}He$ source (see insets). The grey dashed lines contain the field for Baffin Island and West Greenland lavas that are crustally-contaminated (Nb/Th<13, Ce/Pb<20, and/or MgO<10 wt.%), or are insufficiently characterized to identify potential crustal contamination (e.g., many Baffin Island lavas with $^{3}He/^{4}He$ data lack Pb concentration [and Pb isotopic]

data; **Stuart et al., 2003; Starkey et al., 2009**). A global data set for oceanic lavas, including MORB and samples from the four hotspots with $^{3}He/^{4}He$ > 30 Ra, are provided for context (fields are adapted from **Jackson et al., 2007; Jackson et al., 2008**).

1. Introduction

Helium isotopes provide an important tracer of ancient domains that have survived inside the Earth since its accretion. Helium isotopic ratios (normalized to Earth's atmosphere, $^3He/^4He = 1.384x10^{-6}$) are relatively constant in mid-ocean ridge basalts (MORB) (8.8 ± 2.1 R_A, or ratio to atmosphere; (**Graham, 2002**), which passively sample the upper mantle. However, plume-fed hotspots—such as Iceland, Hawaii, Samoa, and Galápagos sample mantle domains with much higher $^3He/^4He$ ratios, thought to be located in the deep mantle (>30 R_A; e.g., **Ellam and Stuart, 2004; Farley et al., 1992; Hilton et al., 1999; Jackson et al., 2007a; Kurz et al., 1982; Macpherson et al., 2005; Saal et al., 2007; Starkey et al., 2009**). The highest observed mantle-derived $^3He/^4He$ (up to 49.8 ± 0.7 R_A) was found in the continental flood basalts associated with the Iceland plume at Baffin Island and West Greenland, erupted at ~60 Ma (**Storey et al., 1998; Rizo et al., 2016; Starkey et al., 2009; Stuart et al., 2003; Graham et al., 1998**), and elevated $^3He/^4He$ ratios were also identified in lavas related to the Iceland plume on east Greenland (Marty et al., 1998). Mid-Miocene lavas in northwest Iceland host the highest observed mantle-derived $^3He/^4He$ of any ocean island basalt (OIB) location (47.5 R_A, **Harðardóttir et al., 2018**; 40.2 R_A, **Mundl et al., 2017**; 37.7 R_A, **Hilton et al., 1999**). Modern Iceland lavas in the neovolcanic zone also have high $^3He/^4He$ (up to 34.3 R_A; **Macpherson et al., 2005**). Therefore, the Iceland plume has hosted elevated $^3He/^4He$ over much of its history and hence is an ideal natural laboratory for studying the high-$^3He/^4He$ mantle domain.

The high-$^3He/^4He$ mantle domain is ancient, requiring preservation in a region of the mantle that is relatively un-degassed and unmixed despite billions of years of mantle convective mixing, melting, and recycling (e.g., **Class and Goldstein, 2005; Tackley, 2000;**

White, 2015; Zindler and Hart, 1986). Recent work examining the short-lived ^{182}Hf-^{182}W system (where ^{182}Hf decays to ^{182}W, $t_{1/2}$ = 8.9 Ma) has demonstrated ^{182}W anomalies in high-$^{3}He/^{4}He$ plume-derived lavas from the Iceland hotspot, Samoa, and Hawaii (**Mundl et al., 2017; Mundl-Petermeier et al., 2019; Rizo et al., 2016**). The presence of these ^{182}W anomalies in plume-related lavas indicates that they are derived from a mantle source that formed when the parent nuclide, ^{182}Hf, was extant (~6 times as long as its half-life, or ~60 Ma following Solar System formation). This is consistent with the observation of a $^{129}Xe/^{130}Xe$ anomaly—different from both atmosphere and MORB—in a moderately high-$^{3}He/^{4}He$ (17.2 R_A) lava from Iceland (**Trieloff et al., 2000**; **Mukhopadhyay, 2012**), which requires formation during the first 100 Ma following terrestrial accretion, within the lifetime of the short-lived parent ^{129}I (where ^{129}I decays to ^{129}Xe, $t_{1/2}$ = 15.7 Ma). Therefore, constraining the composition of the highest $^{3}He/^{4}He$ mantle reservoir observed in the rock record can provide important new insights into the accretionary history and early evolution of Earth's major chemical reservoirs.

This study examines the geochemistry of flood basalts from Baffin Island, Canada (**Figure 1**), and West Greenland, providing new data—He-O-Sr-Nd-Hf-Pb isotopic compositions, as well as whole rock major and trace element concentrations—for 18 lavas from Baffin Island, in order to constrain the composition of the mantle domain with the highest observed $^{3}He/^{4}He$. The Baffin Island and West Greenland lavas constitute a flood basalt province associated with the proto-Icelandic plume that erupted through Archean and Proterozoic continental crust, the assimilation of which could have overprinted their primary

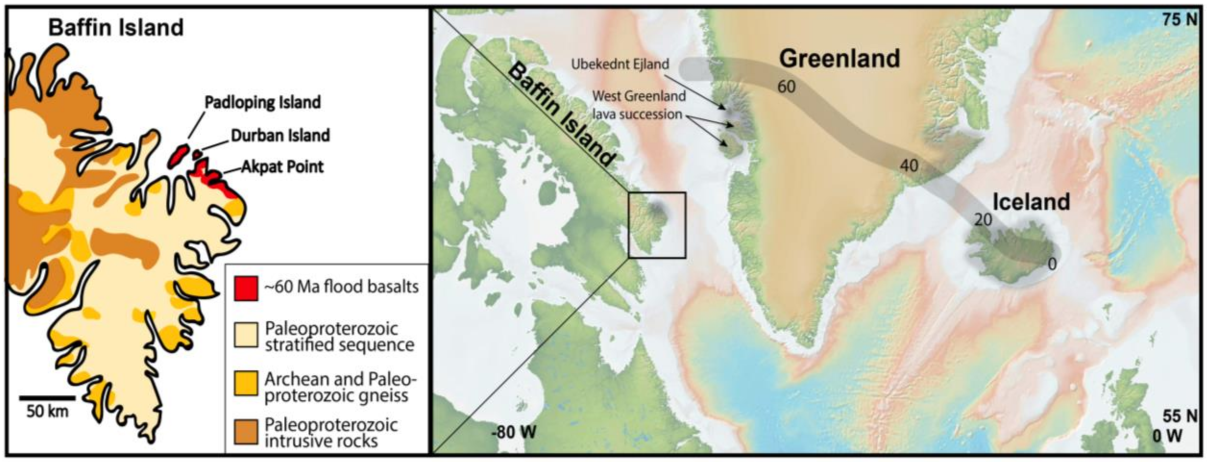

Figure 1. Map of Baffin Island, Greenland, and Iceland. General locations of Iceland plume-derived lavas are shaded in dark grey. The inset shows a simplified geologic map after Wheeler et al. (1996), including the locations of the lavas collected in this study: Padloping Island, Durban Island, and Akpat Point. The hotspot track is a synthetic track with the North American plate fixed through time (modified after **Lawver and Müller [1994]**) and is shown as the grey path. Also shown is the location of the ~60 Ma West Greenland succession samples compiled in Larsen and Pedersen (2009).

mantle signature (e.g., **Saunders et al., 1997; Day, 2016**). Therefore, we identify signatures of crustal assimilation in Baffin Island and West Greenland lavas using a suite of major and trace element filters—whole rock MgO, Ce/Pb, and Nb/Th—sensitive to continental crust assimilation, in order to isolate geochemical signatures of their mantle source. We show that, among high-$^3He/^4He$ lavas globally, the least contaminated lavas from Baffin Island have the most geochemically depleted $^{87}Sr/^{86}Sr$, $^{143}Nd/^{144}Nd$, and $^{176}Hf/^{177}Hf$, and the least radiogenic Pb isotopic compositions. Baffin Island-West Greenland lavas exhibit more geochemically depleted isotopic fingerprints than the high-$^3He/^4He$ lavas erupted in mainland Iceland, demonstrating temporal evolution of the high-$^3He/^4He$ component in the Iceland hotspot. The observation of two geochemically distinct, high-$^3He/^4He$ components in a single hotspot provides important constraints on the origin and evolution of mantle domains hosting high $^3He/^4He$.

2. Methods

2.1. Rock collection, preparation, and analytical methods

The 18 basalts examined in this study were collected at three locations on Baffin Island by Don Francis during the 2004 field season—Padloping Island, Akpat Point, and Durban Island (**Figure 1 and Supplementary Table 1)**. Eleven of the 18 samples in this study have fresh volcanic glass on the margins of the basaltic pillows, a feature that has been identified previously in Baffin Island flood basalt lavas (e.g., **Kent et al., 2004**). The **Supplementary Methods** describe sample preparation and analytical techniques for major and trace element analyses (**Table 1**); He, Sr, Nd, Hf, and Pb isotopic analyses (**Table 2**); oxygen isotopic analyses (**Table 3**); and olivine compositions (**Supplementary Table 2**). Thin section images of all 18 samples are provided in **Supplementary Figure 1.**

3. Data treatment methods

3.1 Filtering for crustal contamination

A primary goal of this study is to identify the mantle source composition of Baffin Island and West Greenland flood basalt lavas. Because these lavas traversed Precambrian continental crust *en route* to the surface, we used MgO contents and two trace element ratios, Nb/Th and Ce/Pb, to identify samples least impacted by crustal contamination to gain insight into primary isotopic ratios.

Lavas with low MgO concentrations erupted in continental settings often have signatures of crustal assimilation **(e.g., Hoernle et al., 2015**). Therefore, lavas with MgO <10

Table 1. Major and trace elements on Baffin Island lavas and reference materials.[1]

	AK-1	AK-6	AK-8b	AK-9	AK-12	AK-13	AK-14	AK-18A	DB-9	DB-13	DB-14	DB-17
XRF												
SiO_2 (wt.%)	45.05	43.80	45.83	45.40	45.30	44.88	44.87	44.81	44.16	44.69	45.10	46.52
TiO_2	0.69	0.54	0.96	0.52	0.69	0.69	0.68	0.70	0.69	0.76	0.77	0.70
Al_2O_3	11.54	8.63	11.04	9.83	11.51	11.61	11.47	11.76	9.86	10.95	10.92	11.60
FeO_T	10.43	10.57	10.88	10.51	10.37	10.60	10.46	10.47	10.53	10.82	10.76	10.13
MnO	0.17	0.17	0.18	0.17	0.17	0.18	0.17	0.18	0.17	0.18	0.18	0.17
MgO	19.31	24.28	19.85	23.63	19.40	19.53	19.65	19.43	23.01	20.81	20.76	18.90
CaO	10.25	7.27	9.41	8.21	10.51	10.07	10.28	10.04	8.26	9.09	9.06	9.76
Na_2O	1.22	0.88	1.30	0.98	1.26	1.27	1.15	1.26	0.88	1.09	1.04	1.23
K_2O	0.02	0.06	0.04	0.01	0.02	0.02	0.01	0.04	0.05	0.01	0.02	0.01
P_2O_5	0.05	0.04	0.07	0.05	0.05	0.05	0.04	0.04	0.06	0.05	0.05	0.05
Total (majors only)[3]	98.74	96.24	99.55	99.32	99.29	98.88	98.79	98.71	97.67	98.46	98.64	99.08
LOI	0.22	3.27	0.00	0.13	0.32	0.00	0.55	0.59	1.37	0.47	0.65	0.05
Total (major, trace oxides, LOI)[3]	99.38	100.05	99.96	99.96	100.03	99.30	99.76	99.72	99.52	99.37	99.73	99.54
Olivine Fo# [2]	87.0	83.7	89.6	89.0	87.2	87.1	87.6	87.3	88.0	87.5	87.0	88.8
XRF												
Rb (ppm)	0.97	1.86	1.18	1.96	1.18	1.26	1.36	0.59	2.35	1.07	1.17	1.10
Sr	63.8	44.7	113.3	47.4	61.5	63.6	60.9	65.4	70.7	77.6	76.9	75.1
Zn	82.0	70.2	75.8	74.0	76.8	76.3	71.8	74.3	82.3	79.4	78.6	73.1
Ni	779	1094	849	1100	789	790	790	778	1038	878	871	763
Cr	1605	2274	1398	2054	1630	1652	1648	1616	1805	1697	1711	1591
V	241	197	248	199	240	239	236	243	212	231	232	235
Cu	108.0	77.7	96.4	68.7	113.7	110.8	110.8	113.3	97.5	97.1	87.5	114.2
Ga	11.4	8.3	11.5	9.7	11.5	11.9	12.5	11.4	10.5	12.0	10.3	12.9
Ba	9.2	8.2	13.7	9.8	9.6	7.5	8.2	5.5	10.9	4.9	9.5	12.0
Y	16.8	11.9	15.9	12.3	16.2	15.7	15.4	16.7	13.4	16.5	15.2	15.6
Nb	0.50	0.10	1.00	0.00	0.60	0.20	0.40	1.19	0.60	0.89	0.10	0.96
Zr	36.4	28.9	53.1	26.0	36.8	36.9	35.4	36.3	39.2	42.4	41.1	36.6
ICP-MS												
Cs (ppm)	0.0027	0.014	0.0020	0.0004	0.0058	0.0011	0.0044	0.0043	0.0081	0.0029	0.0034	0.0055
Rb	0.26	1.08	0.28	0.15	0.30	0.20	0.23	0.42	0.95	0.12	0.17	0.26
Ba	6.04	6.21	11.18	4.77	5.76	4.87	5.84	7.36	7.32	6.55	7.89	9.60
Th	0.194	0.154	0.128	0.040	0.193	0.183	0.188	0.183	0.111	0.088	0.086	0.112
U	0.044	0.037	0.035	0.012	0.044	0.040	0.044	0.049	0.029	0.014	0.016	0.028
Nb	1.12	0.95	1.73	0.51	1.07	1.08	1.08	1.08	1.39	1.17	1.17	1.15
Ta	0.069	0.061	0.112	0.034	0.067	0.066	0.070	0.068	0.089	0.080	0.076	0.069
La	1.59	1.29	2.32	0.70	1.54	1.52	1.51	1.56	1.68	1.47	1.32	1.58
Ce	4.23	3.35	6.43	2.18	4.07	4.10	4.04	4.15	4.63	4.37	4.30	4.02
Pb	0.35	0.22	0.28	0.15	0.33	0.34	0.34	0.37	0.19	0.20	0.20	0.21
Pr	0.69	0.54	1.09	0.42	0.67	0.68	0.67	0.69	0.78	0.77	0.73	0.70
Nd	3.72	2.93	5.71	2.42	3.68	3.65	3.64	3.69	4.03	4.19	3.99	3.79
Sr	64.4	44.4	110.2	48.9	60.2	62.3	60.4	65.7	70.7	77.1	75.7	76.7
Zr	33.9	25.8	50.0	23.8	32.6	33.0	32.8	33.7	36.1	38.5	38.3	34.1
Hf	0.99	0.76	1.38	0.68	0.96	0.97	0.97	0.98	0.98	1.11	1.08	0.94
Sm	1.54	1.18	2.10	1.11	1.52	1.51	1.52	1.48	1.54	1.69	1.61	1.48
Eu	0.65	0.48	0.83	0.46	0.62	0.63	0.63	0.64	0.60	0.66	0.65	0.62
Gd	2.33	1.72	2.69	1.71	2.23	2.27	2.22	2.28	2.09	2.31	2.27	2.22
Tb	0.46	0.33	0.49	0.34	0.43	0.44	0.43	0.44	0.39	0.44	0.42	0.41
Dy	3.02	2.23	3.15	2.30	2.93	2.97	2.92	3.00	2.53	2.87	2.81	2.78
Ho	0.65	0.49	0.64	0.50	0.63	0.63	0.63	0.65	0.54	0.61	0.60	0.60
Y	16.2	12.0	16.0	12.8	15.7	15.8	15.6	16.2	13.5	15.1	14.6	15.0
Er	1.82	1.39	1.73	1.43	1.77	1.79	1.80	1.80	1.50	1.71	1.66	1.69
Tm	0.26	0.20	0.24	0.20	0.25	0.26	0.25	0.26	0.22	0.24	0.24	0.25
Yb	1.66	1.23	1.49	1.33	1.61	1.62	1.60	1.65	1.34	1.53	1.50	1.52
Lu	0.26	0.19	0.23	0.21	0.25	0.25	0.24	0.25	0.21	0.24	0.24	0.23
Sc	36.1	28.9	33.0	31.3	34.4	35.4	34.4	36.1	31.2	34.0	34.0	34.5
Ba/Th	31.2	40.4	87.1	119.8	29.8	26.5	31.0	40.1	65.8	74.5	91.4	85.9
Ce/Pb	12.1	15.5	22.9	14.7	12.3	12.2	11.8	11.2	24.0	22.2	21.7	19.4
Nb/U	25.6	25.8	50.0	42.1	24.3	26.8	24.7	21.8	47.2	86.4	74.4	40.6
Nb/Th	5.8	6.2	13.5	12.8	5.5	5.9	5.7	5.9	12.5	13.3	13.5	10.3
$[La/Sm]_N$	0.65	0.68	0.69	0.39	0.63	0.63	0.62	0.66	0.68	0.55	0.52	0.67
Rb/Cs	95.8	78.1	134.9	359.9	52.1	188.6	52.3	97.6	116.6	42.1	48.7	46.9
Ba/Rb	23.6	5.8	40.7	31.8	19.0	24.5	25.2	17.7	7.7	53.2	47.6	37.0
Th/U	4.4	4.2	3.7	3.3	4.4	4.5	4.3	3.7	3.8	6.5	5.5	3.9

Table 1. ***continued***

	DB-19	PI-10	PI-15	PI-17	PI-18	PI-20	BCR-2	BCR-2	BCR-2 publ	BHVO-2	BHVO-2	BHVO-2 publ
XRF												
SiO_2 (wt.%)	46.11	46.26	44.59	46.28	45.73	45.59	53.96	54.46	54.93	50.04		50.23
TiO_2	1.29	1.00	0.75	0.86	0.84	0.83	2.28	2.30	2.30	2.78		2.77
Al_2O_3	11.38	12.85	10.60	12.18	11.83	11.61	13.56	13.62	13.71	13.68		13.61
FeO_T	10.79	10.75	10.66	10.43	10.59	10.55	12.85	12.62	12.61	11.25		11.29
MnO	0.18	0.18	0.17	0.17	0.17	0.17	0.20	0.20	0.20	0.17		0.17
MgO	17.03	15.17	21.58	17.73	18.48	18.56	3.59	3.53	3.66	7.30		7.35
CaO	9.23	10.86	8.94	10.08	9.77	9.62	7.15	7.16	7.24	11.51		11.54
Na_2O	1.39	1.35	1.08	1.31	1.26	1.21	3.17	3.10	3.17	2.24		2.25
K_2O	0.17	0.02	0.01	0.04	0.04	0.05	1.79	1.79	1.80	0.52		0.52
P_2O_5	0.12	0.07	0.06	0.07	0.07	0.07	0.35	0.35	0.37	0.26		0.27
Total (majors only)[3]	97.71	98.50	98.44	99.16	98.79	98.26	98.92	99.13	100.00	99.74		100.00
LOI	1.18	0.49	0.43	0.56	0.45	0.55	0.10	0.00		0.00		
Total (major, trace oxides, LOI)[3]	99.28	99.30	99.32	100.10	99.64	99.21	99.27	99.39		99.99		
Olivine Fo# [2]	86.4	87.1	88.7	90.4	89.9	90.4						
XRF												
Rb (ppm)	3.38	1.97	1.07	0.97	1.56	1.84	47	47	46	11		9
Sr	170.9	109.0	74.3	99.8	94.8	92.7	340	343	337	397		394
Zn	81.3	77.9	85.9	74.1	77.9	77.1	133	130	130	105		104
Ni	638	486	943	684	734	738	14	13	13	121		120
Cr	1304	1016	1720	1415	1486	1470	9	12	16	283		287
V	288	272	228	245	241	235	405	408	418	321		318
Cu	79.7	119.1	86.2	93.0	83.9	87.6	20	19	20	130		129
Ga	12.3	14.0	11.3	12.5	10.8	11.2	20	22	22	21		21
Ba	74.8	23.0	6.4	18.2	22.6	22.1	676	678	684	139		131
Y	24.7	18.6	14.8	17.5	15.8	16.7	36	36	36	26		26
Nb	7.53	3.15	0.00	4.55	2.59	3.76	12	13	12	16		18
Zr	80.8	54.2	39.8	50.0	49.1	49.4	182	181	187	168		171
ICP-MS												
Cs (ppm)	0.0070	0.0041	0.0032	0.0060	0.0055	0.0093		1.13	1.16		0.098	0.100
Rb	2.95	0.24	0.18	0.31	0.41	0.61		46.3	46.0		8.95	9.26
Ba	71.37	15.20	5.97	21.63	22.76	25.91		679	684		130	131
Th	0.713	0.294	0.098	0.416	0.410	0.392		6.18	5.83		1.26	1.22
U	0.146	0.043	0.018	0.054	0.049	0.063		1.54	1.68		0.41	0.41
Nb	7.85	3.62	1.36	4.26	4.16	4.12		12.6	12.4		19.4	18.1
Ta	0.460	0.211	0.087	0.250	0.242	0.239		0.81	0.79		1.27	1.15
La	6.56	3.51	1.63	3.67	3.18	3.25		26.1	25.1		15.7	15.2
Ce	14.12	8.48	4.69	8.35	8.01	7.93		51.1	53.1		36.3	37.5
Pb	0.80	0.38	0.19	0.36	0.34	0.34		10.0	10.6		1.58	1.65
Pr	1.99	1.31	0.79	1.22	1.10	1.13		6.57	6.83		5.17	5.34
Nd	9.18	6.35	4.32	5.92	5.36	5.51		27.0	28.3		23.3	24.3
Sr	170.7	110.1	74.2	100.7	92.3	91.3		347	337		396	394
Zr	80.1	53.7	38.2	48.9	46.8	46.9		188	187		173	171
Hf	2.06	1.47	1.05	1.31	1.28	1.29		4.81	4.97		4.40	4.47
Sm	3.04	2.26	1.64	2.05	1.87	1.89		7.01	6.55		6.45	6.02
Eu	1.08	0.89	0.64	0.78	0.73	0.74		2.15	1.99		2.24	2.04
Gd	3.84	2.96	2.25	2.69	2.54	2.52		7.11	6.81		6.64	6.21
Tb	0.69	0.53	0.42	0.50	0.47	0.48		1.17	1.08		1.04	0.94
Dy	4.45	3.49	2.74	3.27	3.07	3.10		7.09	6.42		5.87	5.28
Ho	0.95	0.74	0.58	0.69	0.65	0.66		1.42	1.31		1.08	0.99
Y	23.5	18.4	14.6	17.0	16.0	16.2		35.7	36.1		25.9	25.9
Er	2.62	2.04	1.64	1.93	1.81	1.84		3.87	3.67		2.67	2.51
Tm	0.37	0.30	0.23	0.27	0.26	0.26		0.55	0.53		0.34	0.33
Yb	2.35	1.80	1.45	1.71	1.64	1.65		3.38	3.39		2.01	1.99
Lu	0.36	0.28	0.24	0.27	0.25	0.26		0.52	0.505		0.29	0.28
Sc	34.3	38.9	33.4	37.0	35.5	35.7		34.3	33.5		31.7	31.8
Ba/Th	100.1	51.6	60.8	52.0	55.5	66.2		110	117		103	107
Ce/Pb	17.6	22.4	24.1	22.9	23.8	23.3		5.10	5.02		22.99	22.70
Nb/U	53.7	84.0	77.8	78.3	85.3	64.9		8.14	7.39		47.05	43.93
Nb/Th	11.0	12.3	13.9	10.3	10.2	10.5		2.04	2.13		15.42	14.79
$[La/Sm]_N$	1.35	0.98	0.62	1.13	1.06	1.08		2.33	2.40		1.53	1.58
Rb/Cs	424.3	58.1	54.8	52.1	74.1	65.7		41.0	39.7		91.5	93.0
Ba/Rb	24.2	63.6	33.8	69.0	56.2	42.6		14.7	14.9		14.5	14.1
Th/U	4.9	6.8	5.6	7.6	8.4	6.2		4.0	3.5		3.1	3.0

1. Majors and some traces were analyzed by XRF at WSU. The other traces were analyzed by ICP-MS at WSU. Two USGS reference materials, BCR-2 and BHVO-2, were run together with the Baffin lavas as unknowns. These data are provided with preferred values from Jochum et al. (2016) (data are expressed with all Fe as FeO to facilitate comparison with new BCR-2 and BHVO-2 provided here).

2. Olivine forserite compositions are average values of multiple analyses of different olivine grains provided in Supplementary Table 1.

3. Two different totals are incluced for major element analyses. The first total includes major element analyses only. The second total includes major element analyses, LOI (loss on ignition), and the trace element totals expressed as oxides (and includes the following trace elements: Ni, Cr, Sc, V, Ba, Rb, Sr, Zr, Y, Nb, Ga, Cu, Zn, Pb, La, Ce, Th, Nd and U

Table 2. New Sr, Nd, Hf, Pb, He, and O isotopic compositions on Baffin Island lavas.

Sample name	Location	Sample type[1]	$^{87}Sr/^{86}Sr$	2 σ	$^{143}Nd/^{144}Nd$	2 σ	$\varepsilon^{143}Nd$	$^{176}Hf/^{177}Hf$	2 σ	$^{206}Pb/^{204}Pb$	2 σ	$^{207}Pb/^{204}Pb$	2 σ	$^{208}Pb/^{204}Pb$	2 σ	$^{207}Pb/^{206}Pb$	2 σ	$^{208}Pb/^{206}Pb$	2 σ	$\delta^{18}O$ oliv	$^{3}He/^{4}He$ [2]	1 σ	^{4}He cc STP/g	Olivine Mass (g)	Fraction He Blank
AK-1	Akpat Pt.	Glass	0.703559	0.000006	0.512963	0.000006	6.5	0.283231	0.000004	17.6822	0.0013	15.2945	0.0014	37.751	0.003	0.86496	0.00002	2.13501	0.00006	5.21	1.50	0.08	2.76E-09	0.18390	0.06
AK-6	Akpat Pt.	Rock chips	0.703501	0.000006	0.512997	0.000003	7.2	0.283222	0.000005	17.6249	0.0009	15.2887	0.0010	37.664	0.003	0.86747	0.00002	2.13704	0.00008	5.33	2.9	0.8	6.15E-11	0.20507	0.70
AK-8b	Akpat Pt.	Rock chips	0.703009	0.000006	0.513128	0.000003	9.7	0.283266	0.000003	17.7560	0.0010	15.3932	0.0009	37.532	0.002	0.86694	0.00001	2.11373	0.00004	5.03	39.9	0.5	2.30E-08	0.18252	0.01
AK-8b fusion																					20.8	0.5	1.84E-08	0.16757	0.01
AK-9	Akpat Pt.	Rock chips	0.702995	0.000006	0.513174	0.000003	10.6	0.283287	0.000005	17.7715	0.0050	15.3812	0.0045	37.500	0.012	0.86557	0.00003	2.11018	0.00006		56.6	1.1	1.42E-10	0.27417	0.43
AK-9 fusion																					36.3	0.9	5.23E-09	0.25194	0.01
AK-12	Akpat Pt.	Glass	0.703579	0.000007	0.512954	0.000006	6.3	0.283234	0.000004	17.6890	0.0015	15.2932	0.0015	37.738	0.004	0.86458	0.00003	2.13340	0.00006		30.1	0.7	2.77E-10	0.18074	0.37
AK-13 [6]	Akpat Pt.	Glass	0.703579	0.000008	0.512957	0.000005	6.4	0.283212	0.000005	17.6601	0.0018	15.2930	0.0018	37.700	0.005	0.86600	0.00002	2.13480	0.00007	5.32	28.8	0.4	7.83E-09	0.07340	0.05
AK-13 crush replicate [6]																					21.5	0.5	7.07E-10	0.13692	0.24
AK-14	Akpat Pt.	Glass	0.703618	0.000021	0.512956	0.000006	6.4	0.283218	0.000005	17.6951	0.0028	15.3013	0.0025	37.762	0.006	0.86470	0.00003	2.13396	0.00008	5.12	17.9	0.4	5.65E-10	0.19229	0.22
AK-18a	Akpat Pt.	Glass	0.703635	0.000006	0.512952	0.000006	6.3	0.283229	0.000004	17.7029	0.0045	15.3128	0.0040	37.761	0.010	0.86499	0.00003	2.13315	0.00006		15.4	0.4	3.65E-10	0.20209	0.29
DB-9	Durban Is.	Rock chips	0.702997	0.000009	0.513135	0.000003	9.8	0.283272	0.000004	17.9507	0.0031	15.4168	0.0030	37.717	0.008	0.85886	0.00004	2.10123	0.00010	5.10	13.3	0.7	9.27E-11	0.22594	0.59
DB-13	Durban Is.	Glass	0.703021	0.000005	0.513102	0.000003	9.2	0.283265	0.000004	17.9317	0.0025	15.4291	0.0021	37.732	0.006	0.86044	0.00002	2.10434	0.00015	5.03	12.0	0.7	6.75E-11	0.19448	0.70
DB-14	Durban Is.	Glass	0.703021	0.000005	0.513097	0.000003	9.1	0.283284	0.000003	17.9297	0.0025	15.4279	0.0030	37.735	0.007	0.86047	0.00004	2.10453	0.00008	5.09	10.1	0.5	6.56E-11	0.21668	0.68
DB-17	Durban Is.	Rock chips	0.703228	0.000006	0.513104	0.000003	9.2	0.283230	0.000006	17.5114	0.0042	15.2942	0.0037	37.455	0.009	0.87341	0.00002	2.13882	0.00007	5.17	31.2	0.9	7.53E-11	0.20028	0.66
DB-17 fusion																					6.4	0.4	4.68E-09	0.18434	0.01
DB-19	Durban Is.	Rock chips	0.703946	0.000005	0.512937	0.000003	6.0	0.283144	0.000004	18.0095	0.0012	15.3929	0.0009	37.971	0.003	0.85472	0.00002	2.10846	0.00005	5.08	0.2	0.4	1.14E-10	0.19551	0.50
PI-10	Padloping Is.	Rock chips	0.703401	0.000005	0.513028	0.000003	7.8	0.283222	0.000004	17.9607	0.0032	15.4001	0.0035	37.920	0.011	0.85735	0.00003	2.11085	0.00004						
PI-15	Padloping Is.	Glass	0.703008	0.000005	0.513094	0.000003	9.0	0.283279	0.000003	17.9375	0.0029	15.4223	0.0025	37.723	0.008	0.85980	0.00002	2.10296	0.00006	5.21	21.8	0.6	1.93E-10	0.20635	0.42
PI-17	Padloping Is.	Glass	0.703845	0.000006	0.512926	0.000003	5.8	0.283169	0.000004	17.7551	0.0013	15.3663	0.0012	37.662	0.002	0.86545	0.00001	2.12113	0.00015		36.9	0.5	2.42E-09	0.23348	0.05
PI-18	Padloping Is.	Glass	0.703848	0.000006	0.512920	0.000003	5.7	0.283169	0.000004	17.7542	0.0012	15.3680	0.0011	37.660	0.003	0.86560	0.00002	2.12116	0.00004	5.18	36.4	0.6	1.23E-09	0.19692	0.11
PI-20	Padloping Is.	Glass	0.703846	0.000006	0.512923	0.000003	5.7	0.283182	0.000003	17.7540	0.0015	15.3642	0.0015	37.659	0.004	0.86540	0.00002	2.12107	0.00007	5.07	31.1	0.7	7.60E-10	0.23062	0.15
BCR-2 [3]					0.512624	0.000003																			
BCR-2 [3]					0.512621	0.000004																			
BCR-2 [3]					0.512627	0.000004																			
BCR-2 [3, 4]			0.705000	0.000005	0.512621	0.000003																			
AGV-2 [4]			0.703966	0.000006																					
AGV-2 [4]			0.703966	0.000005																					
AGV-2 [4]			0.703972	0.000006																					
BCR-2 [5]								0.282886	0.000003	18.7558	0.0009	15.6251	0.0008	38.7414	0.0022										
AGV-2 [5]								0.282988	0.000006	18.8660	0.0009	15.6174	0.0009	38.5299	0.0032										

1. For the 11 samples with available pillow glass, heavy radiogenic isotopies were measured on glass; for the remaining samples they were measured on rock chips.

2. With three exceptions, all of the helium isotopic analyses were made following crushing olivines *in vacuo*. Using the crushed powders remaining for the $^{3}He/^{4}He$ crush analyses, three fusion experiments were conducted here, on samples DB-17, AK-8b and AK-9.

3. An aliquot of the USGS reference material BCR-2 was run with each analytical session for Nd isotopic analyses.

4. Aliquots of at least one of two USGS reference materials, AGV-2 and BCR-2, were run with each analytical session for Sr isotopic analyses.

5. Hf and Pb isotopic compositions of the USGS reference materials BCR-2 and AGV-2 shown here were reported in Price et al. (2016) and were run in separate analytical sessions from the samples in this study, but in the same laboratory (Lyon) following exactly the same procedures (described in Price et al., 2016).

6. For AK-13, the 28.8 R_A olivine crush values is for a single megacryst (73 mg), and the 21.5 R_A replicate value is from 137 mg of smaller olivine crystals.

7. $\varepsilon^{143}Nd$ is calculated assuming a chondritic value from Bouvier et al. (2008).

wt.% are excluded from consideration here (**Figure 2**). Mantle-derived lavas produced from high degrees of melting (where the degree of melting [F] is >> than the partition coefficients [D] of the incompatible trace elements of interest) have relatively constant Nb/U and Ce/Pb (~47 and ~25 respectively; (Hofmann et al., 1986). These ratios are useful for identifying assimilation of continental crust due to the low values of both ratios in upper (4.44 to 3.71; **Rudnick and Gao, 2003**) and bulk (6.15 to 3.91; **Rudnick and Gao, 2003**) continental crust. By comparison Nb/U and Ce/Pb ratios are significantly higher and relatively constant in global normal MORB (Nb/U = 44.0 ± 1.2 (1σ) and Ce/Pb = 24.0 ± 0.5 (1σ) using the **Gale et al. [2013]** database, and Nb/U = 46.5 ± 7.6 (1σ) and Ce/Pb = 24.3 ± 4.3 (1σ) using the **Jenner and O'Neill [2012]** database).

However, because U is mobile, the Nb/U ratio can be modified during weathering. We therefore use Nb/Th instead, as Th is similarly incompatible, but it is relatively immobile during weathering. Hence, like Nb/U, Nb/Th in melts should reflect the mantle ratio during high degrees of melting (Hofmann, 2003). Nb/Th is also relatively constant in oceanic lavas: Nb/Th = 14.3 ± 2.9 (1σ) (**Gale et al., 2013**) or 15.6 ± 2.6 (1σ) (**Jenner and O'Neill, 2012**). Compared to MORB, Nb/Th is low in both upper (1.14, **Rudnick and Gao, 2003**) and bulk (1.43, **Rudnick and Gao, 2003**) continental crust. Therefore, like both Ce/Pb and Nb/U, the Nb/Th ratio is a sensitive tracer of continental crust assimilation in mantle-derived basalts erupted in continental settings.

We further consider the Baffin Island (**this study, Jackson et al., 2010; Kent et al., 2004; Robillard et al., 1992; Starkey et al., 2009; Stuart et al., 2003; Yaxley et al., 2004**) and associated West Greenland flood basalt lavas (**Larsen and Pedersen, 2009; Starkey et al., 2009**) to be contaminated if they have Nb/Th or Ce/Pb one standard deviation below the average of global MORB glasses by (**Jenner and O'Neill, 2012**; based on glass analyses from the same lab), that is, lavas with Nb/Th < 13.0 and/or Ce/Pb < 20.0 are excluded.

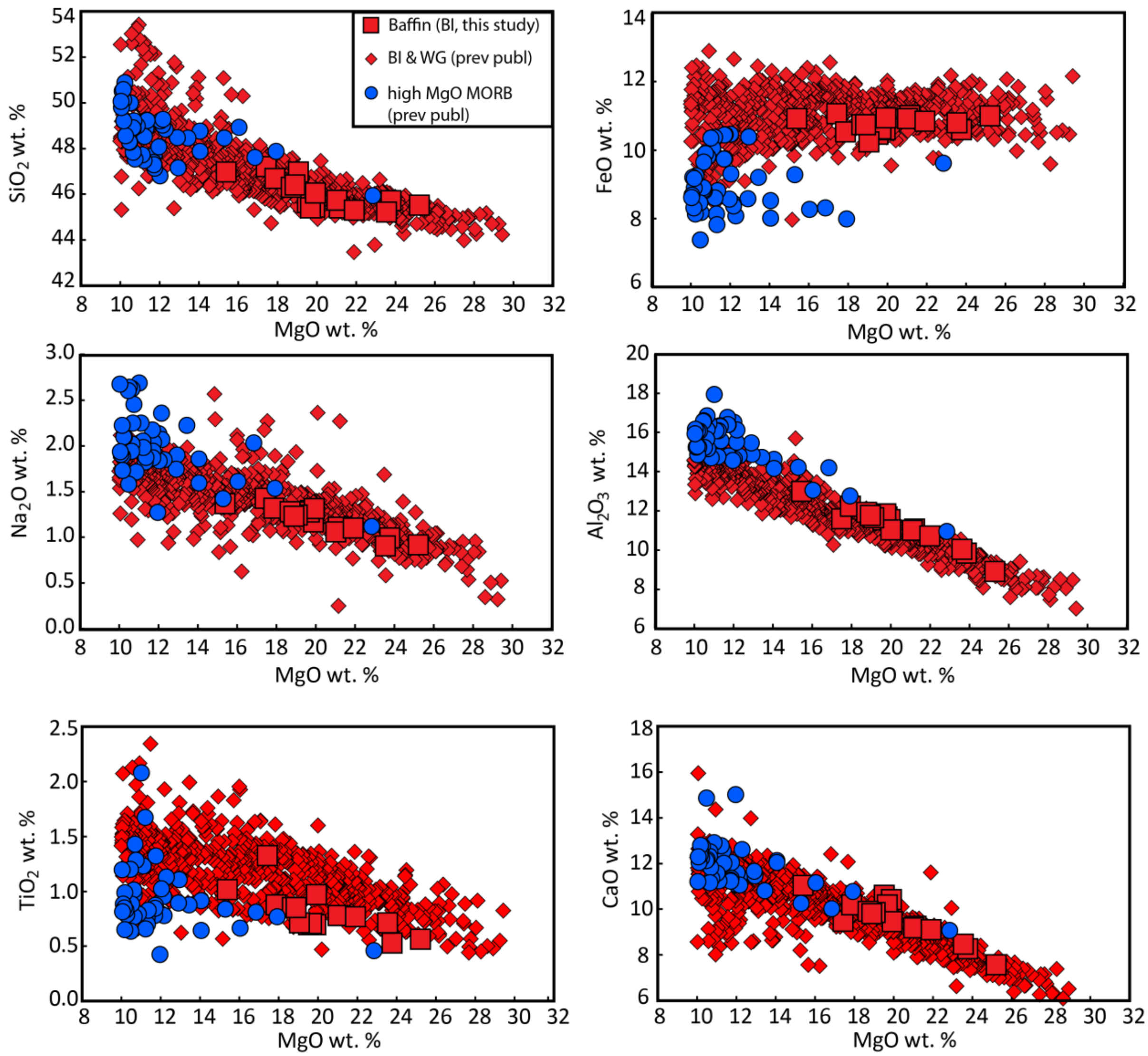

Figure 2. Major element compositions of Baffin Island (BI) lavas from this study (red squares) and other sources (red diamonds**) (Jackson et al., 2010, Starkey et al., 2009, Stuart et al., 2003, Yaxley et al., 2004, Francis et al., 1985**). Also shown are West Greenland (WG) lavas (also red diamonds) from Larsen and Pedersen (2009). Baffin Island and West Greenland lavas are not filtered for crustal assimilation. However, only lavas with MgO > 10 wt. % are shown. High-MgO (> 10 wt. %) MORB samples compiled in **Putirka et al. (2007)** are shown for comparison, but only MORB samples collected >500 km from known hotspots (**King and Adam, 2014**) are shown to avoid a "hotspot" contribution. Major element compositions for Baffin Island and West Greenland differ systematically from MORB such that, for example, the flood basalt lavas have higher FeO at a given MgO. These important petrologic differences are interpreted to be the result of deeper melting and higher melt fraction in the hotter plume setting.

Table 3. Oxygen isotopic compositions of Baffin Island olivines

Sample ID	Mass (mg)	$\delta^{18}O$	1σ	µmol O_2	µmols O_2/mg
AK-1	1.48	5.24	0.07	19.11	12.54
AK-1-replicate	1.43	5.19	0.07	18.79	12.76
sample average		5.21			
AK-6	1.05	5.38	0.07	14.24	13.56
AK-6-replicate	1.20	5.27	0.07	15.38	12.82
AK-6-rep2	0.70	5.35	0.07	9.1	13.00
sample average		5.33			
AK-8b	1.36	5.08	0.07	18.86	13.87
AK-8b-replicate	1.67	4.98	0.07	23.18	13.88
sample average		5.03			
AK-13	1.29	5.24	0.07	17.28	13.40
AK-13-replicate	0.86	5.40	0.10	11.1	12.98
sample average		5.32			
AK-14	0.90	5.12	0.07	11.27	12.16
DB-9	1.32	5.06	0.07	17.45	13.22
DB-9-replicate	1.18	5.14	0.07	15.12	12.81
sample average		5.10			
DB-13	1.40	5.03	0.07	18.36	12.73
DB-14	1.22	5.10	0.07	16.31	13.37
DB-14-replicate	1.25	5.09	0.07	16.77	13.42
sample average		5.09			
DB-17	1.33	5.16	0.07	16.03	12.05
DB-17-replicate	1.21	5.18	0.07	16.78	13.87
sample average		5.17			
DB-19	1.19	5.02	0.07	15.77	13.25
DB-19-replicate	1.23	5.13	0.07	16.29	13.24
sample average		5.08			
PI-15	1.32	5.12	0.07	18.09	13.70
PI-15-replicate	1.27	5.31	0.07	16.72	13.17
sample average		5.21			
PI-18	1.35	5.17	0.07	18.55	13.74
PI-18-replicate	1.25	5.19	0.07	17.36	13.89
sample average		5.18			
PI-20	1.47	4.89	0.07	20.12	13.29
PI-20-replicate	1.64	5.17	0.07	22.23	13.16
PI-20-replicate	1.29	5.15	0.07	17.9	13.88
sample average		5.07			

We acknowledge the possibility that a crustal endmember could contaminate a given lava, yet remain undetected by the present trace element filters. For example, if the isotopic composition of the crustal endmember is significantly different from that of the primary melt, and concentration of that element is relatively high in the primary melt compared to the continental crust, it is conceivable that a very small fraction of continental crust could change the isotopic composition of the resulting lava yet have little impact on the whole-rock trace element ratios. We therefore conservatively refer to Baffin Island and West Greenland lavas with mantle-like Nb/Th (>13) and Ce/Pb (>20), and high MgO (>10 wt.%), as being "least contaminated", instead of "uncontaminated". Additionally, we cannot evaluate a potential continental signature in lavas that lack MgO, Ce/Pb, and Nb/Th data, hence such lavas are excluded from discussion. Oxygen isotopes provide another means of evaluating crustal assimilation. However, due to the lack of olivine

$\delta^{18}O$ measurements from many Baffin Island-West Greenland lavas from previous studies, we do not use $\delta^{18}O$ as a filter for crustal contamination for the extensive dataset examined here. Instead, after filtering lavas for crustal assimilation using MgO, Nb/Th, and Ce/Pb, we examine the $\delta^{18}O$ of the least contaminated lavas to evaluate whether mantle-like compositions have been isolated.

Finally, West Greenland lavas considered to be melts of a metasomatized source by (**Larsen et al., 2003**) are also excluded from further discussion (but shown in the figures with separate symbols). We find such lavas to be enriched in Ba (i.e., Ba/Th > 100), hence all such lavas are excluded from consideration.

3.2. Treatment of MORB geochemical database for comparison with Iceland plume lavas

We compare proto-Iceland plume lavas from Baffin Island-West Greenland with MORB using the database of **Gale et al. (2013)**. In figures and subsequent discussion of radiogenic isotopic (Sr, Nd, Hf, Pb) compositions (see **Sections 4.4 and 4.6**), we exclude MORB influenced by known hotspots—i.e., MORB samples located <500 km from known hotspots, following **Gale et al. (2013)** while employing the hotspot database of **King and Adam (2014)**—and back arc basin lavas. Additionally, for major element investigation of MORB in this study (**Figures 2, 3, and Section 4.1**), we use the MORB database from **Putirka et al. (2007)**. From this database we exclude hotspot-influenced MORB; we also filter lavas with MgO < 10 wt. % to simplify calculation of primary liquids (by avoiding highly differentiated melts; **Figure 3**), and to facilitate direct comparison with Baffin Island and West Greenland lavas (which are also filtered to exclude MgO < 10 wt.%).

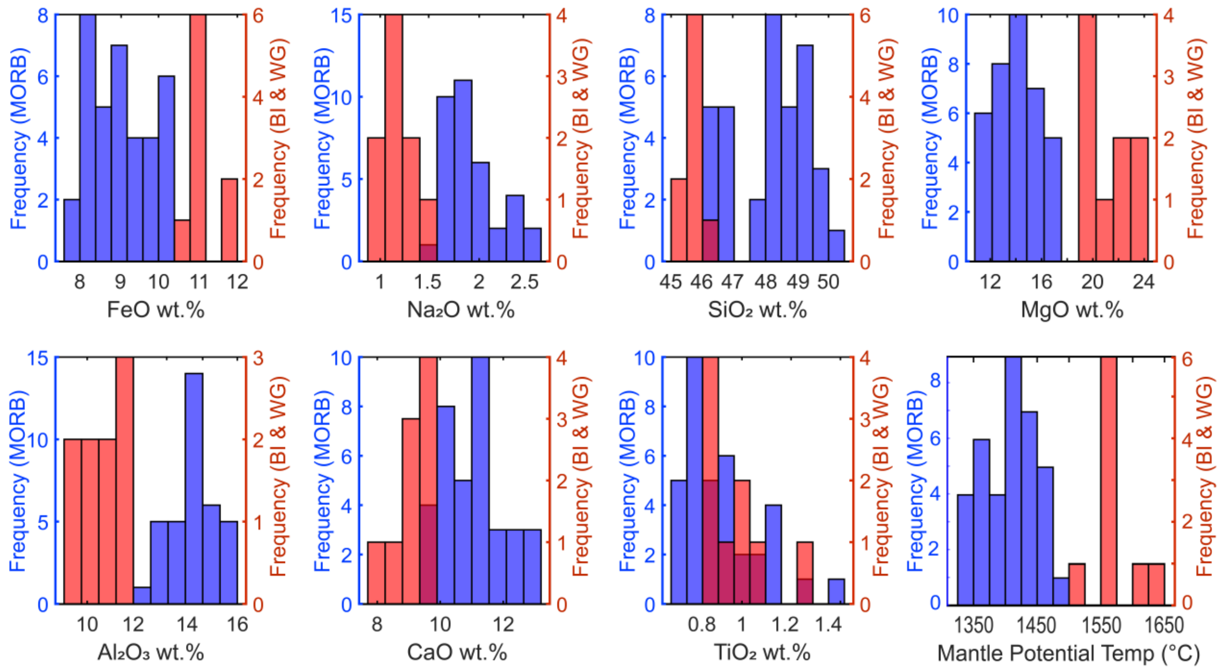

Figure 3. Histogram of calculated primary melt compositions for high-MgO (> 10 wt. %) MORB (blue) located far (>500 km) from hotspots from **Putirka (2007)** and primary melt compositions for Baffin Island (BI) and West Greenland (WG) lavas (red). The data in the histograms are consistent with hotter, deeper melting at BI-WG compared to MORB. BI-WG samples have been filtered for crustal assimilation so that all lavas plotted have Nb/Th > 13, Ce/Pb > 20, and MgO > 10 wt. %; high-Ba/Th (>100) samples from West Greenland are not considered as they are considered altered by mantle metasomatism. Primary melts are calculated using PRIMELT3 from **Herzberg and Asimow (2015)** using Fe_2O_3/TiO_2 = 0.5 and accumulated fractional melting. Mantle potential temperatures calculated with PRIMELT3 software are also shown. The number of samples for BI-WG (N=9) is greater here than in isotope plots because isotopes are not required for petrologic analyses.

3.3. Radiogenic isotopic age corrections and calculation of modern mantle source compositions

In order to compare the isotopic compositions of the ~60 Ma, least contaminated Baffin Island lavas to mid-Miocene and modern neovolcanic zone Iceland lavas, it is necessary to consider the effect of post-eruptive radiogenic ingrowth on the radiogenic isotopic compositions. Therefore, in **Supplementary Table 3**, the Sr, Nd, Hf, and Pb isotopic compositions are back-corrected to 60 Ma. This age correction gives the compositions of the Baffin Island mantle at 60 Ma; however, to facilitate comparison with modern Iceland lavas, the composition of the Baffin Island mantle source *today* (assuming it had not experienced melt extraction at 60 Ma) must be determined. To do this, we start with the initial values from the calculated radiogenic isotopic compositions of Baffin Island lavas at 60 Ma, which reflect the Baffin Island mantle source at the time of flood basalt eruption. We then assume parent-daughter ratios for the Baffin Island mantle source to "age" the radiogenic isotopic compositions of the Baffin Island mantle source from 60 Ma to the present day (**Supplementary Figure 2**). The primary uncertainty in this calculation is the relevant parent-daughter ratios for each radiogenic isotopic system in the Baffin Island *mantle source*. The Nd isotopic compositions of the Baffin Island lavas provide a constraint on possible trace element compositions of the Baffin Island mantle source at 60 Ma. For example, the $^{143}Nd/^{144}Nd$ of the least contaminated Baffin Island lavas overlap with MORB (excluding back arc basins and samples <500 km from known hotspots) (see **Section 4.4**), but are more geochemically depleted (more radiogenic) than chondrites (0.512630; **Bouvier et al., 2008**). Therefore, the Baffin Island mantle source, prior to melt extraction at 60 Ma, was unlikely to have a trace element source more geochemically depleted than depleted MORB mantle (DMM), or more geochemically enriched than chondritic. Thus, the parent-daughter ratios for DMM (Workman and Hart, 2005) and bulk silicate Earth (BSE; **McDonough and Sun, 1995**) are used to "bracket" the lower and upper limits, respectively, of the incompatible trace element composition of the Baffin Island mantle source, and thus the range of calculated radiogenic isotopic compositions of a present-day Baffin Island mantle source (see **Supplementary Figure 2** for a schematic representation of this calculation). The difference in radiogenic isotopic compositions for the calculated Baffin Island mantle today, whether using DMM or BSE as trace element source compositions in the calculation, is minimal, and fields for the present day mantle source isotopic compositions in relevant figures encompass the range of isotopic values arising from the DMM and BSE limits (**Supplementary Table 3**). In fact, the offset among measured, age-corrected, and calculated present-day Baffin Island mantle source fields is small in all isotopic spaces (see **Supplementary Figure 3**), with measured and calculated present-day Baffin Island mantle source isotopic compositions being most similar; of course, for the younger mid-Miocene Iceland lavas, the differences are even smaller (**Supplementary Figure 3**). We do not attempt to age-correct the $^{3}He/^{4}He$ data. Nonetheless, after excluding an influence of cosmogenic ^{3}He, measured $^{3}He/^{4}He$ ratios from olivine *in vacuo* crushing experiments will most likely be lower than the original mantle source compositions due to degassing followed by post-eruptive generation of ^{4}He.

4. Data and Results

4.1. Major element compositions and primary melt compositions

Major element concentrations for the Baffin Island lavas in this study are shown in **Figures 2 and 3** with previously analyzed Baffin Island and West Greenland flood basalt lavas. The lavas are visually fresh and have LOI (loss on ignition) < 1.4 wt.%, with the exception of one lava with LOI = 3.3 wt.% (**Table 2**). The new suite of lavas reported on here are olivine-rich tholeiites with MgO contents ranging from 15–25 wt. % (**Figure 2**) (**Le Bas et al., 1986; Francis, 1985**). To illustrate differences in major element compositions between MORB and the Baffin Island-West Greenland flood basalts, we calculated primary melt compositions of the least contaminated and least evolved (only MgO > 10 wt.% are considered) Baffin Island and West Greenland lavas, as well as high MgO (>10 wt.%) MORB. Relatively few (*N*=9)

Baffin Island-West Greenland lavas remain after filtering for continental crust assimilation using the criteria established in **Section 3.1**. Primary melts are calculated using the PRIMELT3 software assuming an Fe_2O_3/TiO_2 ratio of 0.5 (**Herzberg and Asimow, 2015)**. Relative to MORB, the least contaminated Baffin Island-West Greenland primary melts have higher FeO, but lower Na_2O and Al_2O_3, and generally lower CaO and SiO_2. TiO_2 is not different between the two groups. The Baffin Island-West Greenland primary melts are highly magnesian, with calculated primary melt MgO ranging from 19–24 wt. %, which exceeds the range of calculated MgO (11–17 wt.%) in the MORB primary melts.

4.2. Olivine major and minor element compositions

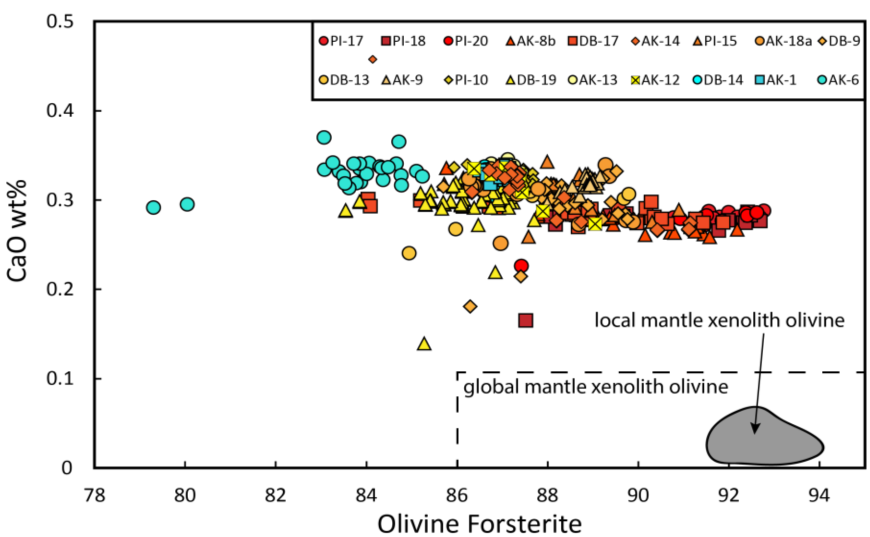

Figure 4. Olivine CaO composition compared to forsterite content of olivines in all 18 samples examined in this study. Color coding reflects maximum forsterite content: red reflects samples with highest maximum forsterite. The CaO at a given forsterite value is distinctly higher in Baffin Island lava olivines compared to olivines found in global mantle xenoliths (from **Hervig et al., 1986**) and local mantle xenoliths from Ubkendt Ejland, West Greenland (**Bernstein et al., 2006**). Higher CaO in the picrite olivines demonstrates that these olivines were not mechanically entrained from the lithospheric mantle during magma ascent.

Olivine forsterite content from the Baffin Island lavas examined here range from forsterite 79.3 to 92.7 for individual spot analyses (**Figure 4 and Supplementary Table 1**). High forsterite olivines in Baffin Island lavas were previously reported by **Francis et al. (1985), Yaxley et al. (2004), and Starkey et al. (2012)**, who found forsterite compositions up to 93.2, 92.9, and 93.0, respectively. Olivines in this suite of Baffin Island lavas have higher CaO for a given forsterite than olivines found in global mantle xenoliths (Hervig et al., 1986) and mantle xenoliths from Ubkendt Ejland, West Greenland, which sample the mantle beneath the Baffin Island-West Greenland flood basalts **(Bernstein et al., 2006**). The CaO content of olivine reflects equilibration temperature and pressure conditions (**Köhler and Brey, 1990**); the high olivine CaO for a given forsterite is typical of high temperature, low pressure magmatic olivine and suggests the olivines in the Baffin Island lavas are likely to be magmatic in origin **(e.g., Jackson and Shirey, 2011**).

4.3. Trace element compositions

Primitive mantle-normalized (McDonough and Sun, 1995) trace element patterns, or spidergrams, are shown in **Figure 5** for the Baffin Island lavas. While one sample (DB-19) has a slightly enriched rare earth element (REE) pattern ($[La/Sm]_N$=1.35, where N reflects normalization to primitive mantle), four lavas (PI-10, PI-17, PI-18, and PI-20) have relatively flat light REE patterns ($[La/Sm]_N$ = 0.98–1.13) and the remaining lavas have depleted LREE patterns (($[La/Sm]_N$ = 0.39–0.70). Some of the relatively fluid-mobile incompatible trace elements exhibit depletions in the lavas relative to elements of similar incompatibility during mantle melting, including Cs, Rb, K, and Pb, and in some cases U. Depletions in Pb are common in mantle-derived lavas (Hart and Gaetani, 2006), and reflect either the mantle source or residual sulfide. In contrast, depletion in U and alkalis may reflect loss of these elements during subaerial weathering. For example, 13 lavas exhibit Th/U greater than the chondritic primitive mantle composition (3.876 ± 0.016; **Blichert-Toft et al., 2010**), with one value as high as 8.4, which likely reflects loss of U relative to immobile Th during weathering. Evidence

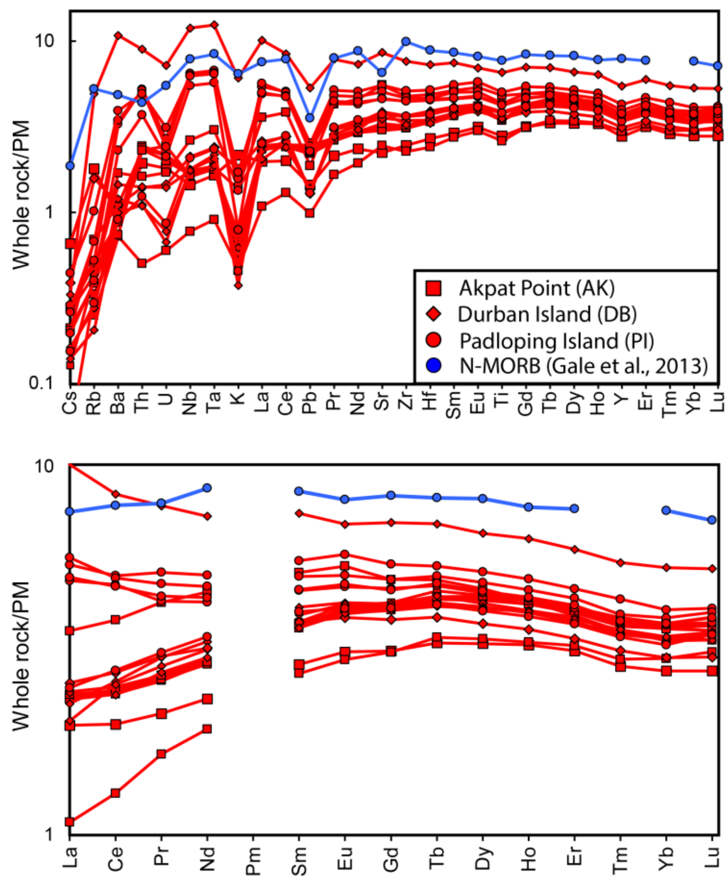

Figure 5. Primitive mantle (**McDonough and Sun, 1995**) normalized trace element patterns for Baffin Island lavas examined in this study plotted with an average N-MORB composition from **Gale et al. (2013)** (using the MORB average that excludes back arc basins and lavas located <500 km from known hotspots). For elements that have both XRF and ICP-MS analyses, ICP-MS data is plotted here.

for alkali mobility is supported by departure of Baffin Island lavas from the canonical Ba/Rb (~12; **Hofmann and White, 1983**) and Rb/Cs (85-95; **Hofmann and White, 1983**) ratios of fresh basalts. In the new suite of Baffin Island lavas Ba/Rb and Rb/Cs vary from 5.8–69.0, and from 42–424, respectively (see **Table 1** for relevant trace element ratios).

As previously noted, large degrees of crustal assimilation are associated with low MgO, Nb/Th, and Ce/Pb in mantle-derived lavas erupted in continental settings. In **Figure 6**, West Greenland basement samples (compiled in **Larsen and Pedersen, 2009**) are shown together with Baffin Island-West Greenland lavas. At lower Nb/Th and Ce/Pb, a subset of Baffin Island-West Greenland lavas trend away from MORB toward compositions identified in the basement, so that ratios in Baffin Island lavas deviation from the relatively constant Nb/Th and Ce/Pb in mantle-derived lavas unmodified by continental crust assimilation.

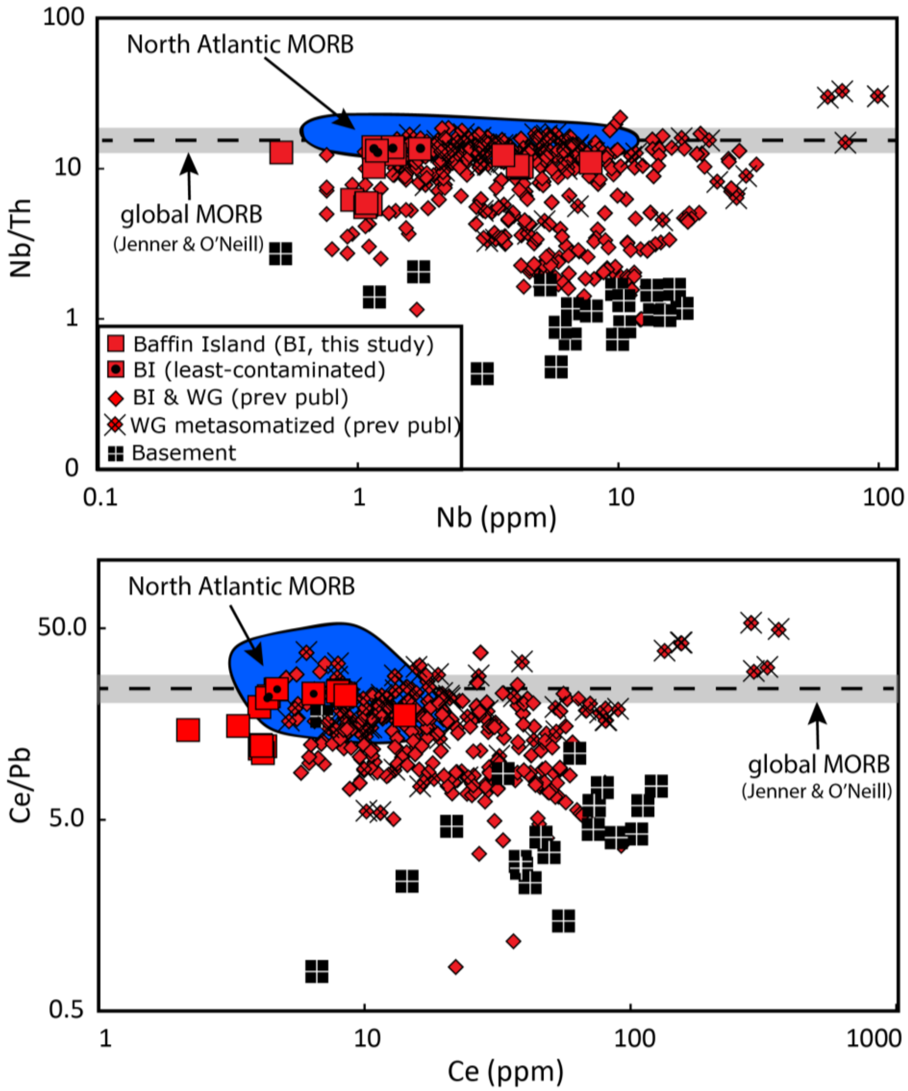

Figure 6. Nb/Th and Ce/Pb plotted against Nb and Ce concentrations, respectively. The least contaminated lavas from this study (*N*=4) are denoted by a small black circle within the red square symbol. Continental crust rocks from West Greenland (WG, **Larsen and Pedersen, 2009**) have low Nb/Th and Ce/Pb. Low Nb/Th and Ce/Pb in Baffin Island and West Greenland lavas therefore are associated with higher degrees of crustal assimilation. Baffin Island (BI) and West Greenland samples considered to be crustally-contaminated have Nb/Th < 13 and/or Ce/Pb < 20 (and/or MgO < 10 wt.%, not shown). These threshold values are the lower limit of the "mantle composition" defined by the MORB database of **Jenner and O'Neill (2012)**, which is shown as a dashed line and grey field (±1 SD) in both panels. Baffin Island and West Greenland lavas from a metasomatized source (Ba/Th>100) are marked with a black "X" over the red diamonds. The North Atlantic MORB field is **from Gale et al. (2013)** and only includes lavas from 50 to 80 °N that are > 500 km from known hotspots.

4.4 Sr-Nd-Hf-Pb isotopic compositions

Measured Sr, Nd, and Hf compositions of the Baffin Island lavas in this dataset range from 0.702995 to 0.703946 for $^{87}Sr/^{86}Sr$, 0.512920 to 0.513174 for $^{143}Nd/^{144}Nd$, and 0.283144 to 0.283287 for $^{176}Hf/^{177}Hf$. The ranges for Pb isotopes span 17.5114 to 18.0095, 15.2887 to 15.4291, and 37.455 to 37.971 for $^{206}Pb/^{204}Pb$, $^{207}Pb/^{204}Pb$, and $^{208}Pb/^{204}Pb$, respectively.

Figure 7 shows that some Baffin Island-West Greenland lavas with low Nb/Th, Ce/Pb, and MgO also have relatively high $^{87}Sr/^{86}Sr$ and lower $^{143}Nd/^{144}Nd$, in some cases approaching radiogenic isotopic values observed in the basement, which has highly geochemically enriched $^{87}Sr/^{86}Sr$ (0.713758 to 0.823010) and $^{143}Nd/^{144}Nd$ (0.510737 to 0.511945) (**Figure 7**). Most basement samples extend to lower $^{206}Pb/^{204}Pb$ than found in MORB, and Baffin Island-West Greenland lavas with the lowest Nb/Th, Ce/Pb, and MgO also tend to have low $^{206}Pb/^{204}Pb$ and extend to the unradiogenic values identified in the basement.

After applying the filters for crustal contamination, only four lavas from the Baffin Island-West Greenland suite—AK-8b, DB-13, DB-14, PI-15—with modern high-precision Sr, Nd, Hf, and Pb isotopic data can be considered "least crustally-contaminated" (see Table 2). (We note that an additional five West Greenland lavas fall in this category but lack Hf and Pb isotopic compositions determined with modern methods; **Larsen and Pedersen, 2009**). While it is unfortunate that so few lavas can be considered (near-)primary, it is preferable to focus only on those lavas that best reflect the composition of the mantle source. The four Baffin Island lavas with mantle-like Nb/Th, Ce/Pb, and high-precision Sr, Nd, Hf, and Pb isotopic data, all from this study, plot in the geochemically depleted region of the $^{143}Nd/^{144}Nd$ versus $^{87}Sr/^{86}Sr$ and $^{176}Hf/^{177}Hf$ versus $^{143}Nd/^{144}Nd$ (**Figure 8, right panels)**.

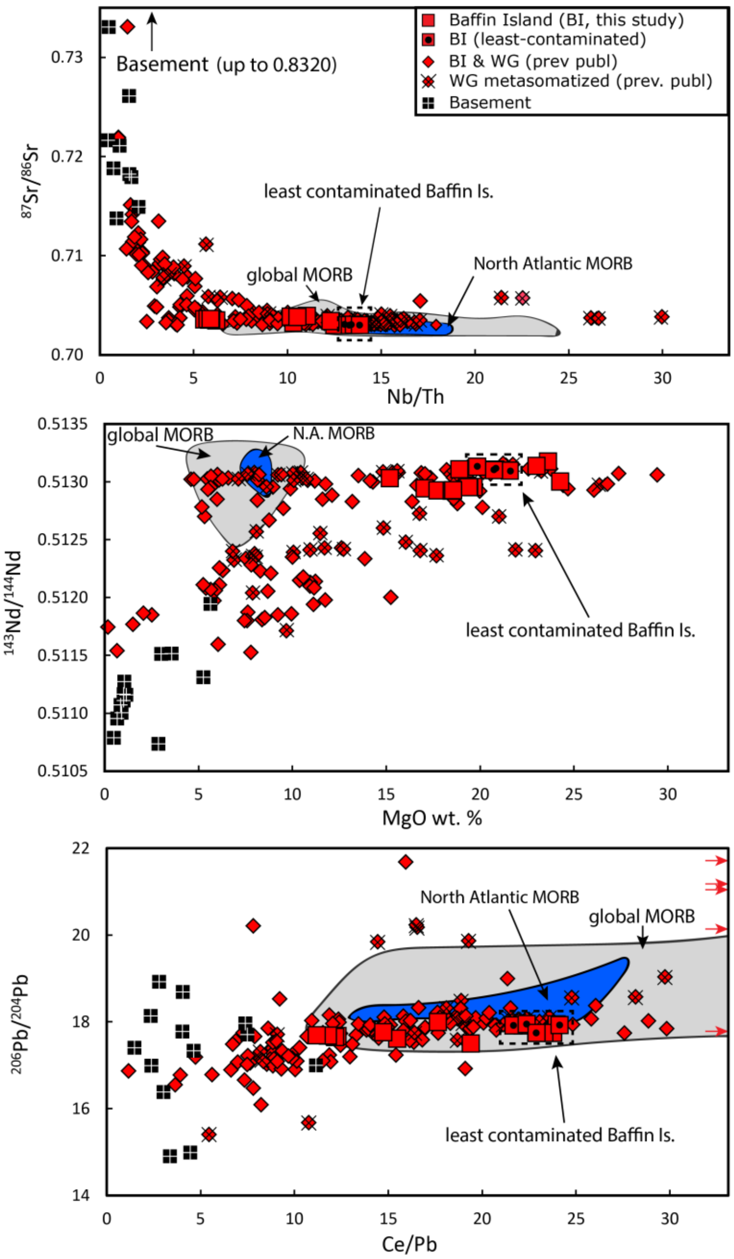

Figure 7. Sr, Nd, and Pb isotope compositions of Baffin Island (BI) and West Greenland (WG) lavas plotted as a function of the three geochemical indicators for crustal assimilation used here: Nb/Th, MgO, and Ce/Pb. All isotope data plotted are measured data. Greater degrees of crustal assimilation are associated with lower Nb/Th, Ce/Pb, and MgO; Baffin and West Greenland lavas with evidence for crustal contamination also have higher $^{87}Sr/^{86}Sr$, lower $^{143}Nd/^{144}Nd$, and generally lower $^{206}Pb/^{204}Pb$. Lavas (*N*=4) identified as the least crustally-contaminated using these criteria are marked with a black dot within the red square and outlined with a dashed box. Baffin Island and West Greenland lavas from a metasomatized source (Ba/Th>100) are marked with a black "X" over the red diamonds. In the bottom panel, five samples (shown with red arrows) with Ba/Th>100 plot outside the panel. The North Atlantic (50 to 80 °N) and global MORB fields are from **Gale et al. (2013)** and only include lavas located > 500 km from known hotspots (**King and Adam, 2014).**

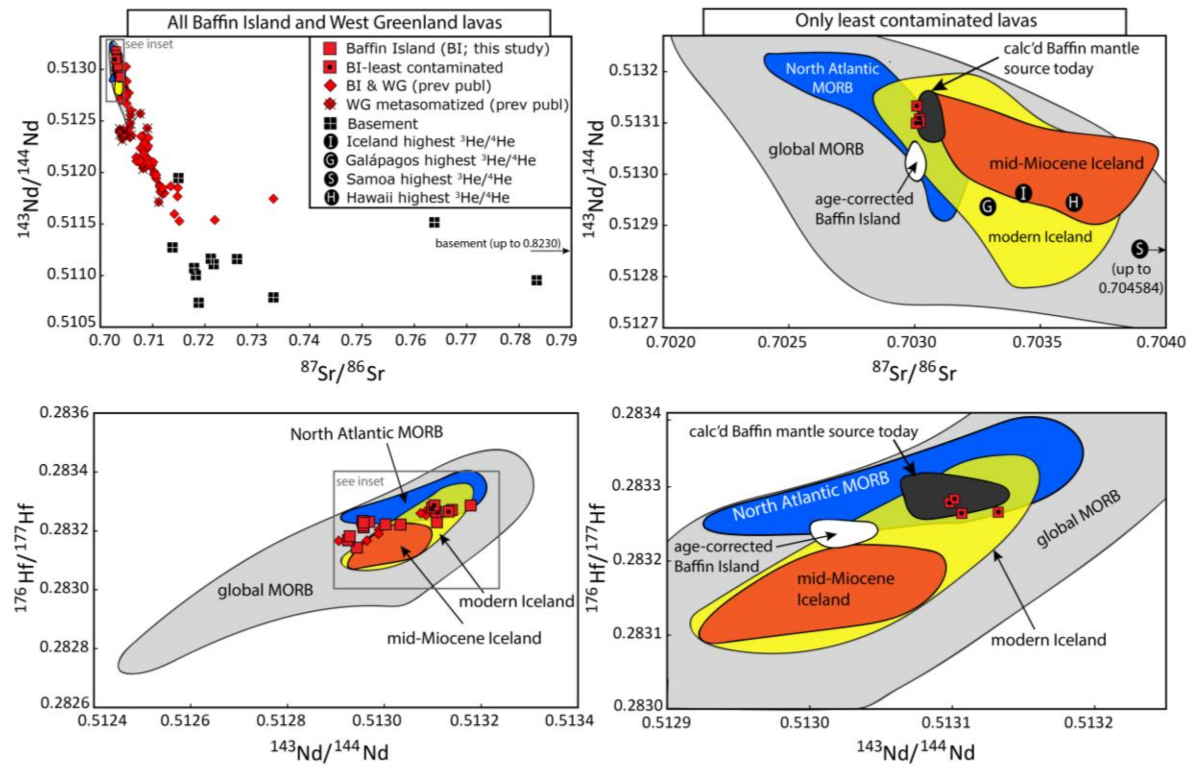

Figure 8. Sr, Nd, and Hf isotopic compositions of Baffin Island (BI) lavas from this study (red squares) shown together with previously published data from Baffin Island and West Greenland (WG) (both as red diamonds) (**Jackson et al., 2010; Starkey et al., 2009; Larsen and Pedersen, 2009; Kent et al., 2004;** and references therein). Data points shown are the measured isotopic compositions, and white and dark grey fields reflect age-corrected and calculated present-day mantle source compositions, respectively (see **Section 3.3 and Supplementary Figure 2)**. Age correction of the mid-Miocene and modern Iceland lavas is negligible (offset is less than the size of the Baffin Island lava symbols; **Supplementary Figure 3**) and the respective fields represent measured data. All isotopic data plotted here are measured data, and age-corrected data, and calculated present-day mantle compositions, are shown as fields in the right panels. Both crustally-contaminated and least crustally-contaminated Baffin Island-West Greenland lavas are show in the left-hand side panels, whereas only the least crustally-contaminated lavas (Nb/Th > 13, Ce/Pb > 20, MgO wt. % > 10) are shown in the right-hand side panels. Paired Hf and Nd isotopic compositions are available from only two studies—this study (red squares) and **Jackson et al. (2010)** (red diamonds), explaining the smaller dataset available for plotting. Mid-Miocene Iceland (orange field), modern Iceland (yellow field), North Atlantic MORB (50° to 80° N) (blue field), and global MORB (light grey field) fields are shown for perspective (Iceland data from GEOROC, http://georoc.mpch-mainz.gwdg.de/georoc/; MORB data from **Gale et al. [2013]**); MORB fields exclude back arc basin lavas and MORB samples < 500 km from nearby hotspots (**Kind and Adam, 2014**). Lavas with the highest $^{3}He/^{4}He$ compositions from Iceland, Galápagos, Hawaii, and Samoa are indicated by the black circles with the letters I, G, H, and S, respectively (**see Jackson et al. [2008]**).

In order to compare Baffin Island with MORB and younger lavas associated with the Iceland plume, we focus on the isotopic compositions calculated for the Baffin Island mantle today (which overlaps the measured isotopic ratios), because the age-corrected data are less appropriate for comparison with the significantly younger high-$^{3}He/^{4}He$ lavas from Iceland (all of which are stratigraphically younger than 14.9 Ma; **Hardarson et al., 1997; McDougall et al., 1984**). The four least crustally-contaminated Baffin Island lavas with mantle-like Nb/Th and Ce/Pb plot within the field for global MORB located far from hotspots in all radiogenic isotopic spaces (**Figures 8 and 9**). However, in plots that include $^{206}Pb/^{204}Pb$, they are offset from the field for North Atlantic MORB (i.e., 50 to 80°N, located far from hotspots), but overlap with it in plots of $^{143}Nd/^{144}Nd$ versus $^{87}Sr/^{86}Sr$ and $^{176}Hf/^{177}Hf$ versus $^{143}Nd/^{144}Nd$. The radiogenic isotopes of the four least contaminated Baffin Island lavas do not consistently overlap with the field for mid-Miocene to modern (neovolcanic zone) Iceland lavas, but partially overlap with the geochemically depleted (Sr, Nd, Hf) and unradiogenic (Pb) portion of the modern (neovolcanic zone) Iceland field. Additionally, they fall on or close to the 4.5 Ga geochron (**Figure 9**), an observation consistent with that made by **Jackson et al. (2010).**

4.5. Oxygen isotopic compositions

In **Figure 10**, the oxygen isotopic compositions measured on Baffin Island olivines from this study are shown together with those previously published (**Kent et al. 2004).** The oxygen isotopic data are compared with olivine forsterite content and basalt Nb/Th. The four least crustally-contaminated Baffin Island lavas also have olivine $\delta^{18}O$ indistinguishable from MORB olivines (5.0–5.2 ‰; **Eiler, 2001**) and all lavas from this study fall within the range defined by mantle olivine $\delta^{18}O$ from **Mattey et al. (1994)** (5.18 ± 0.28 ‰). However, at low

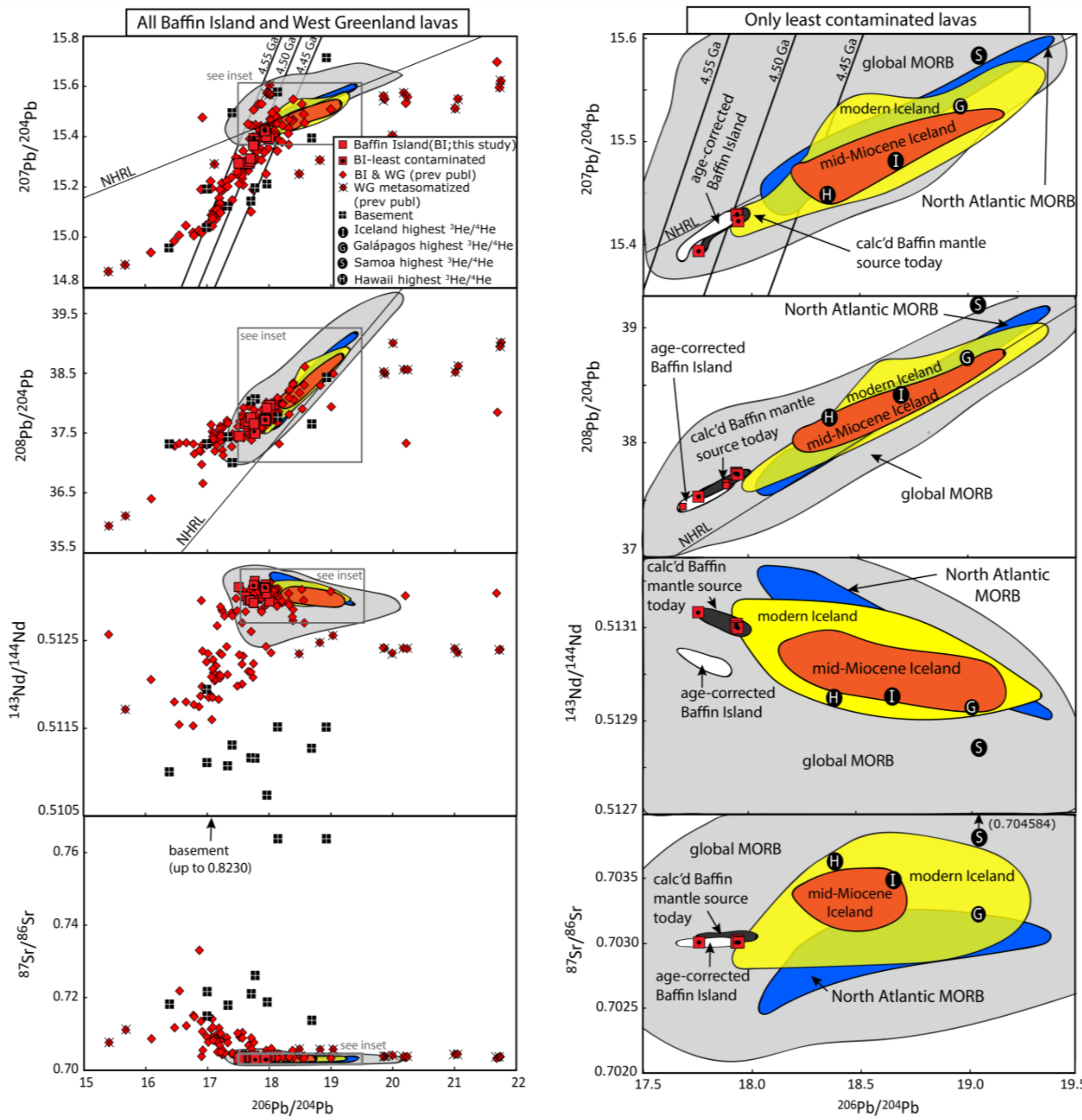

Figure 9. Sr, Nd, and Pb isotopic compositions of Baffin Island (BI) lavas from this study (red squares) shown together with previously published data from Baffin Island and West Greenland (WG) (both red diamonds) (**Jackson et al., 2010; Starkey et al., 2009; Larsen and Pedersen, 2009; Kent et al., 2004;** and references therein). Data points shown are the measured isotopic compositions, while white and dark grey fields reflect age-corrected and calculated present-day mantle source compositions, respectively (see **Section 3.3 and Supplementary Figure 2)**. Age correction of the mid-Miocene and modern Iceland lavas is negligible (offset is less than the size of the Baffin Island lava symbols; **Supplementary Figure 3**) and the respective fields represent measured isotopic ratios. Crustally-contaminated and least crustally-contaminated Baffin Island-West Greenland lavas are show in the left-hand side panels, whereas only the least crustally-contaminated lavas (Nb/Th > 13, Ce/Pb > 20, MgO wt. % > 10) are shown in the right-hand side panels.

Figure 9. *continued*

Mid-Miocene Iceland (orange field), modern Iceland (yellow field), and North Atlantic MORB (50° to 80° N) (blue field) and global MORB (light grey field) fields are shown for perspective (Iceland data from GEOROC, http://georoc.mpch-mainz.gwdg.de/georoc/; MORB data from **Gale et al. [2013])**; MORB fields exclude back arc basin lavas and MORB samples < 500 km from nearby hotspots (**King and Adam, 2014**). For all plots that include Pb isotopes, fields for mid-Miocene and modern Iceland are defined using high-precision MC-ICP-MS data only, while MORB fields also include unspiked Pb isotopic data acquired by TIMS. For Pb isotopic data obtained on Baffin Island and West Greenland, both MC-ICP-MS and unspiked TIMS Pb isotopic data are included in the "global plots" (i.e., left-hand side panels), whereas only samples with MC-ICP-MS Pb isotopic data are shown in the right-hand side panels. In the Sr-Pb panel, mid-Miocene Iceland has a narrower range than other panels because the highest and lowest $^{206}Pb/^{204}Pb$ samples lack Sr isotopic analyses. Lavas with the highest $^{3}He/^{4}He$ compositions from Iceland, Galápagos, Hawaii, and Samoa are indicated by the black circles with the letters I, G, H.

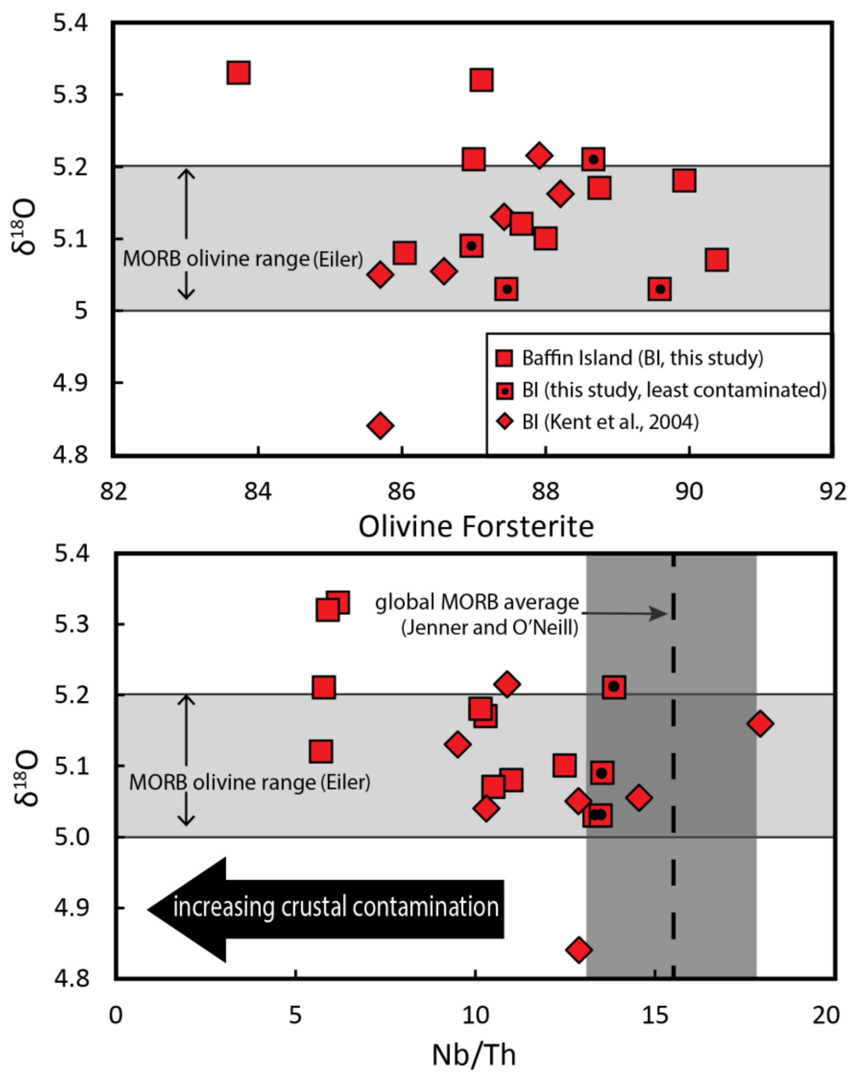

Figure 10. $\delta^{18}O$ compositions of Baffin Island olivines from this study (red squares) and **Kent et al. (2004)** (red diamonds) compared with olivine forsterite and Nb/Th. The range of $\delta^{18}O$ in MORB olivine is from **Eiler (2001).** The range of Nb/Th in MORB is from **Jenner and O'Neil (2012)** and includes 1σ variation. Low Nb/Th, which is associated with higher degrees of crustal assimilation, may relate to somewhat higher $\delta^{18}O$. The four Baffin Island lavas that are "least crustally-contaminated" (based on having high Nb/Th, Ce/Pb, and MgO) also have MORB-like $\delta^{18}O$.

olivine forsterite and low basalt Nb/Th (associated with crustal assimilation), olivine $\delta^{18}O$ values in some of these Baffin lavas plot outside the window defined by MORB olivines.

4.6. Helium concentrations and isotopic compositions

Figure 11 summarizes the helium results for olivine in vacuo crushing determinations for Baffin Island-West Greenland lavas from this and previous studies **(Graham et al., 1998; Stuart et al., 2003; Starkey et al., 2009; Jackson et al., 2010; and Rizo et al., 2016**). Olivine crushing *in vacuo* is the most common helium extraction method because it primarily releases gas from fluid and melt inclusions, which is the best determination of magmatic helium isotopic compositions, due to the possible presence of cosmogenic and/or radiogenic helium in the olivine matrix. The large range in **Figure 11** demonstrates that helium concentrations are highly variable (a factor of 370), most likely reflecting variable abundances of trapped melt and fluid inclusions in the olivines. The olivine crush experiments for the samples in this study yield $^3He/^4He$ ranging from 0.17 to 56.6 R_A, encompassing most of the known values. In general, samples in this study with low ^4He concentrations (< $1.0x10^{-10}$ ^4He cc STP/g) have lower $^3He/^4He$, which owes to greater potential for atmospheric contamination in low ^4He samples (**Hilton et al., 1995**), and to greater sensitivity to reduction in $^3He/^4He$ by post-eruptive radiogenic ingrowth of ^4He. Two samples—AK-9 and DB-17—plot above the trend defined by Baffin Island-West Greenland lavas in $^3He/^4He$ versus ^4He space, and given their low ^4He concentrations, they were selected for fusion experiments (together with AK-8b) on crushed powders to test for cosmogenic ^3He influence.

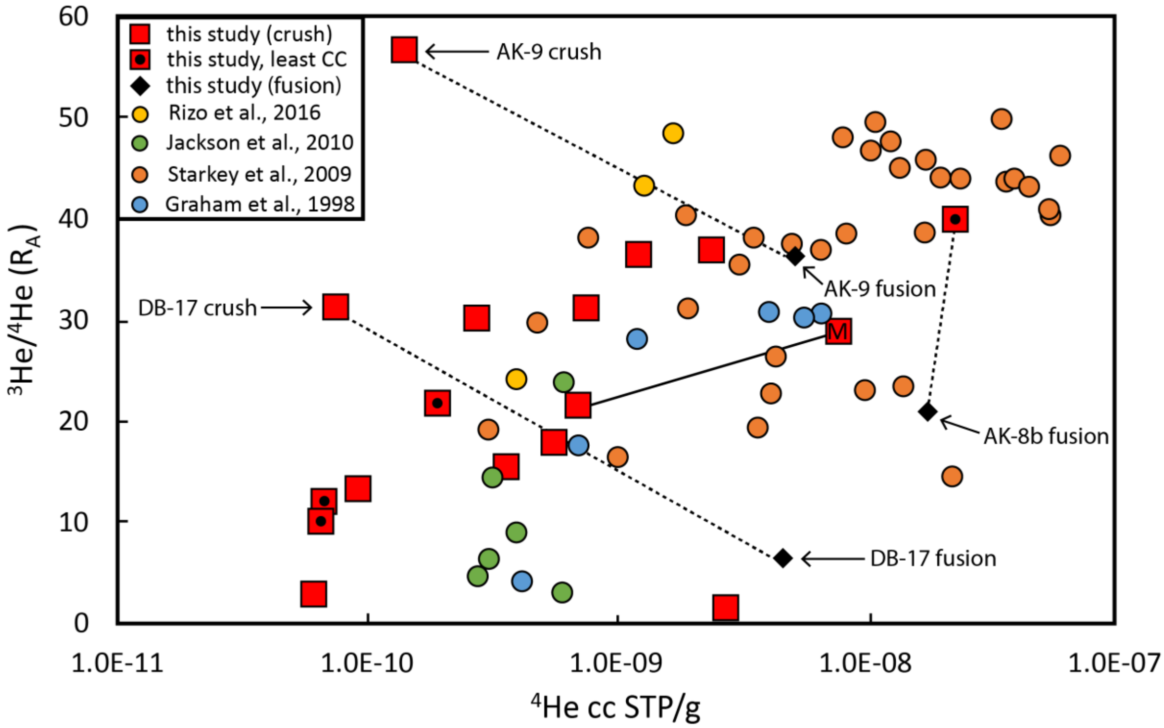

Figure 11. Helium isotopic compositions compared to ^4He concentrations for Baffin Island and West Greenland magmatic olivines. Samples with lower helium concentrations tend to have lower $^3He/^4He$, possibly due to greater sensitivity to post-eruptive radiogenic ingrowth of ^4He. The dashed lines connect the olivine crush experiment data to the respective fusion results for three different samples. The solid line connects a crush experiment on a single olivine megacryst (denoted by an "M" in the symbol) to the crush experiment for muliple olivine phenocrysts from the same lavas (AK-13). CC signifies crustal contamination.

Basaltic olivines with cosmogenic helium typically yield magmatic helium via crushing and extremely high $^3He/^4He$ from fusion, reflecting spallation ^3He in the solid olivine (e.g., **Kurz, 1986**). Sample AK-9, which has the highest $^3He/^4He$ crush experiment in this study (AK-9, 56.6 ± 1.1 R_A), yielded a $^3He/^4He$ of 36.3 R_A and ^4He concentration (5.2 x 10^{-9} cc STP/g) by fusion of the powder remaining after crushing. However, the $^3He/^4He$ from the crush experiment of AK-9 should be treated with caution due to the low ^4He concentration (1.4x10^{-10} cc STP/g) and high (43%) contribution from blank. Another sample that underwent a fusion experiment, DB-17, has a crush $^3He/^4He$ of 31.2 ± 0.9 R_A (^4He = 7.5x10^{-11} cc STP/g), and a fusion $^3He/^4He$ of 6.4 R_A (^4He = 4.7 x 10^{-9} cc STP/g). Critically, the high $^3He/^4He$ value (39.9 ± 0.5 R_A) for an olivine crush experiment, determined in sample AK-8b, also has the highest ^4He concentration (2.3x10^{-8} cc STP/g), and plots within the field of data populated by previously published high-$^3He/^4He$ lavas in the $^3He/^4He$ versus ^4He (cc STP/g) plot, and is considered the most robust high $^3He/^4He$ measurement in this study. A fusion experiment on the AK-8b crushed olivine powder yielded $^3He/^4He$ of 20.8 Ra (and ^4He = 1.84 x10^{-8} cc STP/g). In all three samples with paired crush-powder fusions, the fusion measurements yielded *lower* $^3He/^4He$ than crushing, suggesting that radiogenic helium is a significant contribution. These data demonstrate that cosmogenic helium does not dominate in the olivines and is not a likely contributor to the crushing experiments, because one would expect cosmogenic helium to have *higher* $^3He/^4He$. The lack of high $^3He/^4He$ in the fusion measurements does not exclude the possibility of small amounts of cosmogenic helium, but strongly suggests it is not a contribution to the crushing measurements. Olivine typically has extremely low Th and U abundances (ppb), but radiogenic helium can be implanted into the olivine crystal surfaces from the solid matrix (which has ppm levels of Th and U), which is released by fusion and not by crushing (e.g., **Jackson et al., 2010; Moreira et al., 2012**). The comparison between a megacryst and smaller grain size olivines from the same sample (AK-13) supports the importance of ^4He implantation from the groundmass, i.e. with greater effect on smaller crystals with fewer melt inclusions.

When focusing only on Baffin Island samples with mantle-like Nb/Th and Ce/Pb (i.e., least crustally-contaminated), paired $^3He/^4He$ and Sr-Nd-Pb isotopic measurements show that the least contaminated Baffin Island lavas have a distinct radiogenic isotopic composition from the highest observed $^3He/^4He$ lavas from Iceland, Galápagos, Hawaii, and Samoa (marked as

"I", "G", "H", and "S" in **Figures 8 and 9**). Unfortunately, there are insufficient existing samples with paired $^{3}He/^{4}He$ and $^{176}Hf/^{177}Hf$ to make this comparison. For example, while the upper envelope of $^{3}He/^{4}He$ in Icelandic lavas increases with increasing $^{87}Sr/^{86}Sr$—where the highest $^{3}He/^{4}He$ of 37.7 R_A is at 0.703465—the $^{87}Sr/^{86}Sr$ of the least contaminated Baffin Island lavas defines a narrow range of lower values (0.703008–0.703021) at all $^{3}He/^{4}He$ values (0.703009 at 39.9 R_A) (**Figure 12**). Thus, the Iceland data form a trend that diverges away from the Baffin Island lavas, and this observation holds for both the measured $^{87}Sr/^{86}Sr$ ratio and the calculated present-day $^{87}Sr/^{86}Sr$ for the Baffin Island mantle source. Similarly, a plot of $^{3}He/^{4}He$ versus $^{143}Nd/^{144}Nd$ shows that the highest $^{3}He/^{4}He$ Iceland lavas have lower $^{143}Nd/^{144}Nd$ (0.512969) than the measured $^{143}Nd/^{144}Nd$ (0.513128), and calculated present-day mantle ratio, of the least contaminated high-$^{3}He/^{4}He$ Baffin Island lava, sample AK-8b. Finally, paired $^{3}He/^{4}He$ and $^{206}Pb/^{204}Pb$ compositions of Baffin Island lavas with mantle-like Nb/Th and Ce/Pb do not overlap with Iceland lavas. The highest $^{3}He/^{4}He$ Baffin Island lava has Pb-isotopic compositions ($^{206}Pb/^{204}Pb$ = 17.7560) that are less radiogenic than the highest $^{3}He/^{4}He$ Iceland lava ($^{206}Pb/^{204}Pb$ = 18.653), an observation that holds for both source. There is no evidence that the least contaminated Baffin Island lavas and Iceland high $^{3}He/^{4}He$ lavas converge at a common Sr, Nd, and Pb isotopic composition, even if existing data trends are extrapolated to higher $^{3}He/^{4}He$.

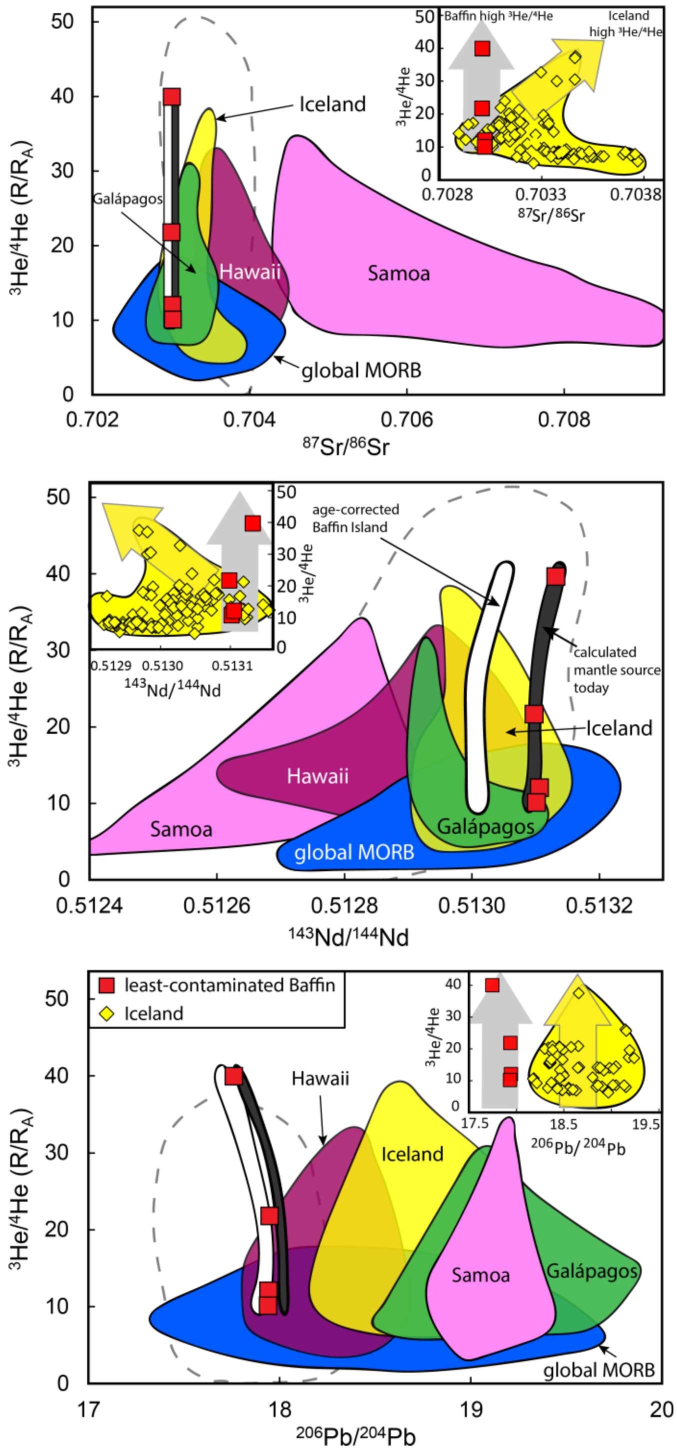

Figure 12. Helium isotopic compositions for several hotspots shown as a function of whole rock ^{87}Sr/^{86}Sr, ^{143}Nd/^{144}Nd, and ^{206}Pb/^{204}Pb. Data points shown are the measured isotopic compositions, and white and dark grey fields reflect age-corrected and calculated present-day mantle source compositions, respectively; ^{3}He/^{4}He data are not age corrected. Lavas with the highest ^{3}He/^{4}He in Iceland (yellow field and symbols) and the least crustally-contaminated Baffin Island lavas (red squares) exhibit different Sr, Nd, and Pb isotopic compositions (the comparisons rely on measured isotopic data [red squares] and calculated present-day isotopic compositions of the mantle source of the Baffin Island lavas; see **Section 3.3**). The least crustally-contaminated lavas from Baffin Island have lower ^{87}Sr/^{86}Sr and ^{206}Pb/^{204}Pb and higher ^{143}Nd/^{144}Nd than the highest ^{3}He/^{4}He Iceland lavas, suggesting a different high-^{3}He/^{4}He source (see insets). The grey dashed lines contain the field for Baffin Island and West Greenland lavas that are crustally-contaminated (Nb/Th<13, Ce/Pb<20, and/or MgO<10 wt.%), or are insufficiently characterized to identify potential crustal contamination (e.g., many Baffin Island lavas with ^{3}He/^{4}He data lack Pb concentration [and Pb isotopic] data; **Stuart et al., 2003; Starkey et al., 2009**). A global data set for oceanic lavas, including MORB and samples from the four hotspots with ^{3}He/^{4}He > 30 Ra, are provided for context (fields are adapted from **Jackson et al., 2007; Jackson et al., 2008**).

5. Discussion

5.1. Two geochemically distinct high-$^3He/^4He$ components in the Iceland plume, or crustal assimilation in Baffin Island high-$^3He/^4He$ lavas?

The highest $^3He/^4He$ lavas from Iceland (that have been characterized with paired radiogenic isotope analyses; up to 37.7 R_A; **Hilton et al., 1999**) Hawaii (35.3 R_A**; Kurz et al., 1983, 1982; Valbracht et al., 1997**), Samoa (33.8 R_A**; Farley et al., 1992; Jackson et al., 2007; Loewen et al., 2019; Workman et al., 2004**), and Galápagos (30.3 R_A; **Graham et al., 1993; Jackson, 2008; Kurz et al., 2014; Kurz and Geist, 1999**) have distinct radiogenic isotopic compositions (see **Figures 8, 9, and 12**). Here we show that the radiogenic isotopic compositions of the least crustally-contaminated high-$^3He/^4He$ lavas from 60 Ma Baffin Island document a mantle domain that is geochemically distinct from mid-Miocene Iceland lavas with the highest $^3He/^4He$. Thus, we argue for the presence of *two* geochemically distinct high-$^3He/^4He$ components within a single mantle plume. However, it is essential to explore whether the difference in radiogenic isotopic compositions between the least crustally-contaminated Baffin Island lavas and Iceland high $^3He/^4He$ lavas reflects temporal evolution of the high-$^3He/^4He$ mantle source sampled by the Iceland hotspot, or continental crust assimilation by the Baffin Island lavas.

Crustal contamination is recorded in high-$^3He/^4He$ continental flood basalts associated with the Icelandic plume at Baffin Island, West Greenland, and East Greenland (e.g., **Day, 2016; Larsen and Pedersen, 2009; Lightfoot et al., 1997; Peate, 2003; Yaxley et al., 2004**). If the Iceland hotspot has a single high-$^3He/^4He$ component, one hypothesis is that the high-$^3He/^4He$ mantle component sampled at the Iceland hotspot has a single Sr-Nd-Hf-Pb isotopic composition over time, and that the difference in Sr-Nd-Hf-Pb between Iceland and the least contaminated Baffin Island high-$^3He/^4He$ lavas is due to melts of the latter having assimilated some amount of continental crust. Radiogenic isotopic compositions for basement samples from West Greenland reported by **Larsen and Pederson (2009)**—which are inferred to be similar to the basement underlying the Baffin Island picrites (St-Onge et al., 2009)—allow us to test this hypothesis by investigating the influence of crustal contamination on the radiogenic isotopic compositions of Baffin Island lavas.

The four least contaminated Baffin Island lavas have lower $^{87}Sr/^{86}Sr$ (0.703009) than the highest $^3He/^4He$ (37.7 Ra) Iceland lava with available $^{87}Sr/^{86}Sr$ data (0.703465 for sample SEL97; **Hilton et al., 1999**). The shift to lower $^{87}Sr/^{86}Sr$ in the least contaminated, highest $^3He/^4He$ Baffin Island lava cannot be explained by continental crust assimilation because assimilation of the local Precambrian crust (which has very high $^{87}Sr/^{86}Sr$—0.713758 to 0.823010—compared to the least crustally-contaminated Baffin Island lavas, 0.703008 to 0.703021) would only serve to *increase* the Baffin Island $^{87}Sr/^{86}Sr$, not decrease it (**Figure 8**). Therefore, lower $^{87}Sr/^{86}Sr$ in the least crustally-contaminated high-$^3He/^4He$ Baffin Island lavas relative to high-$^3He/^4He$ Iceland lavas must relate to differences in their respective mantle source compositions, an observation that holds for both measured and age-corrected $^{87}Sr/^{86}Sr$ in Baffin Island lavas, as well as calculated present-day $^{87}Sr/^{86}Sr$ of the Baffin Island mantle source (**Figure 12**). This argument does not exclude a small contribution of continental crust assimilation in the four least crustally-contaminated Baffin Island lavas, rather, invoking this would only enforce the argument that Baffin Island and Iceland high-$^3He/^4He$ lavas have distinct $^{87}Sr/^{86}Sr$, because any crustal contamination in Baffin Island lavas would be expected to increase the $^{87}Sr/^{86}Sr$, suggesting that hypothetical uncontaminated versions of these lavas would have *even lower* $^{87}Sr/^{86}Sr$ relative to the high-$^3He/^4He$ Iceland lavas.

Neodymium isotopic compositions of Baffin Island lavas yield a similar conclusion. The measured (and calculated Baffin mantle source today) $^{143}Nd/^{144}Nd$ of the four least crustally-contaminated high-$^{3}He/^{4}He$ lavas from Baffin Island have higher $^{143}Nd/^{144}Nd$ than high-$^{3}He/^{4}He$ Iceland lavas (**Figure 12**), an observation that also cannot be explained by crustal assimilation because continental crust—which has very low $^{143}Nd/^{144}Nd$ (0.510737 to 0.511945) compared to the least crustally-contaminated Baffin Island lavas (0.513099 to 0.513133)—would lower the $^{143}Nd/^{144}Nd$ of the Baffin Island lavas (**Figure 8**). Thus, the observation of a more geochemically depleted high-$^{3}He/^{4}He$ component in the proto-Iceland plume, compared to the mid-Miocene to modern Iceland plume, is consistent for both $^{143}Nd/^{144}Nd$ and $^{87}Sr/^{86}Sr$. Unfortunately, insufficient Hf isotopic data exist to verify that his also holds true for $^{176}Hf/^{177}Hf$.

In $^{3}He/^{4}He$ versus $^{206}Pb/^{204}Pb$ isotopic space, there is no overlap in the $^{206}Pb/^{204}Pb$ compositions of the least contaminated Baffin Island lavas and the Iceland field (**Figure 12**). It is also important to evaluate whether the difference in Pb isotopic compositions between Iceland and Baffin Island lavas relates to continental crust assimilation, because Pb isotopes in basalts can be more susceptible to the compositional effects of crustal assimilation than Sr and Nd isotopes. Indeed, Pb is ~60 times more concentrated in the West Greenland basement (from **Larsen and Pedersen [2009]**) than in the least contaminated Baffin Island lavas, whereas Sr and Nd are only ~3 and ~5 times, respectively, more concentrated in the former compared to the latter. Therefore, it is crucial to test the hypothesis that Iceland and Baffin Island high-$^{3}He/^{4}He$ mantle sources actually have the *same* Pb isotopic compositions, and that the apparent shift to lower $^{206}Pb/^{204}Pb$ in Baffin Island lavas is due to assimilation of continental crust with less radiogenic Pb. To test this hypothesis, basement material from **Larsen and Pedersen**

(2009) is mixed with the composition of the highest $^{3}He/^{4}He$ lava (with measured Sr-Nd-Pb isotopes) from Iceland (**Hilton et al., 1999) (see Supplementary Discussion 2.1 and Supplementary Figure 4)**. While crustal assimilation of an Iceland high-$^{3}He/^{4}He$ lava composition can generate the Pb-isotopic compositions of the least contaminated Baffin Island lavas (**Supplementary Figure 4**), it also generates strong crustal contamination signatures (i.e., low continental-like ratios) in Ce/Pb and Nb/Th that are not seen in the least crustally-contaminated Baffin lavas (**Supplementary Discussion 2.1.**). In this light, we find that there is no basement composition in this dataset that, through crustal assimilation, can explain the Sr-Nd-Pb isotopic shift from the composition of the highest $^{3}He/^{4}He$ Iceland lava to the least contaminated Baffin Island lavas while also generating the mantle-like Ce/Pb and Nb/Th in the same lavas (**Supplementary Figure 4**). Furthermore, the observation of mantle-like Ce/Pb, Nb/Th, and $\delta^{18}O$ in the four least contaminated Baffin Island lavas suggests that these four Baffin Island lavas have assimilated very little, if any, continental crust. We conclude that the four Baffin Island lavas are likely very close in composition to their original uncontaminated compositions, and the Pb-isotopic composition of the mantle source of their mantle source must be less radiogenic than (and therefore isotopically distinct from) Iceland high-$^{3}He/^{4}He$ lavas.

It is important to acknowledge that our application of strict trace elements filters, applied to avoid Baffin Island lavas that may have experienced crustal assimilation, may have also filtered out lavas with primary "enriched mantle" signatures, which have been suggested to exist in the Baffin Island mantle (Kent et al., 2004; Robillard et al., 1992; Starkey et al., 2012). For example, the enriched mantle (with higher $^{87}Sr/^{86}Sr$ and lower $^{143}Nd/^{144}Nd$) has low Ce/Pb and Nb/Th due to continental crust recycling **(Hofmann, 1997; Jackson et al., 2007**) and any uncontaminated Baffin Island primary melts sampling enriched mantle (EM) domains with low mantle-derived Ce/Pb and Nb/Th could potentially be eliminated from consideration due to the strict crustal assimilation filters applied to the data set. However, even if enriched mantle lavas with low Ce/Pb and Nb/Th have been filtered out from the Baffin Island data set, this does not negate the finding of a high-$^{3}He/^{4}He$ component in Baffin Island that is *more geochemically depleted* than the Iceland high-$^{3}He/^{4}He$ component (**Figure 12**): the observation remains that there are high-$^{3}He/^{4}He$ Baffin Island lavas with lower $^{87}Sr/^{86}Sr$ and higher $^{143}Nd/^{144}Nd$ that are more geochemically depleted than high-$^{3}He/^{4}He$ Iceland lavas, and these isotopic differences cannot be explained by crustal assimilation.

5.2. A heterogeneous high-$^{3}He/^{4}He$ component: implications for a common component in the mantle and origins of its geochemically depleted nature.

It is intriguing that the least crustally-contaminated Baffin Island lavas have the lowest $^{206}Pb/^{204}Pb$, the most geochemically depleted $^{87}Sr/^{86}Sr$ and $^{143}Nd/^{144}Nd$, of the highest $^{3}He/^{4}He$ of the hotspots with $^{3}He/^{4}He$ >30 R_A (Hawaii, Galápagos, Samoa, and Iceland) (see **Figures 8, 9, and 12**). These observations may provide an important clue to the origin of the high-$^{3}He/^{4}He$ mantle domain. For example, it could be that the extent of geochemical depletion relates to the process that generated high-$^{3}He/(U+Th)$—and thus preserves high $^{3}He/^{4}He$—in the Baffin Island mantle source. For example, if He is less incompatible than U and Th during mantle melting (e.g., **Parman et al., 2005**), then greater geochemical depletion will result in higher $^{3}He/^{4}He$ and higher $^{143}Nd/^{144}Nd$, consistent with the highest $^{3}He/^{4}He$ preserved in Baffin lavas with higher $^{143}Nd/^{144}Nd$ than observed at other high-$^{3}He/^{4}He$ hotspots. However, other studies examining the partitioning of helium during mantle melting are suggest that He is more incompatible than U and Th (Heber et al., 2007; Jackson et al., 2013). Thus, an alternative model for the highly geochemically depleted Sr and Nd (and unradiogenic Pb) isotopes in Baffin Island lavas, compared to other high-$^3He/^4He$ OIB, is that variable quantities of enriched material (e.g., recycled oceanic and/or continental crust) was added to an initially homogeneous, geochemically depleted high-$^3He/^4He$ mantle source (like that observed in Baffin Island lavas) to produce the Sr-Nd-Hf-Pb isotopic variability observed in high-$^3He/^4He$ (>30 Ra) lavas at Hawaii, Galápagos, Samoa and Iceland (Garapić et al., 2015). Consistent with this alternative scenario, radiogenic $^{206}Pb/^{204}Pb$ in the high-$^3He/^4He$ Iceland component, compared to Baffin Island lavas, could result from the addition of a high-U/Pb component. Recycled oceanic crust is an obvious candidate for the high-U/Pb material and would help explain the elevated Ti in high-$^3He/^4He$ OIB lavas relative to Baffin Island (**Garapic et al., 2015**) and the recycled atmospheric heavy noble gas signatures in a moderately high-$^3He/^4He$ Icelandic lava (**Mukhopadhyay, 2012**) and high-$^3He/^4He$ Samoan plume-related lavas in the Lau Basin (Pető et al., 2013). In this scenario, Baffin Island lavas sample the most pristine (or "least modified"; **White, 2015**) surviving relic of an early formed, geochemically depleted high-$^3He/^4He$ mantle domain that has experienced the least overprinting by recycled material over geologic time. Heavy noble gases would provide an ideal test of this hypothesis. $^{129}Xe/^{130}Xe$ data are available for a moderately high-$^3He/^4He$ (17.2 R_A) lava from the neovolcanic zone of Iceland, and a Lau Basin high $^3He/^4He$ lava (28.1 Ra; **Pető et al., 2013**), and they indicate both an early Hadean component in its mantle source and the presence of recycled heavy noble gases. Unfortunately, the heavy noble gas compositions of Baffin Island lavas have not yet been analyzed, so it is not yet possible to use heavy noble gases to evaluate whether the Baffin Island high-$^3He/^4He$ mantle domain has experienced less overprinting by recycled materials compared to other high-$^3He/^4He$ hotspot lavas (Mukhopadhyay and Parai, 2019). Conclusions regarding a recycled atmospheric heavy noble gas component in the highest $^3He/^4He$ mantle domain (e.g., **Mukhopadhyay and Parai, 2019**) will benefit from targeting the Baffin Island-West Greenland suite.

The addition of recycled material to depleted mantle, like that sourcing the high-$^3He/^4He$ Baffin Island lavas, has implications for the origin of Sr-Nd-Pb isotopic heterogeneity in high-$^3He/^4He$ lavas and the "common component" sampled by hotspots. In Sr-Nd-Pb isotopic space, different hotspots form "arrays" that converge on a common region, referred to as FOZO (focus zone; **Hart et al. [1992])** or C (common; **Hanan and Graham [1996])**, and hotspot lavas that sample this common composition are suggested to host high-$^3He/^4He$ (**Hart et al., 1992**). However, the new data from Baffin Island, combined with previously published data from the Iceland hotspot, do not seem to be consistent with convergence on a common high-$^3He/^4He$ component in Sr-Nd-Pb isotopic space: Iceland high $^3He/^4He$ and Baffin high $^3He/^4He$ lavas *diverge* in Figure 12. Rather than a homogeneous high-$^3He/^4He$ domain sampled by all hotspots, a model of heterogeneity in the high-$^3He/^4He$ domain, perhaps due to addition of heterogeneous recycled materials over time to a mantle component similar to Baffin Island may be more consistent with the observed intra-hotspot heterogeneity in the high-$^3He/^4He$ domain(s) sampled by Iceland, and the inter-hotspot Sr-Nd-Pb heterogeneity observed in the highest $^3He/^4He$ lavas from hotspots globally (**Figure 12**).

The origin of the geochemically depleted radiogenic isotopic signatures of lavas with primitive $^3He/^4He$ has eluded explanation since the first geochemical characterization of high $^3He/^4He$ lavas (**Kurz et al., 1982**). With the exception of $^3He/^4He$ and ^{182}W (but for ^{182}W see **Section 5.3**), the least crustally-contaminated Baffin Island resemble MORB in all isotopic spaces explored here (**Figures 8 and 9**)(**Ellam and Stuart, 2004**), as well as $^{142}Nd/^{144}Nd$

(**de Leeuw et al, 2017**), $^{187}Os/^{188}Os$ (**Dale et al., 2009)**, and stable isotopes (e.g., $\delta^{18}O$ [this study], and $\delta^{56}Fe$ and $\delta^{66}Zn$ (McCoy-West et al., 2018)]). One hypothesis is that the proto-Iceland plume head incorporated significant upper mantle material, and concurrent rifting (e.g., **Keen et al., 2012**) may have enhanced upper mantle incorporation, with the result that the upper mantle dominates the non-noble gas isotopic signatures in erupted lavas; the high-$^3He/^4He$ signature from the deep mantle source was retained due to higher concentrations of helium in the deep mantle relative to the upper mantle (Stuart et al., 2003, 2000) (**Section 2.2 of the Supplementary Discussion**). In this model, the composition of the deep mantle domain contributing high $^3He/^4He$ to DMM is unknown because it has been completely overprinted—for everything except for noble gases and possibly W—by mixture with the depleted upper mantle.

Alternatively, an intrinsic depleted component (distinct from the upper mantle MORB source) may reside in the Iceland plume (e.g., **Fitton et al., 2003**), and if the intrinsic component host elevated $^3He/^4He$, it provides an alternative explanation for the geochemically depleted nature of high $^3He/^4He$ material in the Iceland plume. PREMA (Prevalent Mantle) was suggested to be a geochemically depleted lower mantle component sampled by mantle plumes that overlaps with the radiogenic composition of Icelandic high $^3He/^4He$ lavas (**Zindler and Hart, 1986)**. One model proposed for the origin of PREMA is that it is the depleted residue of "significant differentiation of the silicate portion of the Earth [that] occurred contemporaneously with core segregation…and might represent the most primitive remaining mantle, having essentially survived unscathed since the earliest days of Earth history" (**Zindler and Hart, 1986**). In this model, PREMA in the upper mantle convective regime continued to be depleted by crustal extraction and evolved toward DMM (**Zindler and Hart, 1986**). If the least contaminated Baffin Island lavas sample PREMA that was preserved in the lower mantle, the short-lived $^{142}Nd/^{144}Nd$ system (where ^{146}Sm decays to ^{142}Nd, $t_{1/2}$=103 Ma), sensitive to Hadean silicate differentiation, permits investigation of early differentiation that might have generated the geochemically depleted mantle domain with high $^{3}He/^{4}He$. However, no resolvable $^{142}Nd/^{144}Nd$ anomalies are observed in Baffin Island (de Leeuw et al., 2017) or Iceland (Andreasen et al., 2008; Debaille et al., 2007). The implications of the lack of observable $^{142}Nd/^{144}Nd$ anomalies in Iceland hotspot lavas (which contrasts with resolvable $^{142}Nd/^{144}Nd$ variability at other hotspots; **Horan et al., 2018; Peters et al., 2018**) are not yet clear, but may still leave open the possibility of Baffin Island lavas sampling the depleted residue of Hadean terrestrial differentiation (**see Supplementary Discussion 2.2.**), consistent with the primitive Pb isotopic compositions in the least crustally-contaminated Baffin Island lavas (**Jackson et al., 2010**).

5.3. Location of the high-$^{3}He/^{4}He$ mantle domains sampled by the Iceland plume

While it is important to define heterogeneity that exists within the highest $^{3}He/^{4}He$ domain in the mantle, it is also important to constrain where the heterogeneous high-$^{3}He/^{4}He$ domains reside within the mantle. Relationships between $^{3}He/^{4}He$ and geophysical observations at hotspots can provide a clue regarding the location of these domains in the mantle. The hotspot localities with greater contributions from the FOZO-C components (inferred to have high $^{3}He/^{4}He$) have lower seismic shear-wave velocity anomalies in the shallow (200 km) upper mantle (**Konter and Becker, 2012**) and higher buoyancy flux than lower $^{3}He/^{4}He$ hotspots (**Graham, 2002; Jackson et al., 2017; Jellinek and Manga, 2004; Putirka, 2007**), which is consistent with higher $^{3}He/^{4}He$ hotspots sampling hotter mantle domains than lower $^{3}He/^{4}He$ hotspots and MORB (**Putirka et al., 2008; Jackson et al., 2017**).

Here we examine whether the highest $^3He/^4He$ hotspot lavas sampled at Baffin Island-West Greenland also sample a mantle source that was hotter than ambient mantle sampled by MORB (Herzberg and Gazel, 2009; Holm et al., 1993; Putirka et al., 2007; Trela et al., 2017). Using the approach of **Herzberg and Asimow (2015)**, we explore the hypothesis of a hotter-than-ambient-mantle high-$^3He/^4He$ plume by comparing calculated mantle potential temperatures from 1) the least crustally-contaminated Baffin Island-West Greenland compositions, and 2) MORB located >500 km from hotspots (to avoid a "hotspot influence" and isolate the MORB melting signature). The calculated mantle potential temperatures for the least contaminated Baffin Island-West Greenland primary melts range from 1510 to 1630 °C. This range of temperatures is consistent with previously calculated mantle potential temperatures for proto-Iceland plume lavas from **Larsen and Pedersen (2000)** (1520 to 1560 °C), **Herzberg and Gazel (2009)** (1470 to 1650 °C), **Hole and Millett (2016)** (1480 to 1550 °C), and **Putirka et al. (2018)** (1630 ± 65 °C). Critically, the Baffin Island-West Greenland lavas yield higher calculated mantle potential temperatures than the high-MgO MORB considered here (1320 to 1480 °C), the Siqueiros MORB from **Putirka et al. (2018)** (1420 ± 40 °C), the compiled MORB in **Madrigal et al. (2016)** (1320 to 1390 °C), and average MORB from **Cottrell and Kelley (2011)** (1320 ± 39 °C).

Hotter mantle potential temperatures result in higher degrees of melting at Baffin Island and West Greenland (10–30 %, based on results from the PRIMELT3 calculations for the Baffin Island and West Greenland in Figure 3) relative to high-MgO MORB (5–25 %, using PRIMELT3 and lavas in Figure 3**)**. This results in lower Na_2O in Baffin primary liquids (e.g., **Klein and Langmuir, 1987**) **(see Figure 3)**. Similarly, higher mantle potential temperatures will result in greater average melting depths for the Baffin Island-West Greenland lavas compared to MORB, consistent with higher calculated primary melt FeO in the former (i.e., **Klein and Langmuir, 1987**) **(see Figure 3)**. Compared to calculated primary MORB melts, higher temperature of melting in the Baffin Island-West Greenland lavas can also explain higher MgO (owing to higher degrees of melting driving melt closer to olivine compositions), lower SiO_2 (owing to reduced silica activity at greater melting depths), lower Al_2O_3 (due to greater extent of melting in the garnet stability field, thereby leaving Al_2O_3 retained in the source), and lower CaO (because the clinopyroxene phase volume increases at higher pressure melting at the expense of olivine and orthopyroxene; e.g., **Walter, 1998**) **(see Figure 3)**. These findings help to explain the rather large differences in the primary liquid major element compositions between MORB (located far from hotspots) and the least crustally-contaminated Baffin Island-West Greenland lavas (**Figures 2 and 3**), and are consistent with the hypothesis that the high-$^3He/^4He$ domain is sampled by hot plumes (**Putirka, 2008; Jackson et al., 2017**).

A remaining question is why high-$^3He/^4He$ hotspots are hotter than both low-$^3He/^4He$ hotspots (**Jackson et al., 2017**) and MORB located far from hotspots. One hypothesis is that primitive domains are preserved in deep, dense mantle reservoirs (Deschamps et al., 2011; Jellinek and Manga, 2004; Samuel and Farnetani, 2003), and only the hottest mantle plumes are sufficiently buoyant to entrain this material from the deep mantle (**Jackson et al., 2017**). A deep dense domain is ideally suited for preserving primitive geochemical signatures that, like $^3He/^4He$, record the earliest history of the planet despite billions of years of mantle convective mixing. For example, the highest $^3He/^4He$ lavas from Iceland, Samoa, and Hawaii exhibit negative ^{182}W anomalies relative to the terrestrial standard (**Mundl et al., 2017**), and these ^{182}W anomalies date to within ~60 Ma years of terrestrial accretion. In order for modern OIB to have high $^3He/^4He$ and ^{182}W anomalies, there must be domains capable of preserving ancient geochemical signatures within the Earth; however, the exact location of these domains remains unknown.

Two large low-shear-velocity provinces (LLSVPs) that are consistently observed in seismic tomography studies of the deepest mantle (Garnero and McNamara, 2008; Lekic et al., 2012; McNamara, 2019), may represent storage sites for less de-gassed and ancient mantle material, as well as younger subducted oceanic or continental crust (e.g., **Li et al., 2014**). Based on a geographic relationship between hotspots with elevated $^{3}He/^{4}He$ and the location of LLSVPs, LLSVPs have been argued to host elevated $^{3}He/^{4}He$ (Williams et al., 2019). If LLSVPs contain primitive geochemical signatures (**Tackley, 2000**), as well as pockets of heterogenous recycled materials, then variable mixing of primitive and recycled components within LLSVPs could explain the Sr-Nd-Pb-Hf isotopic differences observed between the least contaminated high-$^{3}He/^{4}He$ lavas from Baffin Island-West Greenland and the highest $^{3}He/^{4}He$ OIB lavas at Iceland, Hawaii, Samoa, and Galápagos (**Garapic et al., 2015)**. More importantly for this study, the juxtaposition (and possible mixing) of ancient high-$^{3}He/^{4}He$ and recycled domains in the plume source could explain the isotopic heterogeneity in the Iceland plume through time. Moreover, ultralow-velocity zones (ULVZ) (Garnero et al., 2016; McNamara et al., 2010; Rost et al., 2005**),** which have even slower shear-wave velocity anomalies than LLSVPs, provide a second potential long-term storage site for primitive geochemical signatures (Herzberg et al., 2013; Mundl et al., 2017); the three hotspots observed to have ^{182}W anomalies—Hawaii, Iceland, and Samoa—are all associated with ULVZs (**Mundl et al., 2017; Mundl-Petermeier et al., 2019**). (Note that ^{182}W data are not yet available for Galápagos lavas.) Alternatively, highly viscous mantle domains could lead to the production of isolated convection cells in the mantle, ranging from ~1,000 to 2,200 km depth, called bridgmaniteenriched ancient mantle structures, or BEAMS (Ballmer et al., 2017). Long-term stability of highly viscous portions of the mantle, like BEAMS, may also serve as a storage site for geochemical domains over billions of years. However, further work is needed to explore why material from BEAMS would be preferentially sampled by only the hottest, most buoyant mantle plumes. A contribution from one or more of these domains to rising plume conduits may explain how some isotopic signatures, such as high $^{3}He/^{4}He$ and ^{182}W, have escaped homogenization and have been observed in mantle-derived rocks that erupted during the Cenozoic.

The core is an additional possible residence for both elevated $^{3}He/^{4}He$ and negative ^{182}W anomalies. The possibility of the core as a source of primitive helium in mantle plumes has been explored (**e.g., Bouhifd et al., 2013; Hofmann et al., 1986; Jephcoat, 1998; Porcelli and Halliday, 2001; Roth et al., 2019)**. Tungsten is moderately siderophile, and therefore partitioned into the core during core formation producing a low Hf/W ratio (and thus negative ^{182}W anomalies) in the core relative to the bulk silicate Earth, so a core contribution to mantle plumes would be observed as negative ^{182}W anomalies in hotspot lavas. **Mundl et al. (2017)** and **Mundl-Petermeier et al., 2019** reported negative ^{182}W anomalies in high-$^{3}He/^{4}He$ Iceland lavas, consistent with a core contribution, but **Rizo et al. (2016)** reported positive ^{182}W anomalies in Baffin Island lavas. However, **Kruijer and Kleine (2018**) propose a potential nuclear field shift effect as the origin of the large $\mu^{182}W$ found in a Ontong Java Plateau drill core sample (**Rizo et al., 2016**), leading to their speculation about the validity of the large $\mu^{182}W$ anomaly measured in the Baffin Island sample from the same study. Further, the **Rizo et al. (2016)** result is not consistent recent results of **Mundl-Petermeier et al. (2019),** which show slightly negative ^{182}W anomalies in genetically related West Greenland picrites. Given the sensitivity of ^{182}W in primitive Baffin Island and West Greenland lavas [≤62 ppb W; **Mundl-Petermeier et al., 2019; Rizo et al., 2016**] to being overprinted with continental crust [1000 ppb W; **Rudnick and Gao, 2003**]), additional ^{182}W analyses from Baffin Island lavas, specifically targeting lavas that are identified as being least crustally-contaminated, will be critical for evaluating the presence of $\mu^{182}W$ anomalies in the mantle source of Baffin Island lavas.

If the core is the ultimate source of the anomalous ^{182}W and elevated $^3He/^4He$ at hotspots, and if additional targeting the least crustally-contaminated Baffin Island lavas work reveals anomalous ^{182}W consistent with a core contribution, further investigation of the physical processes and potential geochemical indicators of a core contribution to the mantle is needed to assess this hypothesis. For example, it will also require explanation of the lack of extreme highly siderophile element (HSE: Ru, Rh, Pd, Re, Os, Ir, Pt, Au) enrichment in high-$^3He/^4He$ lavas expected from a core contribution (**e.g., Rizo et al., 2019**). It will also be important to understand the mechanism that links anomalous ^{182}W, high $^3He/^4He$, and the hottest/most buoyant plumes (i.e., the high-$^3He/^4He$ domain is denser and has anomalous ^{182}W, what is the mechanism responsible for the elevated density and how did it acquire anomalous ^{182}W?).

6. Conclusions

The Iceland hotspot has erupted high-$^3He/^4He$ for over 60 My, providing a natural laboratory for investigation of time-integrated chemical evolution in a high-$^3He/^4He$ mantle plume. After filtering Baffin Island-West Greenland lavas that are influenced by continental crust contamination, the least crustally-contaminated Baffin Island-West Greenland lavas host a geochemically depleted high-$^3He/^4He$ component that is more depleted than any other high-

$^{3}He/^{4}He$ lavas globally, including high-$^{3}He/^{4}He$ lavas from Iceland. Compositional differences between the least crustally-contaminated, high-$^{3}He/^{4}He$ Baffin Island-West Greenland lavas and high-$^{3}He/^{4}He$ mainland Iceland lavas cannot be explained by crustal contamination in the former, indicating temporal evolution of the radiogenic isotopic composition in the high-$^{3}He/^{4}He$ component in the Iceland hotspot. Furthermore, there is no evidence yet for compositional convergence of Baffin Island-West Greenland high-$^{3}He/^{4}He$ lavas and Iceland high-$^{3}He/^{4}He$ lavas. Therefore, high-$^{3}He/^{4}He$ lavas from the Iceland hotspot do not support a common high-$^{3}He/^{4}He$ component in the mantle. Geochemically distinct high-$^{3}He/^{4}He$ domains within the Iceland hotspot suggests the plume has sampled at least two high-$^{3}He/^{4}He$ domains with distinct Sr-Nd-Pb isotopic compositions over time. The origin of the highly geochemically depleted radiogenic isotopic compositions in Baffin Island-West Greenland high-$^{3}He/^{4}He$ lavas remains an important outstanding question, but may relate to incorporation of depleted upper mantle during melting in a rift environment, and preservation of elevated $^{3}He/^{4}He$ is due to much higher helium concentrations in the high-$^{3}He/^{4}He$ plume compared to the upper mantle. Alternatively, the geochemically depleted nature of high-$^{3}He/^{4}He$ Baffin Island, the highest on record, may reflect a depleted deep mantle domain, and subsequent variable addition of recycled materials to the ancient noble gas reservoir has generated the isotopic heterogeneity observed at high-$^{3}He/^{4}He$ lavas from other hotspots. Finally, we also find that Baffin Island and related West Greenland lavas, which host elevated $^{3}He/^{4}He$, record hotter temperatures (1510 to 1630 °C) than global MORB erupted far from hotspots (1320 to 1480 °C), consistent with a deep, dense origin for the high-$^{3}He/^{4}He$ mantle domain.

References

Andreasen, R., Sharma, M., Subbarao, K.V., Viladkar, S.G., 2008. Where on Earth is the enriched Hadean reservoir? Earth and Planetary Science Letters 266, 14–28. https://doi.org/10.1016/j.epsl.2007.10.009

Ballmer, M.D., Houser, C., Hernlund, J.W., Wentzcovitch, R.M., Hirose, K., 2017. Persistence of strong silica-enriched domains in the Earth’s lower mantle. Nature Geosci 10, 236–240. https://doi.org/10.1038/ngeo2898

Bas, M.J.L., Maitre, R.W.L., Streckeisen, A., Zanettin, B., 1986. A Chemical Classification of Volcanic Rocks Based on the Total Alkali-Silica Diagram. J Petrology 27, 745–750. https://doi.org/10.1093/petrology/27.3.745

Bernstein, S., Hanghøj, K., Kelemen, P.B., Brooks, C.K., 2006. Ultra-depleted, shallow cratonic mantle beneath West Greenland: dunitic xenoliths from Ubekendt Ejland. Contrib Mineral Petrol 152, 335–347. https://doi.org/10.1007/s00410-006-0109-0

Bouhifd, M.A., Jephcoat, A.P., Heber, V.S., Kelley, S.P., 2013. Helium in Earth’s early core. Nature Geosci 6, 982–986. https://doi.org/10.1038/ngeo1959

Bouvier, A., Vervoort, J.D., Patchett, P.J., 2008. The Lu–Hf and Sm–Nd isotopic composition of CHUR: Constraints from unequilibrated chondrites and implications for the bulk composition of terrestrial planets. Earth and Planetary Science Letters 273, 48–57. https://doi.org/10.1016/j.epsl.2008.06.010

Class, C., Goldstein, S.L., 2005. Evolution of helium isotopes in the Earth’s mantle. Nature 436, 1107. https://doi.org/10.1038/nature03930

Cottrell, E., Kelley, K.A., 2011. The oxidation state of Fe in MORB glasses and the oxygen fugacity of the upper mantle. Earth and Planetary Science Letters 305, 270–282. https://doi.org/10.1016/j.epsl.2011.03.014

Day, J.M.D., 2016. Evidence against an ancient non-chondritic mantle source for North Atlantic Igneous Province lavas. Chemical Geology 440, 91–100. https://doi.org/10.1016/j.chemgeo.2016.07.002

de Leeuw, G.A.M., Ellam, R.M., Stuart, F.M., Carlson, R.W., 2017. 142 Nd/ 144 Nd inferences on the nature and origin of the source of high 3 He/ 4 He magmas. Earth and Planetary Science Letters 472, 62–68. https://doi.org/10.1016/j.epsl.2017.05.005

Debaille, V., Brandon, A.D., Yin, Q.Z., Jacobsen, B., 2007. Coupled 142Nd–143Nd evidence for a protracted magma ocean in Mars. Nature 450, 525–528. https://doi.org/10.1038/nature06317

Deschamps, F., Kaminski, E., Tackley, P.J., 2011. A deep mantle origin for the primitive signature of ocean island basalt. Nature Geosci 4, 879–882. https://doi.org/10.1038/ngeo1295

Eiler, J.M., 2001. Oxygen Isotope Variations of Basaltic Lavas and Upper Mantle Rocks. Reviews in Mineralogy and Geochemistry 43, 319–364. https://doi.org/10.2138/gsrmg.43.1.319

Ellam, R.M., Stuart, F.M., 2004. Coherent He–Nd–Sr isotope trends in high 3He/4He basalts: implications for a common reservoir, mantle heterogeneity and convection. Earth and Planetary Science Letters 228, 511–523. https://doi.org/10.1016/j.epsl.2004.10.020

Farley, K.A., Natland, J.H., Craig, H., 1992. Binary mixing of enriched and undegassed (primitive?) mantle components (He, Sr, Nd, Pb) in Samoan lavas. Earth and Planetary Science Letters 111, 183–199. https://doi.org/10.1016/0012-821X(92)90178-X

Fitton, J.G., Saunders, A.D., Kempton, P.D., Hardarson, B.S., 2003. Does depleted mantle form an intrinsic part of the Iceland plume?: ICELAND PLUME. Geochem. Geophys. Geosyst. 4. https://doi.org/10.1029/2002GC000424

Francis, D., 1985. The Baffin Bay lavas and the value of picrites as analogues of primary magmas. Contr. Mineral. and Petrol. 89, 144–154. https://doi.org/10.1007/BF00379449

Garapić, G., Mallik, A., Dasgupta, R., Jackson, M.G., 2015. Oceanic lavas sampling the high- ^{3}He/ ^{4}He mantle reservoir: Primitive, depleted, or re-enriched? American Mineralogist 100, 2066–2081. https://doi.org/10.2138/am-2015-5154

Garnero, E.J., McNamara, A.K., 2008. Structure and Dynamics of Earth's Lower Mantle. Science 320, 626–628. https://doi.org/10.1126/science.1148028

Garnero, E.J., McNamara, A.K., Shim, S.-H., 2016. Continent-sized anomalous zones with low seismic velocity at the base of Earth's mantle. Nature Geoscience 9, 481–489. https://doi.org/10.1038/ngeo2733

Graham, D.W., 2002. Noble Gas Isotope Geochemistry of Mid-Ocean Ridge and Ocean Island Basalts: Characterization of Mantle Source Reservoirs. Reviews in Mineralogy and Geochemistry 47, 247–317. https://doi.org/10.2138/rmg.2002.47.8

Graham, D.W., Christie, D.M., Harpp, K.S., Lupton, J.E., 1993. Mantle Plume Helium in Submarine Basalts from the Galápagos Platform. Science 262, 2023–2026. https://doi.org/10.1126/science.262.5142.2023

Hanan, null, Graham, null, 1996. Lead and Helium Isotope Evidence from Oceanic Basalts for a Common Deep Source of Mantle Plumes. Science 272, 991–995.

Harðardóttir, S., Halldórsson, S.A., Hilton, D.R., 2018. Spatial distribution of helium isotopes in Icelandic geothermal fluids and volcanic materials with implications for location, upwelling and evolution of the Icelandic mantle plume. Chemical Geology, The noble gases as geochemical tracers – in celebration of Pete Burnard 480, 12–27. https://doi.org/10.1016/j.chemgeo.2017.05.012

Hardarson, B.S., Fitton, J.G., Ellam, R.M., Pringle, M.S., 1997. Rift relocation — A geochemical and geochronological investigation of a palaeo-rift in northwest Iceland. Earth and Planetary Science Letters 153, 181–196. https://doi.org/10.1016/S0012-821X(97)00145-3

Hart, S.R., Gaetani, G.A., 2006. Mantle Pb paradoxes: the sulfide solution. Contrib Mineral Petrol 152, 295–308. https://doi.org/10.1007/s00410-006-0108-1

Hart, S.R., Hauri, E.H., Oschmann, L.A., Whitehead, J.A., 1992. Mantle Plumes and Entrainment: Isotopic Evidence. Science 256, 517–520. https://doi.org/10.1126/science.256.5056.517

Heber, V.S., Brooker, R.A., Kelley, S.P., Wood, B.J., 2007. Crystal–melt partitioning of noble gases (helium, neon, argon, krypton, and xenon) for olivine and clinopyroxene. Geochimica et Cosmochimica Acta 71, 1041–1061. https://doi.org/10.1016/j.gca.2006.11.010

Hervig, R.L., Smith, J.V., Dawson, J.B., 1986. Lherzolite xenoliths in kimberlites and basalts: petrogenetic and crystallochemical significance of some minor and trace elements in olivine, pyroxenes, garnet and spinel. Earth and Environmental Science Transactions of The Royal Society of Edinburgh 77, 181–201. https://doi.org/10.1017/S026359330001083X

Herzberg, C., Asimow, P.D., 2015. PRIMELT3 MEGA.XLSM software for primary magma calculation: Peridotite primary magma MgO contents from the liquidus to the solidus. Geochem. Geophys. Geosyst. 16, 563–578. https://doi.org/10.1002/2014GC005631

Herzberg, C., Asimow, P.D., Ionov, D.A., Vidito, C., Jackson, M.G., Geist, D., 2013. Nickel and helium evidence for melt above the core–mantle boundary. Nature 493, 393–397. https://doi.org/10.1038/nature11771

Herzberg, C., Gazel, E., 2009. Petrological evidence for secular cooling in mantle plumes. Nature 458, 619–622. https://doi.org/10.1038/nature07857

Hilton, D.R., Barling, J., Wheller, G.E., 1995. Effect of shallow-level contamination on the helium isotope systematics of ocean-island lavas. Nature 373, 330. https://doi.org/10.1038/373330a0

Hilton, D.R., Grönvold, K., Macpherson, C.G., Castillo, P.R., 1999. Extreme 3He/4He ratios in northwest Iceland: constraining the common component in mantle plumes. Earth and Planetary Science Letters 173, 53–60. https://doi.org/10.1016/S0012-821X(99)00215-0

Hoernle, K., Rohde, J., Hauff, F., Garbe-Schönberg, D., Homrighausen, S., Werner, R., Morgan, J.P., 2015. How and when plume zonation appeared during the 132 Myr evolution of the Tristan Hotspot. Nat Commun 6, 7799. https://doi.org/10.1038/ncomms8799

Hofmann, A.W., 2003. Sampling Mantle Heterogeneity through Oceanic Basalts: Isotopes and Trace Elements. Treatise on Geochemistry 2, 568. https://doi.org/10.1016/B0-08-043751-6/02123-X

Hofmann, A.W., 1997. Mantle geochemistry: the message from oceanic volcanism. Nature 385, 219. https://doi.org/10.1038/385219a0

Hofmann, A.W., Jochum, K.P., Seufert, M., White, W.M., 1986. Nb and Pb in oceanic basalts: new constraints on mantle evolution. Earth and Planetary Science Letters 79, 33–45. https://doi.org/10.1016/0012-821X(86)90038-5

Hofmann, A.W., White, W.M., 1983. Ba, Rb, and Cs in the Earth's Mantle. Zeitschrift Naturforschung Teil A 38, 256–266. https://doi.org/10.1515/zna-1983-0225

Hole, M.J., Millett, J.M., 2016. Controls of Mantle Potential Temperature and Lithospheric Thickness on Magmatism in the North Atlantic Igneous Province. J Petrology 57, 417–436. https://doi.org/10.1093/petrology/egw014

Holm, P.M., Gill, R.C.O., Pedersen, A.K., Larsen, J.G., Hald, N., Nielsen, T.F.D., Thirlwall, M.F., 1993. The Tertiary picrites of West Greenland: contributions from 'Icelandic' and other sources. Earth and Planetary Science Letters 115, 227–244. https://doi.org/10.1016/0012-821X(93)90224-W

Horan, M.F., Carlson, R.W., Walker, R.J., Jackson, M., Garçon, M., Norman, M., 2018. Tracking Hadean processes in modern basalts with 142-Neodymium. Earth and Planetary Science Letters 484, 184–191. https://doi.org/10.1016/j.epsl.2017.12.017

Jackson, C.R.M., Parman, S.W., Kelley, S.P., Cooper, R.F., 2013. Constraints on light noble gas partitioning at the conditions of spinel-peridotite melting. Earth and Planetary Science Letters 384, 178–187. https://doi.org/10.1016/j.epsl.2013.09.046

Jackson, M.G., 2008. Dismantling the deep earth : geochemical constraints from hotspot lavas for the origin and lengthscales of mantle heterogeneity. Massachusetts Institute of Technology and Woods Hole Oceanographic Institution, Woods Hole, MA. https://doi.org/10.1575/1912/2217

Jackson, M.G., Carlson, R.W., Kurz, M.D., Kempton, P.D., Francis, D., Blusztajn, J., 2010. Evidence for the survival of the oldest terrestrial mantle reservoir. Nature 466, 853–856. https://doi.org/10.1038/nature09287

Jackson, M.G., Hart, S.R., Koppers, A.A.P., Staudigel, H., Konter, J., Blusztajn, J., Kurz, M., Russell, J.A., 2007. The return of subducted continental crust in Samoan lavas. Nature 448, 684–687. https://doi.org/10.1038/nature06048

Jackson, M.G., Konter, J.G., Becker, T.W., 2017. Primordial helium entrained by the hottest mantle plumes. Nature 542, 340–343. https://doi.org/10.1038/nature21023

Jackson, M.G., Shirey, S.B., 2011. Re–Os isotope systematics in Samoan shield lavas and the use of Os-isotopes in olivine phenocrysts to determine primary magmatic compositions. Earth and Planetary Science Letters 312, 91–101. https://doi.org/10.1016/j.epsl.2011.09.046

Jellinek, A.M., Manga, M., 2004. Links Between Long-Lived Hot Spots, Mantle Plumes, D”, and Plate Tectonics. Reviews of Geophysics 42. https://doi.org/10.1029/2003RG000144

Jephcoat, A.P., 1998. Rare-gas solids in the Earth's deep interior. Nature 393, 355–358. https://doi.org/10.1038/30712

Keen, C.E., Dickie, K., Dehler, S.A., 2012. The volcanic margins of the northern Labrador Sea: Insights to the rifting process: VOLCANIC MARGINS, NORTHERN LABRADOR SEA. Tectonics 31, n/a-n/a. https://doi.org/10.1029/2011TC002985

Kent, A.J.R., Stolper, E.M., Francis, D., Woodhead, J., Frei, R., Eiler, J., 2004. Mantle heterogeneity during the formation of the North Atlantic Igneous Province: Constraints from trace element and Sr-Nd-Os-O isotope systematics of Baffin Island picrites: NORTH ATLANTIC IGNEOUS PROVINCE. Geochem. Geophys. Geosyst. 5, n/a-n/a. https://doi.org/10.1029/2004GC000743

King, S.D., Adam, C., 2014. Hotspot swells revisited. Physics of the Earth and Planetary Interiors 235, 66–83. https://doi.org/10.1016/j.pepi.2014.07.006

Klein, E.M., Langmuir, C.H., 1987. Global correlations of ocean ridge basalt chemistry with axial depth and crustal thickness. J. Geophys. Res. 92, 8089. https://doi.org/10.1029/JB092iB08p08089

Köhler, T.P., Brey, G.P., 1990. Calcium exchange between olivine and clinopyroxene calibrated as a geothermobarometer for natural peridotites from 2 to 60 kb with applications. Geochimica et Cosmochimica Acta 54, 2375–2388. https://doi.org/10.1016/0016-7037(90)90226-B

Konter, J.G., Becker, T.W., 2012. Shallow lithospheric contribution to mantle plumes revealed by integrating seismic and geochemical data: SEISMIC AND GEOCHEMICAL CORRELATIONS. Geochem. Geophys. Geosyst. 13, n/a-n/a. https://doi.org/10.1029/2011GC003923

Kruijer, T.S., Kleine, T., 2018. No 182W excess in the Ontong Java Plateau source. Chemical Geology 485, 24–31. https://doi.org/10.1016/j.chemgeo.2018.03.024

Kurz, M.D., 1986. Cosmogenic helium in a terrestrial igneous rock. Nature 320, 435. https://doi.org/10.1038/320435a0

Kurz, M.D., Geist, D., 1999. Dynamics of the Galapagos hotspot from helium isotope geochemistry. Geochimica et Cosmochimica Acta 63, 4139–4156. https://doi.org/10.1016/S0016-7037(99)00314-2

Kurz, M.D., Jenkins, W.J., Hart, S.R., 1982. Helium isotopic systematics of oceanic islands and mantle heterogeneity. Nature 297, 43–47. https://doi.org/10.1038/297043a0

Kurz, M.D., Jenkins, W.J., Hart, S.R., Clague, D., 1983. Helium isotopic variations in volcanic rocks from Loihi Seamount and the Island of Hawaii. Earth and Planetary Science Letters 66, 388–406. https://doi.org/10.1016/0012-821X(83)90154-1

Kurz, M.D., Rowland, S.K., Curtice, J., Saal, A.E., Naumann, T., 2014. Eruption Rates for Fernandina Volcano, in: The Galápagos. American Geophysical Union (AGU), pp. 41–54. https://doi.org/10.1002/9781118852538.ch4

Larsen, L.M., Pedersen, A.K., 2009. Petrology of the Paleocene Picrites and Flood Basalts on Disko and Nuussuaq, West Greenland. Journal of Petrology 50, 1667–1711. https://doi.org/10.1093/petrology/egp048

Larsen, L.M., Pedersen, A.K., 2000. Processes in High-Mg, High-T Magmas: Evidence from Olivine, Chromite and Glass in Palaeogene Picrites from West Greenland. J Petrology 41, 1071–1098. https://doi.org/10.1093/petrology/41.7.1071

Larsen, L.M., Pedersen, A.K., Sundvoll, B., Frei, R., 2003. Alkali Picrites Formed by Melting of Old Metasomatized Lithospheric Mantle: Manˆıtdlat Member, Vaigat Formation, Palaeocene of West Greenland 44, 36.

Lawver, L.A., Müller, R.D., 1994. Iceland hotspot track. Geology 22, 311–314. https://doi.org/10.1130/0091-7613(1994)022<0311:IHT>2.3.CO;2

Lekic, V., Cottaar, S., Dziewonski, A., Romanowicz, B., 2012. Cluster analysis of global lower mantle tomography: A new class of structure and implications for chemical heterogeneity. Earth and Planetary Science Letters 357–358, 68–77. https://doi.org/10.1016/j.epsl.2012.09.014

Li, M., McNamara, A.K., Garnero, E.J., 2014. Chemical complexity of hotspots caused by cycling oceanic crust through mantle reservoirs. Nature Geosci 7, 366–370. https://doi.org/10.1038/ngeo2120

Lightfoot, P.C., Hawkesworth, C.J., Olshefsky, K., Green, T., Doherty, W., Keays, R.R., 1997. Geochemistry of Tertiary tholeiites and picrites from Qeqertarssuaq (Disko Island) and Nuussuaq, West Greenland with implications for the mineral potential of comagmatic intrusions. Contributions to Mineralogy and Petrology 128, 139–163. https://doi.org/10.1007/s004100050300

Loewen, M.W., Graham, D.W., Bindeman, I.N., Lupton, J.E., Garcia, M.O., 2019. Hydrogen isotopes in high 3He/4He submarine basalts: Primordial vs. recycled water and the veil of mantle enrichment. Earth and Planetary Science Letters 508, 62–73. https://doi.org/10.1016/j.epsl.2018.12.012

Macpherson, C., Hilton, D., Day, J., Lowry, D., Gronvold, K., 2005. High-3He/4He, depleted mantle and low-δ18O, recycled oceanic lithosphere in the source of central Iceland magmatism. Earth and Planetary Science Letters 233, 411–427. https://doi.org/10.1016/j.epsl.2005.02.037

Madrigal, P., Gazel, E., Flores, K.E., Bizimis, M., Jicha, B., 2016. Record of massive upwellings from the Pacific large low shear velocity province. Nat Commun 7, 13309. https://doi.org/10.1038/ncomms13309

Marty, B., Upton, B.G.J., Ellam, R.M., 1998. Helium isotopes in early Tertiary basalts, northeast Greenland: Evidence for 58 Ma plume activity in the North Atlantic–Iceland volcanic province. Geology 26, 407–410. https://doi.org/10.1130/0091-7613(1998)026<0407:HIIETB>2.3.CO;2

Mattey, D., Lowry, D., Macpherson, C., 1994. Oxygen isotope composition of mantle peridotite. Earth and Planetary Science Letters 128, 231–241. https://doi.org/10.1016/0012-821X(94)90147-3

McCoy-West, A.J., Fitton, J.G., Pons, M.-L., Inglis, E.C., Williams, H.M., 2018. The Fe and Zn isotope composition of deep mantle source regions: Insights from Baffin Island picrites. Geochimica et Cosmochimica Acta 238, 542–562. https://doi.org/10.1016/j.gca.2018.07.021

McDonough, W.F., Sun, S. -s., 1995. The composition of the Earth. Chemical Geology, Chemical Evolution of the Mantle 120, 223–253. https://doi.org/10.1016/0009-2541(94)00140-4

McDougall, I., Kristjansson, L., Saemundsson, K., 1984. Magnetostratigraphy and geochronology of northwest Iceland. Journal of Geophysical Research: Solid Earth 89, 7029–7060. https://doi.org/10.1029/JB089iB08p07029

McNamara, A.K., 2019. A review of large low shear velocity provinces and ultra low velocity zones. Tectonophysics 760, 199–220. https://doi.org/10.1016/j.tecto.2018.04.015

McNamara, A.K., Garnero, E.J., Rost, S., 2010. Tracking deep mantle reservoirs with ultra-low velocity zones. Earth and Planetary Science Letters 299, 1–9. https://doi.org/10.1016/j.epsl.2010.07.042

Moreira, M., Kanzari, A., Madureira, P., 2012. Helium and neon isotopes in São Miguel island basalts, Azores Archipelago: New constraints on the “low 3He” hotspot origin. Chemical Geology 322–323, 91–98. https://doi.org/10.1016/j.chemgeo.2012.06.014

Mukhopadhyay, S., Parai, R., 2019. Noble Gases: A Record of Earth’s Evolution and Mantle Dynamics. Annu. Rev. Earth Planet. Sci. 47, 389–419. https://doi.org/10.1146/annurev-earth-053018-060238

Mundl, A., Touboul, M., Jackson, M.G., Day, J.M.D., Kurz, M.D., Lekic, V., Helz, R.T., Walker, R.J., 2017. Tungsten-182 heterogeneity in modern ocean island basalts. Science 356, 66–69. https://doi.org/10.1126/science.aal4179

Mundl-Petermeier, A., Walker, R.J., Jackson, M.G., Blichert-Toft, J., Kurz, M.D., Halldórsson, S.A., 2019. Temporal evolution of primordial tungsten-182 and 3He/4He signatures in the Iceland mantle plume. Chemical Geology 525, 245–259. https://doi.org/10.1016/j.chemgeo.2019.07.026

Parman, S.W., Kurz, M.D., Hart, S.R., Grove, T.L., 2005. Helium solubility in olivine and implications for high 3 He/ 4 He in ocean island basalts. Nature 437, 1140. https://doi.org/10.1038/nature04215

Peate, D.W., 2003. The Prinsen af Wales Bjerge Formation Lavas, East Greenland: the Transition from Tholeiitic to Alkalic Magmatism during Palaeogene Continental Break-up. Journal of Petrology 44, 279–304. https://doi.org/10.1093/petrology/44.2.279

Peters, B.J., Carlson, R.W., Day, J.M.D., Horan, M.F., 2018. Hadean silicate differentiation preserved by anomalous 142Nd/144Nd ratios in the Réunion hotspot source. Nature 555, 89–93. https://doi.org/10.1038/nature25754

Pető, M.K., Mukhopadhyay, S., Kelley, K.A., 2013. Heterogeneities from the first 100 million years recorded in deep mantle noble gases from the Northern Lau Back-arc Basin. Earth and Planetary Science Letters 369–370, 13–23. https://doi.org/10.1016/j.epsl.2013.02.012

Porcelli, D., Halliday, A.N., 2001. The core as a possible source of mantle helium. Earth and Planetary Science Letters 192, 45–56. https://doi.org/10.1016/S0012-821X(01)00418-6

Putirka, K., 2008. Excess temperatures at ocean islands: Implications for mantle layering and convection. Geology 36, 283–286. https://doi.org/10.1130/G24615A.1

Putirka, K., Tao, Y., Hari, K.R., Perfit, M.R., Jackson, M.G., Arevalo, R., 2018. The mantle source of thermal plumes: Trace and minor elements in olivine and major oxides of primitive liquids (and why the olivine compositions don't matter). American Mineralogist 103, 1253–1270. https://doi.org/10.2138/am-2018-6192

Putirka, K.D., Perfit, M., Ryerson, F.J., Jackson, M.G., 2007. Ambient and excess mantle temperatures, olivine thermometry, and active vs. passive upwelling. Chemical Geology 241, 177–206. https://doi.org/10.1016/j.chemgeo.2007.01.014

Rizo, H., Andrault, D., Bennett, N.R., Humayun, M., Brandon, A., Vlastelic, I., Moine, B., Poirier, A., Bouhifd, M.A., Murphy, D.T., 2019. 182W evidence for core-mantle interaction in the source of mantle plumes. Geochem. Persp. Let. 6–11. https://doi.org/10.7185/geochemlet.1917

Rizo, H., Walker, R.J., Carlson, R.W., Horan, M.F., Mukhopadhyay, S., Manthos, V., Francis, D., Jackson, M.G., 2016. Preservation of Earth-forming events in the tungsten isotopic composition of modern flood basalts. Science 352, 809–812. https://doi.org/10.1126/science.aad8563

Robillard, I., Francis, D., Ludden, J.N., 1992. The relationship between E- and N-type magmas in the Baffin Bay Lavas. Contr. Mineral. and Petrol. 112, 230–241. https://doi.org/10.1007/BF00310457

Rost, S., Garnero, E.J., Williams, Q., Manga, M., 2005. Seismological constraints on a possible plume root at the core–mantle boundary. Nature 435, 666–669. https://doi.org/10.1038/nature03620

Roth, A.S.G., Liebske, C., Maden, C., Burton, K.W., Schönbächler, M., Busemann, H., 2019. The primordial He budget of the Earth set by percolative core formation in planetesimals. Geochem. Persp. Let. 26–31. https://doi.org/10.7185/geochemlet.1901

Rudnick, R.L., Gao, S., 2003. 3.01 - Composition of the Continental Crust, in: Holland, H.D., Turekian, K.K. (Eds.), Treatise on Geochemistry. Pergamon, Oxford, pp. 1–64. https://doi.org/10.1016/B0-08-043751-6/03016-4

Saal, A., Kurz, M., Hart, S., Blusztajn, J., Blicherttoft, J., Liang, Y., Geist, D., 2007. The role of lithospheric gabbros on the composition of Galapagos lavas. Earth and Planetary Science Letters 257, 391–406. https://doi.org/10.1016/j.epsl.2007.02.040

Samuel, H., Farnetani, C.G., 2003. Thermochemical convection and helium concentrations in mantle plumes. Earth and Planetary Science Letters 207, 39–56. https://doi.org/10.1016/S0012-821X(02)01125-1

Saunders, A.D., Kerr, A.C., Norry, M.J., Kent, R.W., 1997. The North Atlantic Igneous Province. Geophysical Union Monograph, Mahoney, J.J., Coffin, M.F. (Eds.), Large Igneous Provinces 100, 45–93.

Starkey, N.A., Fitton, J.G., Stuart, F.M., Larsen, L.M., 2012. Melt inclusions in olivines from early Iceland plume picrites support high 3He/4He in both enriched and depleted mantle. Chemical Geology 306–307, 54–62. https://doi.org/10.1016/j.chemgeo.2012.02.022

Starkey, N.A., Stuart, F.M., Ellam, R.M., Fitton, J.G., Basu, S., Larsen, L.M., 2009. Helium isotopes in early Iceland plume picrites: Constraints on the composition of high 3He/4He mantle. Earth and Planetary Science Letters 277, 91–100. https://doi.org/10.1016/j.epsl.2008.10.007

St-Onge, M.R., Van Gool, J.A.M., Garde, A.A., Scott, D.J., 2009. Correlation of Archaean and Palaeoproterozoic units between northeastern Canada and western Greenland: constraining the pre-collisional upper plate accretionary history of the Trans-Hudson orogen. Geological Society, London, Special Publications 318, 193–235. https://doi.org/10.1144/SP318.7

Storey, M., Duncan, R.A., Pedersen, A.K., Larsen, L.M., Larsen, H.C., 1998. 40Ar/39Ar geochronology of the West Greenland Tertiary volcanic province. Earth and Planetary Science Letters 160, 569–586. https://doi.org/10.1016/S0012-821X(98)00112-5

Stuart, F.M., Ellam, R.M., Harrop, P.J., Fitton, J.G., Bell, B.R., 2000. Constraints on mantle plumes from the helium isotopic composition of basalts from the British Tertiary Igneous Province. Earth and Planetary Science Letters 177, 273–285. https://doi.org/10.1016/S0012-821X(00)00050-9

Stuart, F.M., Lass-Evans, S., Godfrey Fitton, J., Ellam, R.M., 2003. High 3He/4He ratios in picritic basalts from Baffin Island and the role of a mixed reservoir in mantle plumes. Nature 424, 57–59. https://doi.org/10.1038/nature01711

Tackley, P.J., 2000. Mantle Convection and Plate Tectonics: Toward an Integrated Physical and Chemical Theory. Science 288, 2002–2007. https://doi.org/10.1126/science.288.5473.2002

Trela, J., Gazel, E., Sobolev, A.V., Moore, L., Bizimis, M., Jicha, B., Batanova, V.G., 2017. The hottest lavas of the Phanerozoic and the survival of deep Archaean reservoirs. Nature Geosci 10, 451–456. https://doi.org/10.1038/ngeo2954

Trieloff, M., Kunz, J., Clague, D.A., Harrison, D., Allègre, C.J., 2000. The Nature of Pristine Noble Gases in Mantle Plumes. Science 288, 1036–1038. https://doi.org/10.1126/science.288.5468.1036

Valbracht, P.J., Staudacher, T., Malahoff, A., Allègre, C.J., 1997. Noble gas systematics of deep rift zone glasses from Loihi Seamount, Hawaii. Earth and Planetary Science Letters 150, 399–411. https://doi.org/10.1016/S0012-821X(97)00094-0

Walter, M.J., 1998. Melting of Garnet Peridotite and the Origin of Komatiite and Depleted Lithosphere 39, 32.

Wheeler, J.O., Hoffman, P.F., Card, K.D., Davidson, A., Sandford, B.V., Okulitch, A.V., Roest, W.R., 1996. Geologic Map of Canada, scale 1:5 000 000.

White, W.M., 2015. Isotopes, DUPAL, LLSVPs, and Anekantavada. Chemical Geology 419, 10–28. https://doi.org/10.1016/j.chemgeo.2015.09.026

Williams, C.D., Mukhopadhyay, S., Rudolph, M.L., Romanowicz, B., 2019. Primitive Helium is Sourced from Seismically Slow Regions in the Lowermost Mantle. Geochemistry, Geophysics, Geosystems. https://doi.org/10.1029/2019GC008437

Workman, R.K., Hart, S.R., 2005. Major and trace element composition of the depleted MORB mantle (DMM). Earth and Planetary Science Letters 231, 53–72. https://doi.org/10.1016/j.epsl.2004.12.005

Workman, R.K., Hart, S.R., Jackson, M., Regelous, M., Farley, K.A., Blusztajn, J., Kurz, M., Staudigel, H., 2004. Recycled metasomatized lithosphere as the origin of the Enriched Mantle II (EM2) end-member: Evidence from the Samoan Volcanic Chain. Geochemistry, Geophysics, Geosystems 5. https://doi.org/10.1029/2003GC000623

Yaxley, G.M., Kamenetsky, V.S., Kamenetsky, M., Norman, M.D., Francis, D., 2004. Origins of compositional heterogeneity in olivine-hosted melt inclusions from the Baffin Island picrites. Contrib Mineral Petrol 148, 426–442. https://doi.org/10.1007/s00410-004-0613-z

Zindler, A., Hart, S., 1986. Chemical Geodynamics. Annual Review of Earth and Planetary Sciences 14, 493–571. https://doi.org/10.1146/annurev.ea.14.050186.002425

Appendix

S1. Supplementary Methods

S1.1. Rock preparation, crushing and powdering

Between 20 to 60 g blocks of the freshest interior portion of each sample were cut with a rock saw and sanded with silicon carbide paper to remove any surface contamination. The blocks were then cleaned by sonication in MilliQ H_2O ($\geq$ 18.2 MΩ · cm de-ionized water). The 20 to 60 g rock blocks were crushed and powdered in an agate mill at the GeoAnalytical Lab at Washington State University (WSU) for major and trace element analyses. The agate mill was cleaned with silica between samples to avoid inter-sample contamination. For trace element analyses by ICP-MS, aliquots of powder were dissolved directly in acid in screw-top Teflon PFA vials on a hotplate without use of fusion flux (to reduce blank). For analysis of major (and a subset of trace) elements by X-ray fluorescence (XRF), sample powder was fused with lithium tetraborate to make beads.

For the 11 samples with volcanic glass, 300 mg of pristine glass was separated by hand picking for radiogenic isotopic analyses. For the 7 samples that do not have volcanic glass, additional portions of each sample were crushed with a hammer in a plastic bag and sieved. Between 300-400 mg of (0.5 to 1 mm) rock chips, targeting the freshest portions of the groundmass in the samples, were separated from the lavas for radiogenic isotopic analyses. The rock chips and glass were then cleaned by sonication in MilliQ H_2O. Rock chips were acid leached prior to dissolution, with no powdering step, due to the potential for blank contribution from the powdering apparatus (**Takamasa and Nakai, 2009**).

S1.2. Major and trace element analyses

The concentrations of major elements and select trace elements (Rb, Sr, Zn, Ni, Cr, V, Cu, Ga, Ba, Y, Nb, Zr) were determined by XRF at the WSU Geoanalytical Laboratory. Measurements of SiO_2, Al_2O_3, TiO_2, and P_2O_5 in basalts have a precision of 0.1 – 0.3% (1σ) of the amount present, and 0.4 – 0.7% (1σ) of the amount present for FeO, MgO, CaO, Na_2O, MnO and K_2O **(Johnson et al., 1999**).

Two USGS reference materials, BHVO-2 and BCR-2, were analyzed as unknowns together with the samples in this study. Major element analyses of two separate aliquots of the USGS reference material BCR-2 are within 2% of the preferred values from **Jochum et al. (2016)**, with the exceptions of MgO (within 2.0 to 2.3%), Na_2O (2.3% for one of the aliquots), and P_2O_5 (4 to 5%). For BHVO-2 all major element analyses are within 1% except P_2O_5 (2.5%). A subset of the trace elements (Sr, Zn, Cu, Ga, Ba, Y, V and Rb) measured by XRF on the BCR-2 reference material are within 6% of the preferred measured values from Jochum et al. (2016). Elements that showed somewhat poorer agreement include Ni (9%), Ga (10%), and Cr (21 to 44 %). The BHVO-2 XRF trace element measurements generally showed better agreement with the preferred literature values from **Jochum et al. (2016)**, and are within 2% of the preferred **Jochum et al. (2016)** values, except for Ba (6%), Nb (11%), and Rb (19%).

A suite of trace elements (Cs, Rb, Ba, Th, U, Nb, Ta, La, Ce, Pb, Pr, Nd, Sr, Zr, Hf, Sm, Eu, Gd, Tb, Dy, Ho, Y, Er, Tm, Yb, Lu, Sc) were measured by inductively coupled plasma mass spectrometry (ICP-MS) at WSU and instrumental drift was corrected for using Rh, In, and Re internal standards. **Knaack et al. (1994)** previously reported the precision for trace element analysis using this method. For the BCR-2 and BHVO-2 reference materials analyzed in this study, most trace element concentrations are within 5% of the **Jochum et al.'s (2016)** preferred values for both reference materials (BCR-2 and BHVO-2). Analyses of the remaining trace elements (Cs, Th, U, Ta, Pb, Sm, Eu, Tb, Dy, Ho, and Er) agree to within 12% or better of the published values for both reference materials. Major and trace element data for aliquots of BHVO-2 and BCR-2 reference basalt powders, processed as unknowns with the Baffin Island samples within the same analytical session, are presented in **Table 2**.

S1.3. Olivine major and trace elements

Olivine grains from each sample were picked under a binocular microscope from 500-850 micron crushed whole rock fractions. Grains with visible alteration were avoided. Approximately 10 to 15 different grains from each sample were then placed into epoxy mounts, polished, and carbon coated for electron probe microanalysis on the Cameca SX-100 electron microprobe at the University of California Santa Barbara. Primary standards used were synthetic Mg_2SiO_4 (synthetic forsterite) for Mg, Si; Fe_2SiO_4 (synthetic fayalite) for Fe; MnO synthetic for Mn; Ni_2SiO_4 (synthetic) for Ni; diopside (Chesterman) for Ca; orthoclase MAD-10 for Al; and chromite (UC # 523-9) for Cr. Matrix correction was performed using ZAF or Phi-Rho-Z calculations and the mass absorption coefficients dataset were from FFAST.

S1.4. Helium isotopic analysis

Between 73 to 274 mg of the freshest olivine crystals, selected by visual inspection under a binocular microscope, were separated from the Baffin Island lavas for He isotopic analyses. Analyses were carried out at the Woods Hole Oceanographic Institution in the Isotope Geochemistry Facility following methods presented in **Kurz et al. (2009; 2004)**. Samples were crushed *in vacuo*, and then analyzed on a dual-collection, statically operated He isotope mass spectrometer. Following crushing, powders from several olivine samples (AK-8b, AK-9, and DB-17) were selected for fusion *in vacuo*. The helium released by fusion from the sample with highest crush $^3He/^4He$ ratio (56.6 R_A), AK-9, has relatively high $^3He/^4He$ ratios (36.3 R_A) from fusion; nonetheless, the helium concentration measured by crushing in this sample is low and we do not interpret it to reflect mantle $^3He/^4He$. Sample DB-17, with 31.2 R_A by crushing, as low $^3He/^4He$ from the fusion experiment (6.4 R_A) and does not suggest a cosmogenic ^3He component. Finally, AK-8b (39.9 R_A) was also selected for $^3He/^4He$ analysis by fusion of crushed powders, and the fusion analyses yielded a $^3He/^4He$ of 20.8 R_A which is not consistent with a cosmogenic ^3He being responsible for the elevated $^3He/^4He$ in the crush experiment.

Helium gas concentrations varied from 6.15×10^{-11} to 2.3×10^{-8} cc ^4He STP/g for crush experiments, and in-run precision was ±0.1 to ±1.1 R_A (1σ) on the $^3He/^4He$ measurements. Additionally, two $^3He/^4He$ analyses were made on one sample (AK-13): one by crushing an olivine megacryst (28.8 R_A) and one by crushing multiple smaller olivine crystals (21.5 R_A). Helium isotopic compositions are summarized in **Table 1**.

S1.5. δ^{18}O methods

Oxygen isotopic compositions of olivines from a subset of the Baffin Island lavas in this study (**Table 3**) were analyzed by laser fluorination in the Stable Isotope Laboratory at the University of Oregon. Multiple olivine grains from a single rock sample were pooled for each oxygen isotopic analysis, with total olivine mass analyzed ranging from 0.9 to 1.7 mg. Oxygen isotopic analyses follow the methods described in **Bindeman et al. (2008)**. A 35W CO_2-laser was used, and olivines were reacted with purified BrF_5 to release oxygen. Gases were purified cryogenically using liquid N_2 and by using a Hg-diffusion pump to eliminate traces of F_2 gas formed by fluorination. Oxygen was then converted to CO_2 by reaction with platinum-graphite, and the yields were measured by a baratron gauge (all were at the 12.8 to 13.9 μmols/mg range). Then the CO_2 was analyzed on a MAT 253 mass spectrometer. Internal precision varied from 0.07 to 0.10 ‰ (1 SD). The standards used with these analyses include San Carlos olivine (δ^{18}O = 5.25 ‰), Gore Mt Garnet (UWG2, δ^{18}O = 5.80 ‰, **Valley et al., 1995**) and OUG University of Oregon Garnet (δ^{18}O = 6.52 ‰). Olivines from 13 lavas were analyzed, 11 of which had duplicate or triplicate analyses, where different olivines were selected for the replicate analysis: analyses of different olivine from the same hand sample agree to within 0.01 to 0.28 ‰. δ^{18}O of standards varied 0.01 to 0.14 ‰ over the course of the study, and were used to correct for day-to-day variability and absolute oxygen isotopic compositions on the SMOW scale.

S1.6. Sr, Nd, Hf, and Pb isotopic analyses

Prior to dissolution, all samples were acid leached at the Ecole Normale Supérieure de Lyon (ENS Lyon) following the "light leach" method of **Price et al. (2014)**. Wet chemistry, including sample dissolution and separation of Hf and Pb, follows **Blichert-Toft and Albarède (2009)**. Hf and Pb isotopic compositions were determined using the multi-collector (MC-)ICP-MS Nu Plasma 500 HR housed at ENS Lyon.

Hf isotopic ratios were corrected for mass fractionation assuming an exponential law and assuming a ^{179}Hf/^{177}Hf ratio of 0.7325. ^{173}Yb, ^{175}Lu, ^{181}Ta, and ^{183}W were monitored for isobaric interferences on masses 180 (^{180}W and ^{180}Ta) and 176 (^{176}Lu and ^{176}Yb), but corrections were nominal. The JMC-475 standard was analyzed repeatedly throughout Hf analytical sessions, and always overlap with the preferred value of 0.282163 ± 0.000009 (**Blichert-Toft et al., 1997**); samples were thus not renormalized for offset between measured and preferred $^{176}Hf/^{177}Hf$ values. New Hf-isotopic data are reported in **Table 1**.

Pb isotopic compositions were corrected for mass bias by Tl-addition, assuming an exponential law and a $^{205}Tl/^{203}Tl$ ratio of 2.388; ^{202}Hg was monitored to make the isobaric correction for ^{204}Hg on mass 204. Sample unknowns were corrected for the offset between measured and preferred (from **Eisele et al., 2003**) values for NBS981. External reproducibility is estimated based on repeat analyses of SRM981, and is 100 to 200 ppm for $^{206}Pb/^{204}Pb$, $^{207}Pb/^{204}Pb$, and $^{208}Pb/^{204}Pb$, and 50 ppm for $^{207}Pb/^{206}Pb$ and $^{208}Pb/^{206}Pb$. New Pb-isotopic data are reported in Table 1.

Sr and the rare earth element (REE) fractions were collected from the HBr washes from the Pb chemistry at ENS Lyon described above. The Sr fractions were brought up and dried down in 8N HNO_3 twice to get rid of any residual HBr from Pb extraction. At UCSB, the Sr fractions were brought up and dried down in 8N HNO_3 twice to eliminate any residual HBr from Pb extraction at Lyon. Samples were then brought up in 3N HNO_3 at 120°C for 30 minutes, sonicated for 30 min, and then centrifuged for 4 to 5 minutes. Eichrom Sr-spec columns were made from custom cut and acid-cleaned 1 mL pipette tips each containing ~100 µL of Sr-spec resin (see **Price et al., 2017**). After Sr was collected from the first round of Sr-spec columns, each sample went through its respective Sr-spec column a second time for final collection of Sr. At UCSB, the REE fractions from Lyon were brought up and dried down in 8N HNO_3 twice to eliminate any residual HBr from Pb extraction. Samples were then brought up in 1N HNO_3 at 120°C for 30 minutes, sonicated for 30 min, and then centrifuged for 4 to 5 minutes. Neodymium was separated from the REE fractions using a two-column procedure. First, Eichrom Tru-spec resin was added to custom cut and acid-cleaned 1 mL pipette tips and the REE fractions were passed through the resin and relevant REE fractions were collected (see **Price et al., 2017**). The collected REE fractions were then passed through LN resin column to purify Nd (see **Price et al., 2017).**

Strontium isotopic analyses were performed by thermal ionization mass spectrometry (TIMS) on a Thermo Scientific Triton Plus™ Multicollector Thermal Ionization Mass

Spectrometer at the University of California Santa Barbara (UCSB). Approximately 500 ng of Sr (dissolved in 3 N HNO_3) was loaded with TaCl ion emitter onto zone refined Re filaments (99.999% pure, from H Cross USA) using a parafilm dam to control for sample location on the filament. The NBS987 Sr standard was measured every 3-4 samples during each of three analytical sessions. Analyses used 10^{11} Ω resistors in the amplifier feedback loop, with a 3.3 picoamp gainboard, and typical beam intensities were 4 V (on 10^{11} Ω resistors) on mass 88. Analyses consisted of ~75 minutes of analysis (21 minutes of which consisted of baseline measurements), with amplifier gains analyzed every three or four samples. Amplifier rotation was used for all analyses, and baselines were taken before each block (where five blocks constitute a full rotation of the amplifiers). The average $^{87}Sr/^{86}Sr$ value of the NBS987 Sr standards during the first analytical session was 0.710246 ± 0.000008 (2SD, N=4), 0.710248 ± 0.000013 (2SD, N=5) for the second analytical session, and 0.710248 ± 0.000013 (2SD, N=2) for the third analytical session. The measured $^{87}Sr/^{86}Sr$ ratios for all samples and USGS reference materials are corrected for the offset between preferred (0.710240) and measured $^{87}Sr/^{86}Sr$ values for NBS987 within each analytical session (i.e., a single barrel). The $^{88}Sr/^{86}Sr$ ratio was used to correct for mass fractionation using the exponential law and assuming a canonical $^{86}Sr/^{88}Sr$ ratio of 0.1194. Interference correction for ^{87}Rb was nominal and was performed by measuring ^{85}Rb and assuming a canonical ratio of $^{87}Rb/^{85}Rb$ = 0.386. At least one of two USGS reference materials (AGV-2 and BCR-2) was run with each analytical session, processed with Baffin Island sample unknowns through column chemistry at UCSB. After correction to the preferred NBS987 value, the average measured $^{87}Sr/^{86}Sr$ for AGV-2 was 0.703968 (± 0.000007 2SD, N=3) and for BCR-2 was 0.705000 (± 0.000005 2SE, N=1) (Table 2). The AGV-2 and BCR-2 yielded $^{87}Sr/^{88}Sr$ ratios within error of values reported by Weis et al. (2006): 0.703973 ± 0.000010 (2SD, N=10) and 0.705005 ± 0.000011 (2SD, N=13), respectively, after renormalization of their data to the preferred NBS987 values used here. The total Sr procedural blanks were <60 pg.

Neodymium isotopic compositions were also run by TIMS at UCSB. Approximately 200 ng of Nd, dissolved in 1N HNO_3, was loaded onto zone refined Re filaments (99.999% pure, from H Cross USA) using a parafilm dam. Analyses used 10^{11} Ω resistors in the feedback loop of the amplifiers, with a 3.3 picoamp gainboard, and typical beam intensities were 2.5 V (on 10^{11} Ω resistors) on mass 144. Analyses were typically ~75 minutes (21 minutes of which consisted of baseline measurements), with amplifier gains measured every three or four samples. Amplifier rotation was used for all analyses, and baselines were taken before each block (where five blocks constitute a full rotation of the amplifiers). Isotopic compositions were corrected for instrumental mass fractionation relative to $^{146}Nd/^{144}Nd$ of 0.7219 using the exponential law. Multiple JNdi Nd standards were run during each of four analytical sessions (i.e., where each analytical session consists of a single barrel) and gave the following averages: $^{143}Nd/^{144}Nd$ of 0.512100 ± 0.000004 (2SD, N=5); $^{143}Nd/^{144}Nd$ of 0.512100 ± 0.000005 (2SD, N=4); $^{143}Nd/^{144}Nd$ of 0.512101 ± 0.000005 (2SD, N=6); and $^{143}Nd/^{144}Nd$ of 0.512098 ± 0.000005 (2SD, N=2). The measured $^{143}Nd/^{144}Nd$ ratios for all USGS reference materials and unknowns are corrected for the offset between the measured and the preferred JNdi $^{143}Nd/^{144}Nd$ of 0.512099 (**Garçon et al., 2018**). The total procedural Nd blank was <5 pg. Interference correction for ^{144}Sm on ^{144}Nd was negligible, and was performed by measuring ^{147}Sm. Aliquots of the USGS reference material, BCR-2, were processed with unknowns through column chemistry at UCSB and run during each TIMS analytical session. Following renormalization to the preferred JNdi value within each analytical session, the average measured $^{143}Nd/^{144}Nd$ for BCR-2 was 0.512623±0.000006 (2SD, N=4) (Table 2). The average BCR-2 value from Weis et al. (2006) is 0.512618 ± 0.000012 (2SD, N=11) (after renormalizing their data to the preferred JNdi reference frame using the La Jolla to JNdi conversion of 1.000503 from **Tanaka et al. [2000]**).

S2. Supplementary Discussion

S2.1. Modelled crustal assimilation scenarios

A goal of this modelling exercise to evaluate whether the Baffin Island and high $^3He/^4He$ Iceland mantle sources have different Pb-isotopic compositions, or whether the difference in their Pb-isotopic compositions is the result of continental crust to an Iceland-like high $^3He/^4He$ endmember to generate the Pb-isotopic compositions in the least contaminated Baffin Island lavas. Selecting the most representative basement composition for this test is challenging because the Pb isotopic compositions of the basement samples envelop the Baffin Island-West Greenland field (**Figure 9**), making it difficult to discern the direction of a contamination trend in Pb-isotopic space. Additionally, no single available basement sample can be mixed with the highest $^{3}He/^{4}He$ Iceland lava composition to produce the Pb isotopic compositions of the least crustally-contaminated Baffin Island lavas. However, after many iterations of modelling individual and combined basement compositions, we find that combining basement samples 177375 (Karrat Group gneiss) and 113450 (Nordfjord shale), combined in equal proportions by mass, yields a successful crustal endmember composition. That is, the Pb isotopic composition of this crustal compositions, when mixed with the highest $^{3}He/^{4}He$ Iceland lava, can successfully generate the $^{206}Pb/^{204}Pb$, $^{207}Pb/^{204}Pb$, and $^{208}Pb/^{204}Pb$ isotopic compositions of the least crustally-contaminated Baffin Island lavas with 3% continental crust contribution; see black mixing line in **Supplementary Figure 4**). At face value, this would imply that the difference between Baffin Island and Iceland high $^{3}He/^{4}He$ lavas is simply the result of 3% addition of continental crust to an Iceland-like high $^{3}He/^{4}He$ endmember. However, there are geochemical consequences for this mixing scenario that make it untenable. For example, the hypothetical mixture of basement (3%) and high-$^{3}He/^{4}He$ Iceland lava (97%) yields a Ce/Pb of 11.0 and a Nb/Th of 8.7, values that are far lower than the Ce/Pb and Nb/Th ratios in the four least crustally-contaminated Baffin Island lavas in this study (21.7 to 24.1 and 13.3 to 13.9, respectively). Additionally, this mixing scenario fails for Sr and Nd isotopes because it predicts higher $^{87}Sr/^{86}Sr$ and lower $^{143}Nd/^{144}Nd$ than observed in the four least contaminated Baffin Island lavas.

To solve the problems associated with $^{87}Sr/^{86}Sr$ and $^{143}Nd/^{144}Nd$ in the mixing model above, we develop a hypothetical uncontaminated Baffin Island endmember with lower $^{87}Sr/^{86}Sr$ and higher $^{143}Nd/^{144}Nd$. Therefore, we explore a mixing scenario where the hypothetical uncontaminated Baffin Island endmember has Pb isotopic compositions like the highest $^{3}He/^{4}He$ Iceland lava, but with lower $^{87}Sr/^{86}Sr$ and higher $^{143}Nd/^{144}Nd$, such that a mixture of this composition with basement will generate the observed Sr, Nd, and Pb isotopic compositions in the least contaminated Baffin Island lavas (see blue mixing line in **Supplementary Figure 4**). In order for the hypothetical uncontaminated Baffin Island melt with Iceland-like Pb isotopes to acquire, through crustal assimilation, the $^{87}Sr/^{86}Sr$, $^{143}Nd/^{144}Nd$ and Pb-isotopic compositions observed in the least contaminated Baffin Island lavas, the $^{143}Nd/^{144}Nd$ must be relatively high (approximately 0.5134) and the $^{87}Sr/^{86}Sr$ must be very low (approximately 0.7025) (where the Sr and Nd isotopic compositions are chosen to “force” the model to successfully capture the Sr, Nd, and Pb isotopic compositions of the least contaminated Baffin Island lavas measured in this study; see blue mixing line in **Supplementary Figure 4**). The successful model requires ~3% continental crust, but this also results in Ce/Pb (11.0) and Nb/Th (8.7) ratios in the hypothetical mixture that are much lower than observed in the least contaminated Baffin lavas (21.7 to 24.1 and 13.3 to 13.9, respectively). Thus, an important conclusion of this modelling exercise is that, even if we design a hypothetical uncontaminated Baffin Island endmember that will force the mixing model (i.e., mix continental crust with hypothetical uncontaminated Baffin Island lavas) to generate the Sr, Nd, and Pb radiogenic isotopic compositions measured in the least crustally-contaminated Baffin Island lavas, such a mixing scenario can be rejected because the resulting Ce/Pb and Nb/Th ratios in the mixture are much lower than observed in these four lavas. We find this result to be true for a range of continental crust compositions, owing to the high concentrations of Pb and Th, and low Ce/Pb and Nb/Th, in continental crust compared to the lavas: even small quantities of continental crust in Baffin Island lavas quantitatively reduce the Ce/Pb and Nb/Th ratios in crustally contaminated lavas. We cannot generate the Sr, Nd, and Pb isotopic composition of the least contaminated Baffin Island lavas by mixing the Iceland high $^{3}He/^{4}He$ component with continental crust, the implication being that the Baffin Island source has distinct Sr, Nd, and Pb isotopic compositions from the Iceland high $^{3}He/^{4}He$ mantle. Indeed, the four least contaminated Baffin Island lavas are likely to have Sr, Nd, and Pb isotopic compositions very close to their original uncontaminated compositions.

S2.2. Signals from ^{142}Nd

The ^{146}Sm–^{142}Nd decay system is another short-lived isotopic system that has produced isotopic anomalies in modern mantle-derived rocks **(Horan et al., 2018; Peters et al., 2018**). ^{146}Sm has a half-life of 103 Ma, and therefore was extant for only ~500 million years following Solar System formation. Due to the lithophile nature of Sm and Nd (assuming the core is not highly enriched in sulfur; **Kiseeva and Wood, 2015**), the presence of ^{142}Nd anomalies in modern plume-derived lavas would record the preservation of an early silicate differentiation event. Pairing of ^{182}W and ^{142}Nd can provide additional constraints on the timing and processes that produced Hadean signatures preserved in hotspot lavas. However, Baffin Island lavas from two studies do not show resolvable $\mu^{142}Nd$ differences from the terrestrial standard: **de Leeuw et al. (2017)** measure an average $\mu^{142}Nd$ of −1.4 ± 6.3 ppm (2SD, N = 15), and (**Rizo et al.,**

2016) measured an average μ^{142}Nd of 4.0 ± 5.4 ppm (2SD, *N* = 7) (where $\mu^{142}Nd = 10^6 \times [^{142}Nd/^{144}Nd_{sample} - {}^{142}Nd/^{144}Nd_{terrestrial\ standard}]/^{142}Nd/^{144}Nd_{terrestrial\ standard}$, and the terrestrial standard is JNdi). Furthermore, **Andreasen et al. (2008)** and **Debaille et al. (2007)** did not identify resolvable μ^{142}Nd anomalies in lavas from Iceland, including mid-Miocene lavas. A question that arises is whether the Iceland lavas with μ^{182}W anomalies have μ^{142}Nd anomalies: while **Andreasen et al. (2008)** did not identify μ^{142}Nd anomalies in Iceland lavas, none of the Iceland samples containing μ^{182}W anomalies (**Mundl et al., 2017; Mundl-Petermeier et al., 2019**) were analyzed for μ^{142}Nd (and none of Iceland lavas analyzed for high-precision ^{142}Nd/^{144}Nd have been characterized for ^{3}He/^{4}He).

Nonetheless, it is important to use the lack of resolvable ^{142}Nd/^{144}Nd anomalies as a constraint for any model for the origin of the Baffin Island mantle source. The least crustally-contaminated Baffin Island lavas have superchondritic ^{143}Nd/^{144}Nd (ε^{143}Nd = + 9.0 to 9.7) and primitive Pb isotopic compositions that fall on the 4.50 Ga Geochron, and the Pb isotopic compositions are consistent with an early (~4.50 Ga) differentiation event that fractionated U from Pb. If U/Pb fractionation resulted from silicate differentiation, then silicate melt extraction from the mantle at 4.50 Ga would also have been expected to produce superchondritic Sm/Nd responsible for the positive (geochemically depleted) ε^{143}Nd in the residual mantle that became the source of Baffin Island mantle, and the superchondritic Sm/Nd would generate anomalously high ^{142}Nd/^{144}Nd (because differentiation occurred during the lifetime of ^{146}Sm). But no ^{142}Nd anomalies are observed in Baffin lavas.

However, it is possible that the ^{142}Nd/^{144}Nd in the Icelandic plume source is distinct from the ambient upper mantle, but has been overprinted by mixing with upper mantle. The Iceland plume first erupted at Baffin Island and West Greenland in a rift environment as the Labrador Sea was spreading in the Late Cretaceous (**Keen et al., 2012**). Therefore, if a high ^{3}He/^{4}He mantle sampled by the Iceland plume interacted with local DMM (μ^{142}Nd = 0) in the rifting environment, then plume's ^{142}Nd anomaly could be greatly attenuated by mixing (**de Leeuw et al., 2017**). For example, if the Baffin Island lavas represent a mixture of the moderately high-^{3}He/^{4}He plume mantle like that found in Reunion (μ^{142}Nd = 7.0 ± 1.9) and DMM (μ^{142}Nd = 0), then mixing of these two reservoirs in 25:75 (Reunion:DMM) mixture would yield ^{142}Nd/^{144}Nd (μ^{142}Nd = 2.9) indistinguishable from the terrestrial standard, assuming Nd concentrations for the two mantle sources of 1.25 ppm and 0.581 ppm, respectively (**McDonough and Sun, 1995; Workman and Hart, 2005)**. This result is consistent with the lack of resolvable $^{142}Nd/^{144}Nd$ in Baffin Island lavas. In this mixing scenario, the high-$^{3}He/^{4}He$ signature of the mixture (i.e., like that in the least crustally contaminated Baffin lavas) is not significantly overprinted by low $^{3}He/^{4}He$ of DMM if the plume mantle has at least ten times higher concentration of He compared to the DMM (e.g., **de Leeuw et al., 2017**) and the plume has a $^{3}He/^{4}He$ of 50 R_A and DMM is 8 R_A. For example, in the 25:75 mixing scenario, the $^{3}He/^{4}He$ of the mixture is 40.3 R_A (or 48.8 R_A) if the plume mixing endmember has 10 (or 100) times higher helium concentrations than the depleted upper mantle. If the $^{3}He/^{4}He$ of the plume is higher than 50 R_A, then achieving even higher $^{3}He/^{4}He$ in the mixture is feasible at even lower mixing proportions of the plume endmember.

Another possible model for Baffin Island lavas having $^{142}Nd/^{144}Nd$ similar to the terrestrial standard is discussed in **de Leeuw et al (2017)**, who suggest that some, but not all (**Bouvier and Boyet, 2016**), of the $^{142}Nd/^{144}Nd$ difference between Earth and chondrites may still be attributed to ^{146}Sm decay in the early Earth's mantle. The Earth and enstatite chondrites appear to have the same nucleosynthetic mix for several elements including oxygen, Cr and Ti, but the $^{142}Nd/^{144}Nd$ of the accessible Earth is on the order of 8 to 10 ppm higher than the average measured for enstatite chondrites (**Burkhardt et al., 2016; Gannoun et al., 2011**). This difference in $^{142}Nd/^{144}Nd$ of the accessible Earth relative to enstatite chondrites could be the result of superchondritic Sm/Nd in the accessible Earth. For example, if we assume that the accessible Earth has $^{142}Nd/^{144}Nd$ that is 8 ppm higher than bulk Earth with enstatite chondrite-like $^{142}Nd/^{144}Nd$, then global differentiation of the silicate Earth at 4.4 Ga to from an incompatible element depleted reservoir with superchondritic Sm/Nd ($^{147}Sm/^{144}Nd$ = 0.2123) would yield $\mu^{142}Nd$ = 0 and a modern "PREMA-like" $^{143}Nd/^{144}Nd$ = 0.513105. These $\mu^{142}Nd$ and $^{143}Nd/^{144}Nd$ compositions match Baffin Island lavas (and, in particular, the $^{143}Nd/^{144}Nd$ of the least crustally contaminated lavas). In other words, if the bulk-Earth has $\mu^{142}Nd$ = -8, then $\mu^{142}Nd$ = 0 reflects an early-formed depleted mantle source that also would have superchondritic $^{143}Nd/^{144}Nd$ today. Global-scale differentiation of the Earth could be caused by a Moon-forming impact, which may have occurred as late as 4.4 Ga (e.g., **Carlson, 2019**). This leaves open the interpretation of **Jackson et al. (2010)** and **Jackson and Carlson, (2011)**, with the only difference being that the early differentiation event is no longer limited to the first 30 Ma following terrestrial accretion by the assumption that the bulk-Earth has μ^{142}Nd = -20, as would be the case if it had the same isotopic composition as ordinary chondrites, but instead can be pushed to later times following terrestrial accretion using an enstatite chondrite composition. The lack of correlation of ^{142}Nd/^{144}Nd and ^{182}W/^{184}W in high ^{3}He/^{4}He lavas is most easily explained if the event that fractionated Sm/Nd occurred after ^{182}Hf was dead as Hf/W also would be expected to fractionate during a magma ocean scenario. Additionally, ocean island basalts with reported μ^{142}Nd anomalies (i.e., μ^{142}Nd > 0 or μ^{142}Nd < 0), like those at Reunion (**Peters et al., 2018**), may reflect the range of Sm/Nd ratios in different reservoirs produced by the global differentiation event.

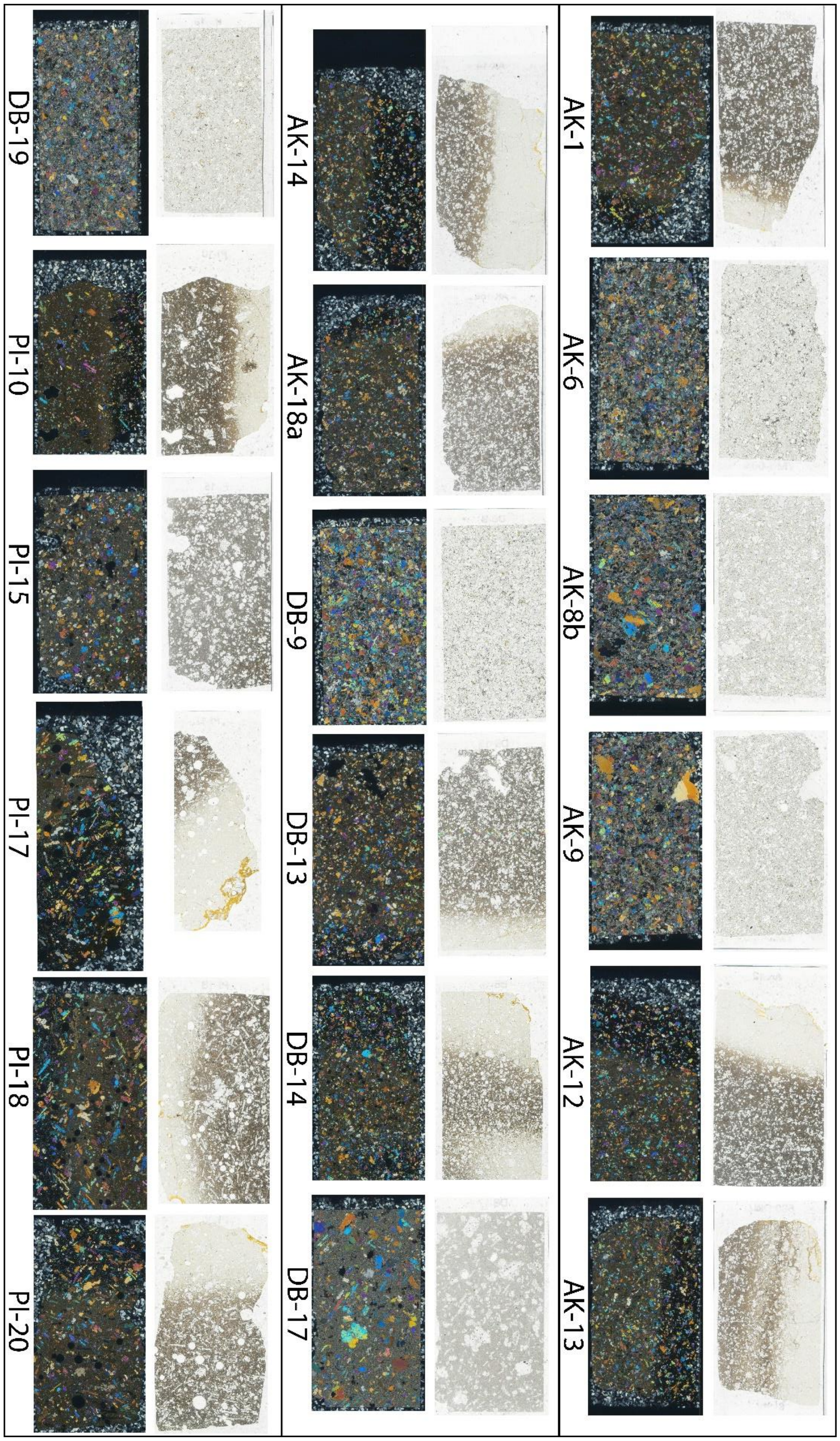

Figure S1. Thin sections (1" x 1 7/8") of the eighteen new Baffin Island lavas in this study are shown in plain polarized light and cross polarized light. Glassy margins are visible in a number of samples including: AK-8b, AK-12, AK-13, AK-14, AK-18a, DB-13, DB-14, PI-10, PI-17, PI-18, PI-20.

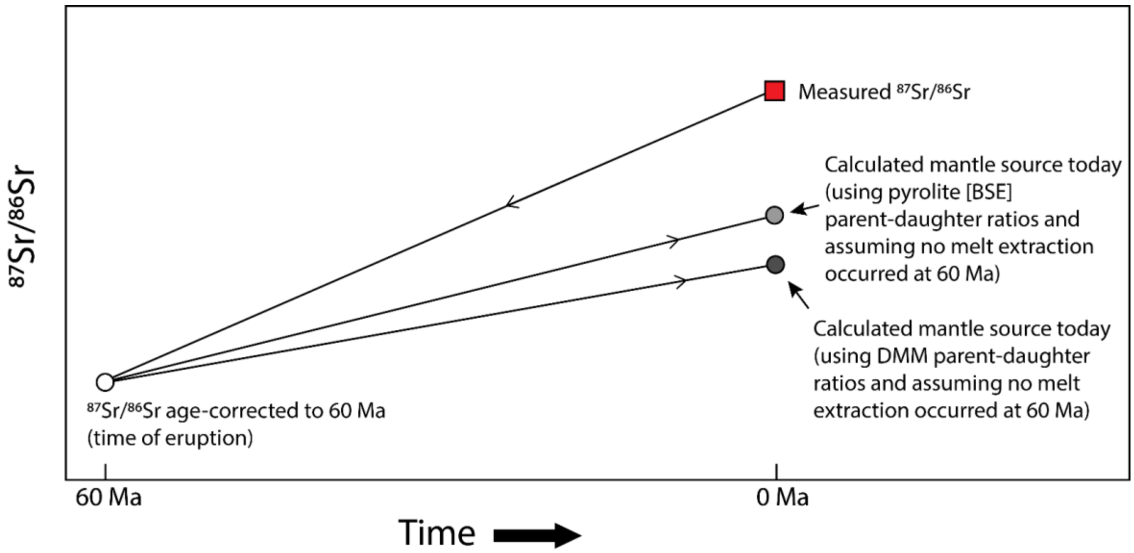

Figure S2. A schematic diagram illustrating the relationship between the measured $^{87}Sr/^{86}Sr$, age-corrected (to 60 Ma) $^{87}Sr/^{86}Sr$, and calculated present-day mantle source $^{87}Sr/^{86}Sr$. The age-corrected $^{87}Sr/^{86}Sr$ is calculated using the measured Rb/Sr and isotopic composition of the Baffin Island lavas and an eruption age of 60 Ma. In order to calculate the Baffin mantle source today, the age-corrected $^{87}Sr/^{86}Sr$ at 60 Ma is taken to be the starting mantle source composition. Assuming this mantle source did not undergo melt extraction at 60 Ma to generate Baffin Island lavas, the age-corrected $^{87}Sr/^{86}Sr$ is then "forward aged" from 60 Ma to 0 Ma using two different mantle source compositions: For a depleted mantle scenario, the Rb/Sr from DMM (Workman and Hart, 2005) is used to calculate what the $^{87}Sr/^{86}Sr$ of the Baffin mantle source today would be if it had not experienced melt extraction at 60 Ma; for a primitive mantle scenario, the Rb/Sr from pyrolite (McDonough and Sun, 1995) is used to calculate the $^{87}Sr/^{86}Sr$ of the Baffin mantle source today (**see Section 3.3 of the text**). Of course, the Rb/Sr ratio of the Baffin Island mantle source is unknown, but the range of source trace element compositions captured by DMM and pyrolite provide upper and lower limits on the possible range of the time evolution of radiogenic isotopic compositions of the Baffin Island mantle source. This is because the Baffin Island source is clearly more geochemically depleted than pyrolite (as evidenced by Sr, Nd, and Hf isotopic compositions in Baffin lavas), but not more depleted than DMM (again, as evidenced by the same radiogenic isotopic compositions).

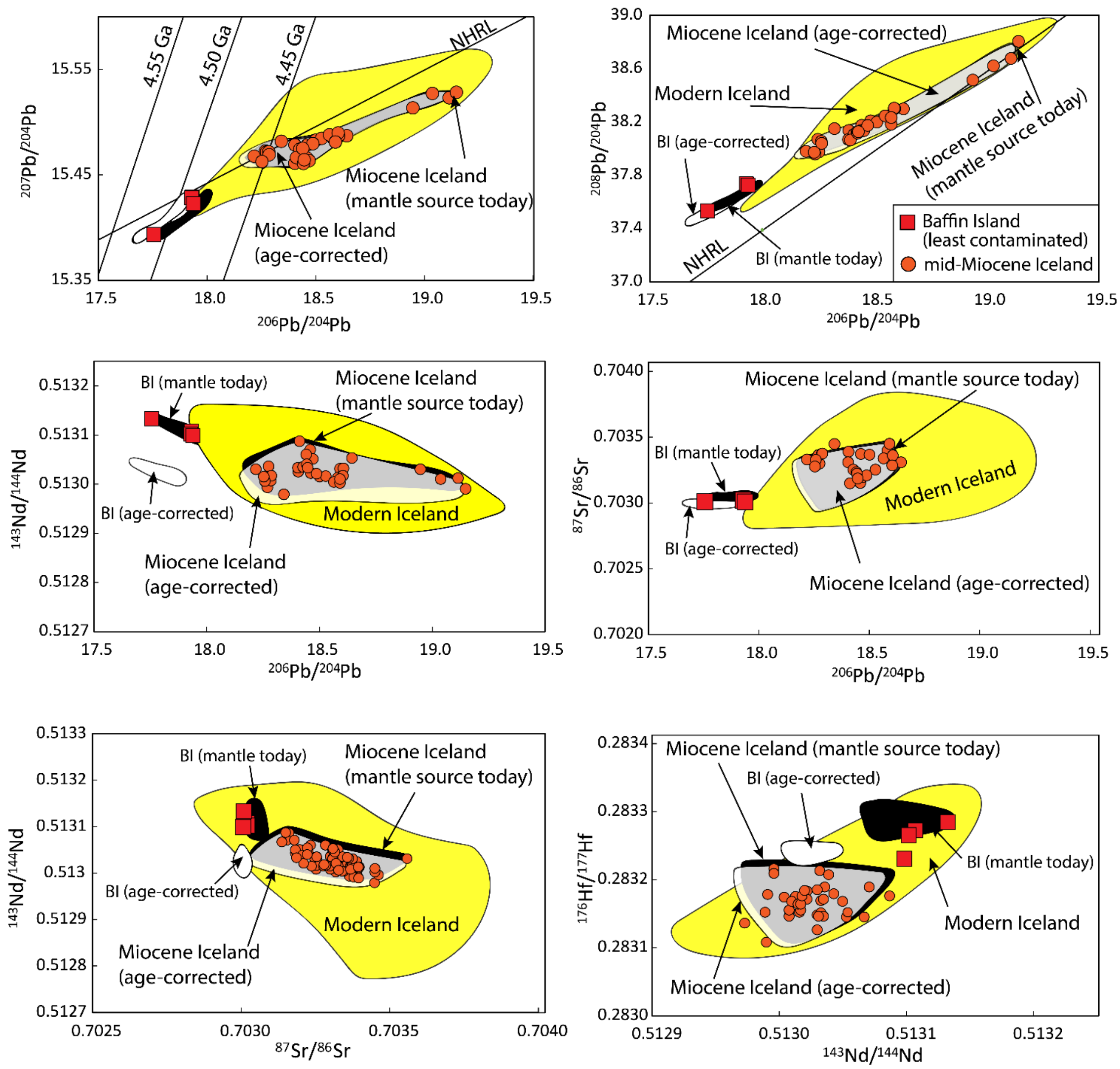

Figure S3. The measured isotopic ratios for Baffin Island (BI, red squares), and Miocene Iceland (orange circles), are shown with the field for their respective age-corrected data (white fields) and range of calculated mantle sources today (black fields). In all isotopic spaces, there is overlap between the measured ratios and the range of "calculated mantle today" ratios. Use of either measured or calculated present day radiogenic isotopic compositions for Baffin Island lavas does not change the conclusions of this study (**see Section 4.4 of the text**), but we argue that age-corrected radiogenic isotopic compositions of Baffin Island lavas are difficult to meaningfully compare to radiogenic isotopic compositions in modern Iceland lavas. For Miocene to modern Iceland lavas, the offset among measured, age-corrected, and calculated mantle source today compositions is insignificant.

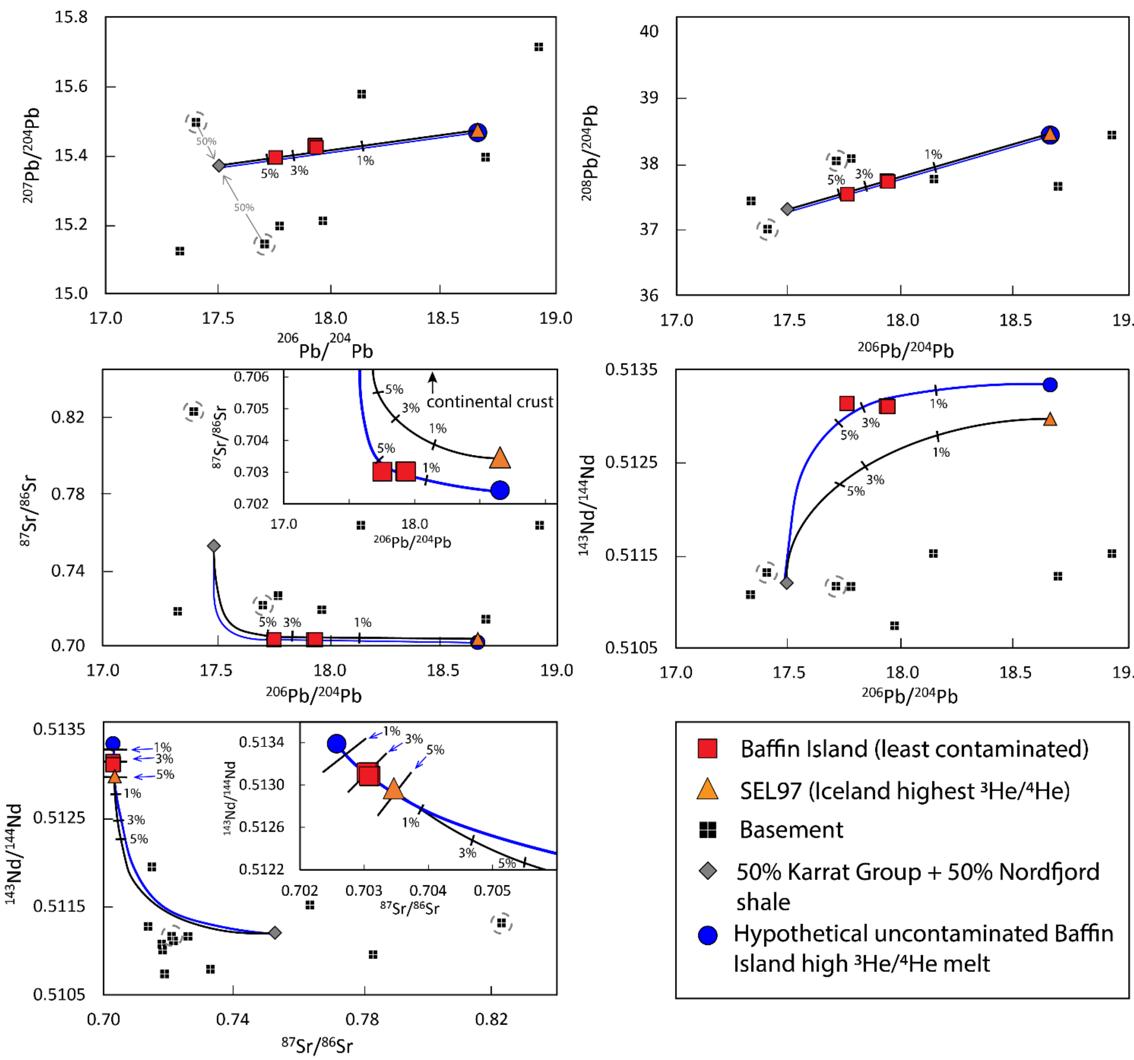

Figure S4. Two mixing models are shown here (**see Section 5.1 of the text**). The basement endmember is a mixture of 50% Karrat Group gneiss sample 177375 combined with 50% Nordfjord shale sample 113450 (radiogenic isotopic compositions and trace element concentrations are in **Larsen and Pedersen, 2009**). The two basement samples that are mixed are outlined in dashed grey circles. Black lines show the mixing scenario between the basement endmember and the highest $^{3}He/^{4}He$ lava from Iceland that has measured Sr-Nd-Pb isotopic compositions (SEL97). The isotopic compositions for SEL97 can be found in **Hilton et al. (1999)** and trace element concentrations are reported in **Jackson et al. (2008)**. While the Pb isotopic compositions of the least crustally contaminated Baffin Island lavas can be generated by assimilation of ~3% of the basement endmember into an Iceland high $^{3}He/^{4}He$ melt, the mixing model fails to capture the Baffin Island lavas in Sr-Pb, Nd-Pb, or Sr-Nd isotopic spaces. Therefore, blue lines show the mixing scenario between the basement and a hypothetical uncontaminated Baffin Island high $^{3}He/^{4}He$ melt that, while unlike any measured Baffin Island lava, is designed (to have lower $^{87}Sr/^{86}Sr$ and higher $^{143}Nd/^{144}Nd$) to make a successful mixing model such that a mixture of this composition with basement will generate observed isotopic compositions in the least contaminated Baffin Island lavas (**see Section 5.1 of the text**): the Pb isotopic composition of the hypothetical uncontaminated melt is the same as that in SEL97, but the $^{87}Sr/^{86}Sr$ and $^{143}Nd/^{144}Nd$ ratios of the hypothetical uncontaminated Baffin Island high $^{3}He/^{4}He$ end member are 0.7025 and 0.5134, respectively (where values are chosen to generate a successful isotopic mixing model). In order for the hypothetical uncontaminated melt mixing model to generate the least crustally contaminated Baffin Island compositions in all isotope spaces (i.e., blue line), the Sr concentration required for the hypothetical uncontaminated melt is 400 ppm, and the Nd concentration required is 15 ppm. The blue line shows that mixing the hypothetical uncontaminated Baffin melt with ~3% of the basement endmember can generate all of the radiogenic isotopic compositions observed in least crustally contaminated Baffin Island lavas. However, the Ce/Pb and Nb/Th of the mixture would be much lower (~11 and ~9, respectively) than observed in the least crustally contaminated Baffin Island lavas (21.7 to 24.1 and 13.3 to 13.9, respectively), allowing us to reject such a model.

Supplementary Table 1: Baffin Island sample notes

Sample no.	Name		Easting	Northing	Elevation (m)
Akpak Point	NTS: 16K/13/14, NAD 27, UTM Zone 20				
AK-1	Pillow Fragment	lower pillows	554821	7423575	80
AK-6	Beach Stone - Flow Interior		554975	7424264	1
AK-8b	Flow Interior	summit Flow	553724	7422689	895
AK-9	Flow Interior		553468	7422641	860
AK-12	Pillow Fragment	lower pillows	554924	7424118	
AK-13	Pillow Fragment	lower pillows	554924	7424118	
AK-14	Pillow Fragment	lower pillows	554924	7424118	
AK-18a	Pillow Fragment	lower pillows	554924	7424118	
Durban Island	NTS: 16 M/1 & N/4, NAD 27, UTM Zone 20				
DB-9	Flow Base		533580	7440411	345
DB-13	Pillow Fragment	upper pillows	533409	7440566	435
DB-14	Pillow Fragment	upper pillows	533409	7440566	435
DB-17	Flow Base	second subaerial flow	533409	7440566	460
DB-19	Flow Interior		536577	7441613	625
Padloping Island	NTS: 16 M/1 & N/4, NAD 27, UTM Zone 20				
PI-10	Pillow Fragment	lowermost pillows	524244	7451382	25
PI-15	Pillow Fragment	upper pillows	523777	7450813	340
PI-17	Pillow Fragment	upper pillows	523777	7450813	340
PI-18	Pillow Fragment	upper pillows	523777	7450813	340
PI-20	Pillow Fragment	upper pillows	523777	7450813	340

Table S1.

1. All the exposures are remnants of flat lying successions of lavas exposed as cliffs along the coast.
2. Elevation is thus equivalent to stratigraphic position at any one of the three sampling sites (i.e., Akpat Point, Durban Island, Padloping Island), but cannot be used for cross comparison between sampling sites.
3. The samples without elevations (AK-12, 13, 14 and 18a) were collected on the beach from large blocks that had fallen from the cliff.

Supplementary Table 2: Major and trace oxide compositions of olivines measured by electron probe microanalysis.

Sample	NiO	MnO	SiO_2	MgO	FeO	Al_2O_3	Cr_2O_3	CaO	TOTAL	Fo#
AK-1	0.33	0.19	40.43	46.67	12.18	0.04	0.06	0.32	100.21	87.2
AK-1	0.32	0.20	40.37	46.65	12.23	0.08	0.07	0.33	100.25	87.2
AK-1	0.33	0.18	40.37	46.55	12.23	0.04	0.06	0.32	100.10	87.2
AK-1	0.34	0.19	40.32	46.58	12.25	0.06	0.07	0.34	100.13	87.1
AK-1	0.33	0.19	40.37	46.65	12.27	0.05	0.06	0.32	100.24	87.1
AK-1	0.33	0.19	40.41	46.79	12.31	0.05	0.06	0.33	100.48	87.1
AK-1	0.33	0.20	40.18	46.53	12.25	0.06	0.06	0.33	99.94	87.1
AK-1	0.34	0.19	40.27	46.69	12.30	0.05	0.07	0.33	100.24	87.1
AK-1	0.33	0.18	40.13	46.43	12.26	0.12	0.12	0.33	99.91	87.1
AK-1	0.33	0.19	40.34	46.76	12.36	0.05	0.06	0.34	100.42	87.1
AK-1	0.33	0.20	40.16	46.49	12.31	0.08	0.08	0.34	99.99	87.1
AK-1	0.34	0.18	40.31	46.64	12.35	0.09	0.07	0.33	100.32	87.1
AK-1	0.34	0.19	40.23	46.51	12.32	0.07	0.07	0.34	100.06	87.1
AK-1	0.33	0.19	40.33	46.69	12.38	0.05	0.06	0.32	100.35	87.1
AK-1	0.33	0.19	40.33	46.71	12.39	0.05	0.07	0.33	100.41	87.0
AK-1	0.31	0.19	40.34	46.58	12.36	0.08	0.07	0.33	100.27	87.0
AK-1	0.34	0.20	40.15	46.49	12.38	0.06	0.06	0.34	100.02	87.0
AK-1	0.33	0.18	40.29	46.59	12.43	0.05	0.06	0.33	100.27	87.0
AK-1	0.34	0.20	40.28	46.62	12.44	0.05	0.07	0.33	100.33	87.0
AK-1	0.32	0.19	40.26	46.56	12.43	0.09	0.07	0.33	100.26	87.0
AK-1	0.34	0.18	40.29	46.41	12.41	0.04	0.06	0.33	100.06	87.0
AK-1	0.33	0.19	40.21	46.42	12.47	0.08	0.09	0.32	100.11	86.9
AK-1	0.34	0.20	40.29	46.46	12.50	0.07	0.06	0.33	100.25	86.9
AK-1	0.32	0.20	40.13	46.15	12.59	0.07	0.09	0.32	99.86	86.7
AK-1	0.32	0.20	40.30	46.28	12.64	0.05	0.07	0.32	100.18	86.7
AK-1	0.32	0.20	40.00	46.21	12.68	0.09	0.08	0.33	99.92	86.7
AK-1	0.33	0.20	40.05	46.06	12.82	0.08	0.09	0.33	99.98	86.5
sample ave	0.33	0.19	40.26	46.52	12.39	0.07	0.07	0.33	100.17	87.0
2SD	0.01	0.01	0.21	0.36	0.30	0.04	0.03	0.01	0.34	0.3
AK-6	0.30	0.21	39.97	45.19	13.96	0.07	0.05	0.33	100.07	85.2
AK-6	0.31	0.22	39.42	44.65	13.94	0.07	0.07	0.33	99.01	85.1
AK-6	0.31	0.21	39.93	44.96	14.40	0.06	0.06	0.32	100.25	84.8
AK-6	0.29	0.23	39.82	44.88	14.38	0.03	0.06	0.33	100.01	84.8
AK-6	0.29	0.22	39.86	44.46	14.31	0.14	0.07	0.37	99.72	84.7
AK-6	0.29	0.21	39.52	44.55	14.39	0.08	0.07	0.34	99.46	84.7
AK-6	0.30	0.21	39.77	44.62	14.62	0.07	0.05	0.34	99.99	84.5
AK-6	0.30	0.22	39.70	44.65	14.75	0.08	0.08	0.32	100.12	84.4
AK-6	0.31	0.23	39.81	44.71	14.81	0.06	0.06	0.34	100.33	84.3
AK-6	0.30	0.23	39.46	44.36	14.74	0.05	0.07	0.34	99.54	84.3
AK-6	0.30	0.24	39.56	44.45	14.93	0.04	0.05	0.34	99.91	84.1
AK-6	0.31	0.23	39.44	44.14	14.92	0.09	0.09	0.34	99.57	84.1
AK-6	0.29	0.24	39.54	44.26	15.03	0.05	0.05	0.33	99.79	84.0
AK-6	0.30	0.23	39.53	44.20	15.15	0.04	0.06	0.32	99.83	83.9
AK-6	0.29	0.24	39.59	44.14	15.16	0.04	0.04	0.34	99.84	83.8
AK-6	0.29	0.24	39.48	44.22	15.19	0.04	0.06	0.34	99.85	83.8
AK-6	0.29	0.24	39.64	44.13	15.24	0.04	0.06	0.32	99.96	83.8
AK-6	0.29	0.24	39.66	44.09	15.29	0.06	0.06	0.34	100.03	83.7
AK-6	0.28	0.23	39.78	44.18	15.44	0.03	0.05	0.31	100.30	83.6
AK-6	0.29	0.24	39.72	44.06	15.49	0.04	0.05	0.32	100.21	83.5
AK-6	0.29	0.23	39.72	44.00	15.51	0.06	0.07	0.33	100.22	83.5
AK-6	0.29	0.23	39.66	43.97	15.61	0.06	0.05	0.33	100.19	83.4
AK-6	0.28	0.24	39.53	43.85	15.72	0.04	0.05	0.34	100.05	83.3
AK-6	0.28	0.25	39.22	43.59	15.84	0.09	0.07	0.33	99.68	83.1

AK-6	0.30	0.25	39.25	43.41	15.78	0.18	0.07	0.37	99.61	83.1
AK-6	0.26	0.27	38.85	41.34	18.38	0.04	0.05	0.30	99.48	80.0
AK-6	0.25	0.29	38.60	40.79	18.98	0.03	0.04	0.29	99.27	79.3
sample ave	0.29	0.23	39.56	44.07	15.26	0.06	0.06	0.33	99.86	83.7
2SD	0.03	0.04	0.61	1.91	2.24	0.07	0.02	0.03	0.66	2.6
AK-8b	0.48	0.12	41.16	50.25	7.59	0.07	0.11	0.27	100.05	92.2
AK-8b	0.46	0.13	41.11	49.82	8.17	0.06	0.12	0.26	100.13	91.6
AK-8b	0.45	0.12	41.25	49.94	8.33	0.06	0.12	0.26	100.53	91.4
AK-8b	0.48	0.13	41.03	49.66	8.40	0.10	0.16	0.27	100.23	91.3
AK-8b	0.47	0.13	41.08	49.81	8.46	0.08	0.12	0.27	100.43	91.3
AK-8b	0.45	0.13	40.99	49.65	8.48	0.10	0.13	0.27	100.20	91.3
AK-8b	0.44	0.13	41.09	49.53	8.57	0.09	0.14	0.28	100.27	91.1
AK-8b	0.45	0.14	41.06	49.35	8.91	0.09	0.15	0.26	100.41	90.8
AK-8b	0.45	0.14	40.92	49.07	8.96	0.12	0.16	0.26	100.09	90.7
AK-8b	0.44	0.15	40.76	48.69	9.48	0.09	0.16	0.26	100.03	90.2
AK-8b	0.41	0.15	40.91	48.88	9.62	0.07	0.10	0.28	100.43	90.1
AK-8b	0.42	0.15	40.75	48.35	10.16	0.11	0.14	0.27	100.35	89.5
AK-8b	0.41	0.16	40.68	48.21	10.23	0.09	0.12	0.28	100.17	89.4
AK-8b	0.40	0.15	40.74	48.22	10.39	0.07	0.10	0.28	100.34	89.2
AK-8b	0.39	0.16	40.77	48.13	10.55	0.05	0.10	0.29	100.43	89.1
AK-8b	0.38	0.17	40.38	47.45	11.16	0.08	0.10	0.29	100.01	88.3
AK-8b	0.38	0.18	40.38	47.03	11.66	0.07	0.09	0.28	100.09	87.8
AK-8b	0.37	0.17	40.26	47.00	11.66	0.09	0.11	0.28	99.95	87.8
AK-8b	0.36	0.18	40.21	46.31	12.43	0.10	0.10	0.29	99.99	86.9
AK-8b	0.32	0.20	40.10	45.61	13.50	0.06	0.08	0.34	100.20	85.8
AK-8b	0.32	0.20	40.07	45.64	13.56	0.05	0.06	0.32	100.22	85.7
sample ave	0.42	0.15	40.75	48.41	10.01	0.08	0.12	0.28	100.22	89.6
2SD	0.09	0.05	0.74	2.85	3.52	0.04	0.05	0.04	0.34	3.8
AK-9	0.37	0.17	40.81	48.16	10.44	0.06	0.10	0.33	100.44	89.2
AK-9	0.38	0.16	40.75	48.08	10.48	0.05	0.07	0.32	100.29	89.1
AK-9	0.35	0.16	40.54	47.82	10.43	0.05	0.07	0.32	99.75	89.1
AK-9	0.35	0.16	40.70	48.06	10.52	0.05	0.09	0.31	100.25	89.1
AK-9	0.36	0.16	40.32	47.76	10.45	0.05	0.09	0.32	99.49	89.1
AK-9	0.37	0.16	40.70	48.04	10.54	0.05	0.10	0.32	100.29	89.0
AK-9	0.36	0.16	40.05	47.49	10.44	0.04	0.07	0.31	98.93	89.0
AK-9	0.38	0.16	40.68	48.00	10.55	0.06	0.08	0.32	100.22	89.0
AK-9	0.36	0.17	40.74	48.17	10.59	0.06	0.07	0.32	100.47	89.0
AK-9	0.37	0.16	40.59	47.77	10.51	0.05	0.07	0.32	99.84	89.0
AK-9	0.36	0.17	40.91	48.20	10.62	0.05	0.09	0.32	100.73	89.0
AK-9	0.36	0.16	40.13	47.55	10.48	0.04	0.07	0.31	99.11	89.0
AK-9	0.37	0.16	40.71	48.01	10.58	0.05	0.08	0.32	100.29	89.0
AK-9	0.38	0.17	40.61	47.93	10.58	0.05	0.07	0.32	100.10	89.0
AK-9	0.37	0.17	40.70	48.07	10.62	0.05	0.08	0.32	100.38	89.0
AK-9	0.36	0.16	40.26	47.74	10.55	0.08	0.10	0.31	99.55	89.0
AK-9	0.37	0.18	40.86	48.14	10.64	0.05	0.07	0.32	100.64	89.0
AK-9	0.36	0.17	40.99	48.21	10.66	0.05	0.08	0.32	100.84	89.0
AK-9	0.38	0.16	40.94	48.15	10.66	0.05	0.07	0.32	100.74	88.9
AK-9	0.36	0.17	40.85	48.03	10.64	0.05	0.08	0.32	100.51	88.9
AK-9	0.37	0.16	40.49	47.90	10.62	0.04	0.06	0.32	99.97	88.9
AK-9	0.38	0.18	40.69	47.87	10.61	0.08	0.10	0.32	100.23	88.9
AK-9	0.36	0.16	40.95	48.15	10.68	0.07	0.09	0.32	100.79	88.9
AK-9	0.37	0.16	40.87	48.09	10.67	0.05	0.07	0.33	100.61	88.9
AK-9	0.37	0.16	40.73	47.96	10.69	0.05	0.08	0.33	100.37	88.9
AK-9	0.37	0.16	40.69	48.00	10.72	0.05	0.08	0.32	100.39	88.9

AK-9	0.37	0.17	40.52	47.93	10.71	0.09	0.09	0.32	100.18	88.9
AK-9	0.35	0.18	40.74	47.90	10.70	0.05	0.08	0.32	100.33	88.9
AK-9	0.37	0.17	40.51	47.86	10.70	0.08	0.10	0.32	100.11	88.9
AK-9	0.36	0.16	39.97	46.93	10.50	0.06	0.08	0.32	98.38	88.8
AK-9	0.35	0.17	39.81	47.07	10.54	0.06	0.08	0.32	98.40	88.8
AK-9	0.36	0.17	40.63	47.73	10.70	0.05	0.08	0.33	100.05	88.8
AK-9	0.35	0.18	40.83	47.85	10.75	0.08	0.09	0.31	100.44	88.8
AK-9	0.36	0.16	40.72	47.82	10.75	0.05	0.08	0.32	100.26	88.8
AK-9	0.36	0.16	40.79	47.81	10.84	0.06	0.08	0.30	100.41	88.7
AK-9	0.37	0.18	40.39	47.37	10.93	0.11	0.11	0.31	99.77	88.5
AK-9	0.35	0.17	40.51	47.50	11.14	0.11	0.13	0.31	100.22	88.4
AK-9	0.37	0.18	40.49	47.31	11.21	0.11	0.11	0.31	100.08	88.3
AK-9	0.36	0.17	39.66	46.64	11.35	0.11	0.12	0.30	98.71	88.0
sample ave	0.37	0.17	40.61	47.90	10.58	0.06	0.08	0.32	100.08	89.0
2SD	0.02	0.01	0.60	0.60	0.18	0.02	0.02	0.01	1.28	0.2

AK-12	0.40	0.15	40.56	47.71	10.47	0.08	0.14	0.27	99.78	89.0
AK-12	0.37	0.17	40.10	46.60	11.45	0.09	0.11	0.29	99.17	87.9
AK-12	0.34	0.18	40.18	46.55	11.93	0.09	0.09	0.31	99.66	87.4
AK-12	0.32	0.18	40.52	46.75	12.01	0.04	0.06	0.33	100.21	87.4
AK-12	0.32	0.19	40.37	46.80	12.04	0.04	0.06	0.33	100.14	87.4
AK-12	0.32	0.17	40.31	46.60	12.05	0.04	0.07	0.33	99.90	87.3
AK-12	0.32	0.18	40.28	46.64	12.06	0.10	0.13	0.32	100.04	87.3
AK-12	0.32	0.18	40.52	46.75	12.09	0.08	0.08	0.33	100.36	87.3
AK-12	0.32	0.19	40.36	46.58	12.05	0.04	0.06	0.32	99.93	87.3
AK-12	0.32	0.18	40.29	46.49	12.04	0.04	0.06	0.33	99.76	87.3
AK-12	0.32	0.18	40.27	46.51	12.05	0.06	0.08	0.33	99.80	87.3
AK-12	0.32	0.18	40.18	46.43	12.07	0.05	0.06	0.33	99.62	87.3
AK-12	0.34	0.18	40.30	46.72	12.17	0.05	0.06	0.33	100.16	87.2
AK-12	0.32	0.18	40.09	46.29	12.08	0.04	0.06	0.33	99.38	87.2
AK-12	0.32	0.20	40.25	46.63	12.18	0.05	0.05	0.33	100.01	87.2
AK-12	0.33	0.19	40.35	46.76	12.23	0.08	0.09	0.33	100.37	87.2
AK-12	0.32	0.18	39.92	46.10	12.07	0.06	0.07	0.33	99.06	87.2
AK-12	0.33	0.18	40.20	46.60	12.23	0.05	0.05	0.32	99.97	87.2
AK-12	0.32	0.18	40.21	46.64	12.25	0.05	0.07	0.33	100.06	87.2
AK-12	0.33	0.19	40.24	46.65	12.27	0.08	0.08	0.33	100.16	87.1
AK-12	0.32	0.18	40.12	46.11	12.13	0.07	0.07	0.32	99.33	87.1
AK-12	0.33	0.19	40.19	46.61	12.26	0.11	0.09	0.33	100.10	87.1
AK-12	0.35	0.19	40.15	46.73	12.29	0.05	0.07	0.33	100.16	87.1
AK-12	0.33	0.18	40.20	46.61	12.26	0.05	0.06	0.33	100.02	87.1
AK-12	0.34	0.19	40.21	46.67	12.29	0.05	0.06	0.33	100.14	87.1
AK-12	0.33	0.19	40.21	46.57	12.27	0.11	0.09	0.33	100.10	87.1
AK-12	0.34	0.18	40.11	46.54	12.27	0.05	0.06	0.33	99.88	87.1
AK-12	0.33	0.18	40.28	46.56	12.27	0.05	0.08	0.33	100.07	87.1
AK-12	0.33	0.19	40.30	46.75	12.36	0.14	0.09	0.33	100.49	87.1
AK-12	0.31	0.18	39.86	46.04	12.17	0.06	0.07	0.33	99.03	87.1
AK-12	0.34	0.19	40.07	46.56	12.32	0.07	0.07	0.33	99.94	87.1
AK-12	0.31	0.19	40.05	46.14	12.24	0.05	0.06	0.34	99.36	87.1
AK-12	0.34	0.20	40.08	46.28	12.29	0.05	0.08	0.33	99.65	87.0
AK-12	0.34	0.20	40.32	46.63	12.39	0.06	0.07	0.33	100.35	87.0
AK-12	0.32	0.18	39.44	45.44	12.08	0.06	0.06	0.33	97.90	87.0
AK-12	0.33	0.18	40.08	46.21	12.32	0.06	0.07	0.33	99.57	87.0
AK-12	0.31	0.19	40.11	46.28	12.34	0.10	0.10	0.33	99.76	87.0
AK-12	0.32	0.19	40.35	46.53	12.44	0.05	0.06	0.33	100.27	87.0
AK-12	0.33	0.20	40.42	46.74	12.49	0.05	0.07	0.33	100.63	87.0

AK-12	0.31	0.19	40.24	46.30	12.44	0.04	0.05	0.33	99.89	86.9
AK-12	0.32	0.19	39.54	45.35	12.39	0.08	0.07	0.33	98.26	86.7
AK-12	0.31	0.20	40.16	46.05	12.95	0.06	0.06	0.34	100.12	86.4
sample ave	0.3	0.2	40.2	46.5	12.2	0.1	0.1	0.3	99.8	87.2
2SD	0.03	0.02	0.43	0.75	0.68	0.05	0.04	0.02	1.08	0.7
AK-13	0.32	0.18	40.07	46.30	11.89	0.07	0.09	0.33	99.24	87.4
AK-13	0.31	0.19	40.19	46.33	11.91	0.07	0.07	0.33	99.40	87.4
AK-13	0.34	0.19	40.48	46.83	12.04	0.08	0.07	0.31	100.34	87.4
AK-13	0.34	0.18	40.45	46.79	12.14	0.08	0.09	0.32	100.38	87.3
AK-13	0.32	0.19	40.39	46.74	12.14	0.08	0.07	0.33	100.27	87.3
AK-13	0.32	0.18	39.95	46.12	11.99	0.06	0.05	0.33	99.00	87.3
AK-13	0.34	0.19	40.50	46.85	12.19	0.08	0.09	0.33	100.56	87.3
AK-13	0.34	0.18	40.38	46.69	12.15	0.05	0.07	0.33	100.20	87.3
AK-13	0.32	0.18	40.29	46.69	12.16	0.06	0.08	0.33	100.12	87.2
AK-13	0.34	0.19	40.27	46.74	12.18	0.08	0.09	0.34	100.22	87.2
AK-13	0.33	0.19	40.50	46.65	12.17	0.08	0.09	0.33	100.34	87.2
AK-13	0.33	0.18	40.35	46.66	12.19	0.05	0.07	0.33	100.17	87.2
AK-13	0.34	0.20	40.29	46.54	12.16	0.05	0.07	0.33	99.97	87.2
AK-13	0.32	0.18	40.07	46.39	12.15	0.05	0.08	0.33	99.57	87.2
AK-13	0.32	0.19	40.28	46.64	12.24	0.11	0.08	0.33	100.20	87.2
AK-13	0.34	0.20	40.30	46.59	12.23	0.07	0.09	0.33	100.15	87.2
AK-13	0.32	0.19	40.25	46.57	12.24	0.11	0.10	0.32	100.10	87.2
AK-13	0.33	0.19	40.19	46.60	12.26	0.10	0.10	0.33	100.11	87.1
AK-13	0.33	0.19	40.38	46.61	12.29	0.06	0.07	0.33	100.26	87.1
AK-13	0.34	0.19	40.24	46.55	12.27	0.05	0.07	0.33	100.03	87.1
AK-13	0.33	0.19	40.22	46.55	12.28	0.06	0.06	0.35	100.03	87.1
AK-13	0.33	0.18	40.32	46.56	12.29	0.05	0.08	0.33	100.14	87.1
AK-13	0.33	0.19	40.37	46.57	12.31	0.07	0.07	0.34	100.24	87.1
AK-13	0.32	0.19	40.10	46.38	12.31	0.05	0.08	0.33	99.77	87.0
AK-13	0.32	0.19	40.20	46.36	12.35	0.05	0.05	0.33	99.85	87.0
AK-13	0.33	0.19	40.05	46.25	12.35	0.05	0.06	0.33	99.62	87.0
AK-13	0.32	0.19	40.24	46.46	12.42	0.09	0.08	0.33	100.13	87.0
AK-13	0.32	0.19	40.07	46.16	12.36	0.09	0.08	0.34	99.61	86.9
AK-13	0.32	0.20	40.09	46.10	12.55	0.04	0.06	0.34	99.70	86.8
AK-13	0.33	0.19	40.19	46.42	12.64	0.05	0.05	0.33	100.21	86.7
AK-13	0.32	0.20	40.03	45.96	12.52	0.05	0.05	0.33	99.46	86.7
AK-13	0.32	0.18	39.91	46.00	12.62	0.07	0.08	0.33	99.51	86.7
AK-13	0.32	0.20	39.97	46.02	12.62	0.05	0.11	0.33	99.60	86.7
sample ave	0.33	0.19	40.23	46.47	12.26	0.07	0.08	0.33	99.95	87.1
2SD	0.02	0.01	0.32	0.50	0.37	0.04	0.03	0.01	0.74	0.4
AK-14	0.43	0.13	40.92	49.39	8.55	0.05	0.11	0.27	99.85	91.1
AK-14	0.46	0.13	41.10	49.37	8.58	0.08	0.13	0.27	100.11	91.1
AK-14	0.44	0.14	40.92	48.83	9.22	0.06	0.11	0.27	99.99	90.4
AK-14	0.33	0.16	40.18	47.41	10.72	0.06	0.09	0.28	99.22	88.7
AK-14	0.35	0.16	40.62	47.37	11.12	0.05	0.13	0.30	100.09	88.4
AK-14	0.41	0.16	40.54	47.43	11.32	0.10	0.13	0.28	100.36	88.2
AK-14	0.32	0.18	40.56	46.72	12.03	0.04	0.09	0.33	100.27	87.4
AK-14	0.32	0.18	40.43	46.72	12.05	0.06	0.08	0.32	100.16	87.4
AK-14	0.32	0.18	40.29	46.43	11.99	0.05	0.06	0.32	99.65	87.4
AK-14	0.32	0.18	40.26	46.54	12.02	0.04	0.06	0.32	99.76	87.3
AK-14	0.33	0.18	40.30	46.71	12.07	0.07	0.08	0.33	100.07	87.3
AK-14	0.32	0.18	40.38	46.65	12.06	0.04	0.06	0.32	100.01	87.3
AK-14	0.32	0.18	40.22	46.58	12.04	0.05	0.06	0.33	99.78	87.3

AK-14	0.32	0.18	40.06	46.34	11.99	0.07	0.07	0.33	99.37	87.3
AK-14	0.32	0.17	40.19	46.42	12.03	0.06	0.08	0.32	99.59	87.3
AK-14	0.32	0.19	40.13	46.33	12.05	0.04	0.06	0.33	99.44	87.3
AK-14	0.32	0.18	40.25	46.54	12.11	0.04	0.07	0.33	99.84	87.3
AK-14	0.32	0.18	39.92	46.10	12.00	0.04	0.06	0.33	98.95	87.3
AK-14	0.32	0.18	40.12	46.41	12.09	0.09	0.08	0.33	99.61	87.2
AK-14	0.32	0.18	40.01	46.30	12.08	0.04	0.07	0.32	99.33	87.2
AK-14	0.31	0.18	40.36	46.65	12.19	0.07	0.07	0.33	100.16	87.2
AK-14	0.33	0.17	40.11	46.38	12.15	0.05	0.05	0.34	99.58	87.2
AK-14	0.32	0.18	40.29	46.46	12.17	0.04	0.07	0.33	99.86	87.2
AK-14	0.31	0.18	40.38	46.52	12.19	0.07	0.07	0.33	100.05	87.2
AK-14	0.32	0.18	40.11	46.31	12.14	0.08	0.08	0.32	99.55	87.2
AK-14	0.32	0.19	40.35	46.48	12.21	0.03	0.06	0.31	99.95	87.2
AK-14	0.31	0.19	40.23	46.43	12.22	0.04	0.07	0.33	99.82	87.1
AK-14	0.33	0.19	40.24	46.46	12.25	0.05	0.06	0.33	99.90	87.1
AK-14	0.32	0.19	40.23	46.57	12.28	0.05	0.08	0.33	100.06	87.1
AK-14	0.33	0.18	40.20	46.35	12.22	0.05	0.07	0.33	99.72	87.1
AK-14	0.34	0.18	40.11	46.43	12.29	0.12	0.10	0.33	99.90	87.1
AK-14	0.33	0.19	40.25	46.46	12.32	0.09	0.09	0.32	100.05	87.1
AK-14	0.33	0.18	40.30	46.54	12.34	0.05	0.06	0.33	100.14	87.0
AK-14	0.32	0.19	40.04	46.15	12.26	0.05	0.07	0.33	99.41	87.0
AK-14	0.31	0.18	40.38	46.44	12.47	0.08	0.09	0.34	100.28	86.9
AK-14	0.31	0.19	40.25	46.35	12.48	0.07	0.07	0.33	100.06	86.9
AK-14	0.30	0.19	40.14	45.94	12.55	0.04	0.06	0.33	99.54	86.7
AK-14	0.35	0.19	39.77	45.48	12.84	0.08	0.12	0.31	99.13	86.3
sample ave	0.33	0.18	40.29	46.71	11.83	0.06	0.08	0.32	99.81	87.6
2SD	0.07	0.03	0.52	1.64	1.96	0.04	0.04	0.04	0.68	2.2
AK-18a	0.37	0.14	40.94	48.60	9.75	0.07	0.12	0.28	100.28	89.9
AK-18a	0.36	0.15	40.99	48.60	9.92	0.07	0.13	0.28	100.50	89.7
AK-18a	0.33	0.15	40.84	48.25	10.24	0.03	0.08	0.33	100.26	89.4
AK-18a	0.34	0.16	40.73	48.16	10.31	0.05	0.08	0.34	100.15	89.3
AK-18a	0.35	0.15	40.75	47.79	10.87	0.08	0.11	0.27	100.37	88.7
AK-18a	0.36	0.17	40.43	47.19	11.71	0.06	0.07	0.31	100.30	87.8
AK-18a	0.31	0.18	39.81	46.33	11.95	0.07	0.08	0.31	99.02	87.4
AK-18a	0.30	0.21	39.55	45.90	11.88	0.05	0.06	0.31	98.24	87.3
AK-18a	0.33	0.19	40.26	46.67	12.10	0.05	0.06	0.33	99.98	87.3
AK-18a	0.33	0.18	40.37	46.57	12.09	0.04	0.07	0.32	99.99	87.3
AK-18a	0.32	0.18	39.81	46.25	12.02	0.05	0.06	0.33	99.02	87.3
AK-18a	0.32	0.18	40.21	46.61	12.12	0.06	0.08	0.33	99.89	87.3
AK-18a	0.33	0.18	39.79	46.24	12.04	0.07	0.09	0.32	99.06	87.3
AK-18a	0.34	0.19	40.22	46.57	12.14	0.07	0.07	0.33	99.92	87.2
AK-18a	0.33	0.19	40.33	46.64	12.17	0.06	0.07	0.33	100.13	87.2
AK-18a	0.33	0.19	40.21	46.64	12.17	0.08	0.08	0.33	100.04	87.2
AK-18a	0.33	0.18	39.77	46.27	12.08	0.04	0.05	0.33	99.05	87.2
AK-18a	0.32	0.17	39.94	46.58	12.17	0.09	0.08	0.33	99.69	87.2
AK-18a	0.31	0.18	39.76	46.06	12.06	0.07	0.08	0.31	98.83	87.2
AK-18a	0.33	0.18	40.32	46.44	12.16	0.04	0.07	0.33	99.87	87.2
AK-18a	0.32	0.18	39.79	46.40	12.15	0.05	0.07	0.33	99.29	87.2
AK-18a	0.34	0.19	40.33	46.68	12.24	0.04	0.06	0.33	100.21	87.2
AK-18a	0.32	0.19	40.29	46.64	12.23	0.05	0.06	0.33	100.10	87.2
AK-18a	0.33	0.19	40.27	46.60	12.23	0.07	0.10	0.33	100.12	87.2
AK-18a	0.32	0.18	39.76	46.25	12.14	0.04	0.06	0.33	99.08	87.2

AK-18a	0.33	0.18	40.19	46.49	12.21	0.05	0.05	0.33	99.82	87.2
AK-18a	0.33	0.18	40.42	46.64	12.25	0.05	0.05	0.33	100.26	87.2
AK-18a	0.33	0.18	39.78	46.20	12.15	0.05	0.06	0.33	99.07	87.1
AK-18a	0.33	0.19	40.25	46.53	12.24	0.09	0.09	0.32	100.04	87.1
AK-18a	0.33	0.18	39.70	46.09	12.13	0.05	0.07	0.33	98.88	87.1
AK-18a	0.31	0.18	39.93	46.40	12.21	0.08	0.08	0.33	99.51	87.1
AK-18a	0.32	0.18	39.68	46.11	12.16	0.04	0.06	0.32	98.88	87.1
AK-18a	0.32	0.18	39.69	46.07	12.31	0.05	0.08	0.25	98.95	87.0
AK-18a	0.32	0.19	40.17	46.20	12.51	0.05	0.06	0.33	99.83	86.8
AK-18a	0.31	0.18	39.39	45.68	12.42	0.04	0.05	0.33	98.39	86.8
AK-18a	0.33	0.19	40.27	46.32	12.61	0.05	0.05	0.33	100.16	86.8
AK-18a	0.32	0.19	40.22	46.39	12.69	0.14	0.10	0.33	100.39	86.7
AK-18a	0.33	0.19	40.29	46.13	12.63	0.05	0.06	0.33	100.02	86.7
AK-18a	0.33	0.20	40.23	46.27	12.67	0.05	0.08	0.32	100.14	86.7
AK-18a	0.31	0.19	39.32	45.38	12.49	0.07	0.06	0.33	98.16	86.6
AK-18a	0.34	0.19	40.16	46.13	12.74	0.05	0.07	0.31	99.99	86.6
AK-18a	0.32	0.20	40.12	46.02	12.82	0.08	0.07	0.33	99.95	86.5
AK-18a	0.32	0.21	40.13	45.94	12.88	0.05	0.06	0.31	99.90	86.4
AK-18a	0.32	0.20	40.20	45.92	12.92	0.05	0.06	0.32	99.98	86.4
AK-18a	0.32	0.19	40.08	46.01	13.00	0.06	0.07	0.31	100.04	86.3
AK-18a	0.33	0.20	40.23	46.07	13.08	0.06	0.08	0.32	100.38	86.3
sample ave	0.33	0.18	40.13	46.52	12.09	0.06	0.07	0.32	99.70	87.3
2SD	0.03	0.03	0.75	1.40	1.48	0.04	0.03	0.04	1.24	1.6
DB-9	0.45	0.15	40.69	48.52	9.86	0.09	0.11	0.28	100.15	89.8
DB-9	0.42	0.15	40.69	48.40	9.89	0.06	0.10	0.28	100.01	89.7
DB-9	0.43	0.14	40.60	48.32	10.05	0.07	0.13	0.29	100.02	89.6
DB-9	0.37	0.15	40.69	48.29	10.07	0.06	0.10	0.33	100.07	89.5
DB-9	0.40	0.17	40.44	48.01	10.15	0.04	0.10	0.30	99.60	89.4
DB-9	0.40	0.16	40.59	48.03	10.34	0.06	0.10	0.32	100.00	89.2
DB-9	0.42	0.15	40.46	47.96	10.34	0.07	0.11	0.28	99.80	89.2
DB-9	0.41	0.16	40.41	47.82	10.66	0.10	0.14	0.29	99.98	88.9
DB-9	0.40	0.17	40.56	47.89	10.98	0.06	0.11	0.30	100.46	88.6
DB-9	0.38	0.17	40.44	47.44	11.06	0.05	0.09	0.29	99.93	88.4
DB-9	0.41	0.17	40.31	47.30	11.16	0.08	0.11	0.32	99.86	88.3
DB-9	0.37	0.17	40.26	47.31	11.22	0.10	0.12	0.29	99.83	88.3
DB-9	0.39	0.17	40.36	47.43	11.30	0.08	0.10	0.30	100.12	88.2
DB-9	0.39	0.17	40.49	47.54	11.36	0.08	0.09	0.30	100.42	88.2
DB-9	0.37	0.17	40.37	47.28	11.40	0.04	0.07	0.30	100.02	88.1
DB-9	0.37	0.18	40.43	47.27	11.52	0.04	0.07	0.32	100.20	88.0
DB-9	0.37	0.17	40.34	47.25	11.55	0.07	0.10	0.31	100.17	87.9
DB-9	0.36	0.17	40.38	47.17	11.61	0.05	0.07	0.30	100.11	87.9
DB-9	0.36	0.19	40.16	46.88	11.85	0.07	0.10	0.32	99.93	87.6
DB-9	0.36	0.18	40.16	46.67	11.93	0.04	0.08	0.32	99.75	87.5
DB-9	0.30	0.18	40.18	46.79	12.02	0.04	0.07	0.21	99.80	87.4
DB-9	0.35	0.19	40.37	46.86	12.12	0.05	0.07	0.32	100.33	87.3
DB-9	0.37	0.19	39.96	46.43	12.08	0.08	0.09	0.30	99.51	87.3
DB-9	0.35	0.19	40.18	46.60	12.35	0.04	0.06	0.32	100.09	87.1
DB-9	0.34	0.19	40.18	46.40	12.38	0.05	0.06	0.32	99.91	87.0
DB-9	0.34	0.18	40.20	46.26	12.61	0.05	0.07	0.31	100.01	86.7
DB-9	0.35	0.19	40.20	46.31	12.62	0.05	0.06	0.32	100.11	86.7
DB-9	0.34	0.20	40.00	45.81	12.89	0.04	0.07	0.32	99.66	86.4
DB-9	0.24	0.21	40.06	46.12	13.06	0.03	0.04	0.18	99.94	86.3
DB-9	0.33	0.21	39.95	45.59	13.56	0.07	0.07	0.31	100.08	85.7
sample ave	0.37	0.17	40.34	47.20	11.47	0.06	0.09	0.30	100.00	88.0
2SD	0.08	0.03	0.42	1.59	2.01	0.04	0.05	0.06	0.44	2.2

DB-13	0.37	0.15	40.87	48.62	9.86	0.07	0.08	0.31	100.32	89.8
DB-13	0.36	0.15	40.60	48.35	9.91	0.06	0.06	0.30	99.80	89.7
DB-13	0.36	0.18	40.30	46.84	11.76	0.05	0.07	0.31	99.87	87.7
DB-13	0.37	0.18	40.46	47.02	11.85	0.06	0.06	0.31	100.31	87.6
DB-13	0.33	0.18	40.44	46.99	11.93	0.06	0.07	0.32	100.31	87.5
DB-13	0.34	0.17	40.26	46.85	11.99	0.06	0.06	0.31	100.05	87.4
DB-13	0.34	0.19	40.34	46.55	12.37	0.04	0.05	0.32	100.21	87.0
DB-13	0.32	0.19	40.19	46.35	12.43	0.06	0.06	0.33	99.92	86.9
DB-13	0.27	0.22	40.06	45.83	13.33	0.03	0.03	0.27	100.04	86.0
DB-13	0.25	0.23	39.90	45.09	14.25	0.03	0.03	0.24	100.01	84.9
sample ave	0.33	0.18	40.34	46.85	11.97	0.05	0.06	0.30	100.08	87.5
2SD	0.08	0.05	0.55	2.10	2.68	0.03	0.03	0.05	0.39	2.9
DB-14	0.35	0.18	40.30	46.77	12.20	0.05	0.06	0.32	100.24	87.2
DB-14	0.33	0.19	40.34	46.76	12.21	0.06	0.06	0.32	100.26	87.2
DB-14	0.34	0.19	40.15	46.58	12.17	0.05	0.06	0.32	99.86	87.2
DB-14	0.34	0.19	40.33	46.81	12.28	0.05	0.06	0.33	100.39	87.2
DB-14	0.35	0.19	40.23	46.59	12.32	0.04	0.04	0.33	100.10	87.1
DB-14	0.33	0.19	40.09	46.13	12.25	0.05	0.05	0.33	99.42	87.0
DB-14	0.34	0.19	40.06	46.35	12.31	0.05	0.05	0.33	99.67	87.0
DB-14	0.34	0.20	40.23	46.53	12.37	0.05	0.04	0.33	100.09	87.0
DB-14	0.34	0.20	40.14	46.49	12.40	0.07	0.06	0.33	100.02	87.0
DB-14	0.33	0.19	40.18	46.55	12.51	0.07	0.07	0.33	100.24	86.9
DB-14	0.32	0.20	40.15	46.28	12.48	0.05	0.06	0.33	99.85	86.9
DB-14	0.33	0.20	40.04	46.37	12.53	0.07	0.06	0.33	99.94	86.8
DB-14	0.33	0.20	40.09	46.30	12.55	0.07	0.07	0.30	99.91	86.8
DB-14	0.33	0.20	39.88	46.05	12.50	0.06	0.05	0.31	99.38	86.8
DB-14	0.34	0.19	40.21	46.34	12.63	0.05	0.05	0.33	100.14	86.7
DB-14	0.33	0.20	39.98	46.01	12.69	0.06	0.05	0.34	99.66	86.6
sample ave	0.34	0.19	40.15	46.43	12.40	0.06	0.06	0.33	99.95	87.0
2SD	0.02	0.01	0.25	0.49	0.32	0.02	0.02	0.02	0.59	0.4
DB-17	0.44	0.13	41.16	50.25	7.93	0.07	0.11	0.28	100.36	91.9
DB-17	0.43	0.12	41.17	50.34	8.41	0.08	0.18	0.27	101.00	91.4
DB-17	0.45	0.12	41.05	49.71	8.49	0.09	0.14	0.28	100.34	91.3
DB-17	0.43	0.14	40.92	49.26	9.07	0.09	0.13	0.27	100.31	90.6
DB-17	0.41	0.15	40.89	49.04	9.17	0.09	0.15	0.28	100.18	90.5
DB-17	0.43	0.14	40.92	49.00	9.33	0.07	0.11	0.28	100.29	90.3
DB-17	0.43	0.14	40.92	49.35	9.46	0.07	0.12	0.28	100.77	90.3
DB-17	0.41	0.15	41.10	49.22	9.45	0.09	0.14	0.30	100.86	90.3
DB-17	0.41	0.15	40.90	48.90	9.51	0.10	0.13	0.29	100.38	90.2
DB-17	0.41	0.15	40.78	48.69	9.69	0.09	0.11	0.27	100.20	90.0
DB-17	0.40	0.16	40.84	48.49	9.97	0.11	0.13	0.28	100.39	89.7
DB-17	0.40	0.16	40.76	48.37	10.05	0.08	0.11	0.29	100.23	89.6
DB-17	0.40	0.16	40.51	47.85	10.59	0.09	0.10	0.29	99.99	89.0
DB-17	0.39	0.17	40.82	48.16	10.70	0.06	0.07	0.28	100.64	88.9
DB-17	0.39	0.16	40.59	47.86	10.76	0.06	0.09	0.29	100.20	88.8
DB-17	0.38	0.16	40.71	47.92	10.82	0.06	0.10	0.28	100.43	88.8
DB-17	0.39	0.16	40.59	47.76	10.80	0.06	0.09	0.29	100.14	88.7
DB-17	0.39	0.17	40.60	47.81	10.89	0.08	0.10	0.27	100.30	88.7
DB-17	0.39	0.17	40.30	47.63	10.94	0.09	0.11	0.29	99.91	88.6
DB-17	0.38	0.17	40.50	47.64	11.00	0.08	0.10	0.28	100.15	88.5
DB-17	0.39	0.16	40.27	47.44	11.06	0.09	0.11	0.29	99.80	88.4
DB-17	0.37	0.17	40.43	47.60	11.17	0.09	0.10	0.29	100.21	88.4

DB-17	0.37	0.18	40.40	47.31	11.54	0.09	0.11	0.30	100.28	88.0
DB-17	0.34	0.19	40.41	46.88	11.95	0.09	0.10	0.31	100.28	87.5
DB-17	0.34	0.18	40.30	46.87	12.00	0.09	0.08	0.32	100.17	87.4
DB-17	0.34	0.19	40.14	46.27	12.37	0.08	0.09	0.32	99.80	87.0
DB-17	0.34	0.20	40.15	46.27	12.65	0.07	0.09	0.29	100.07	86.7
DB-17	0.32	0.22	39.83	45.28	14.03	0.09	0.08	0.30	100.15	85.2
DB-17	0.30	0.23	39.64	44.47	15.01	0.08	0.07	0.29	100.08	84.1
DB-17	0.31	0.25	39.68	44.37	15.03	0.08	0.07	0.30	100.09	84.0
sample ave	0.39	0.17	40.58	47.87	10.79	0.08	0.11	0.29	100.27	88.8
2SD	0.08	0.06	0.82	2.98	3.53	0.03	0.05	0.02	0.55	3.9
DB-19	0.36	0.17	39.73	46.48	11.61	0.04	0.07	0.28	98.74	87.7
DB-19	0.34	0.18	40.24	46.83	11.92	0.05	0.06	0.32	99.93	87.5
DB-19	0.32	0.18	39.76	46.26	11.95	0.06	0.07	0.31	98.91	87.3
DB-19	0.34	0.17	40.20	46.53	12.09	0.05	0.06	0.32	99.77	87.3
DB-19	0.33	0.18	39.62	46.10	12.02	0.07	0.09	0.30	98.69	87.2
DB-19	0.33	0.18	39.68	46.14	12.10	0.07	0.07	0.30	98.87	87.2
DB-19	0.32	0.19	39.87	46.22	12.13	0.06	0.07	0.30	99.14	87.2
DB-19	0.33	0.20	40.29	46.53	12.22	0.04	0.05	0.31	99.97	87.2
DB-19	0.32	0.19	39.81	46.20	12.16	0.04	0.06	0.29	99.05	87.1
DB-19	0.32	0.19	39.83	46.24	12.23	0.05	0.05	0.31	99.21	87.1
DB-19	0.32	0.18	39.74	46.17	12.23	0.07	0.07	0.31	99.08	87.1
DB-19	0.32	0.18	39.77	46.07	12.20	0.03	0.05	0.31	98.94	87.1
DB-19	0.33	0.19	40.27	46.49	12.33	0.04	0.05	0.31	100.01	87.0
DB-19	0.32	0.20	40.45	46.84	12.46	0.05	0.06	0.31	100.70	87.0
DB-19	0.32	0.18	39.77	46.06	12.25	0.04	0.06	0.30	98.98	87.0
DB-19	0.32	0.19	39.56	45.87	12.29	0.08	0.07	0.29	98.67	86.9
DB-19	0.32	0.19	39.62	45.95	12.32	0.04	0.05	0.30	98.78	86.9
DB-19	0.33	0.19	40.20	46.58	12.51	0.04	0.04	0.30	100.20	86.9
DB-19	0.26	0.15	39.33	45.32	12.23	0.09	0.07	0.22	97.68	86.8
DB-19	0.32	0.19	39.66	45.97	12.42	0.03	0.06	0.31	98.97	86.8
DB-19	0.32	0.20	40.23	46.53	12.62	0.04	0.05	0.31	100.30	86.8
DB-19	0.31	0.19	39.63	45.76	12.46	0.04	0.05	0.29	98.72	86.8
DB-19	0.31	0.19	39.38	45.49	12.54	0.06	0.07	0.30	98.34	86.6
DB-19	0.32	0.19	39.65	45.63	12.59	0.06	0.07	0.31	98.80	86.6
DB-19	0.31	0.21	40.24	46.28	12.84	0.03	0.05	0.30	100.25	86.5
DB-19	0.30	0.19	40.13	46.26	12.91	0.07	0.06	0.27	100.19	86.5
DB-19	0.31	0.19	39.77	45.76	12.86	0.03	0.05	0.29	99.28	86.4
DB-19	0.32	0.20	39.98	45.75	13.11	0.04	0.05	0.30	99.75	86.2
DB-19	0.28	0.20	39.66	45.64	13.09	0.03	0.04	0.32	99.28	86.1
DB-19	0.31	0.21	40.15	45.92	13.18	0.03	0.05	0.29	100.15	86.1
DB-19	0.31	0.19	39.60	45.51	13.08	0.03	0.05	0.30	99.07	86.1
DB-19	0.32	0.21	40.10	45.88	13.19	0.04	0.04	0.31	100.08	86.1
DB-19	0.31	0.21	40.11	45.95	13.24	0.03	0.05	0.29	100.20	86.1
DB-19	0.27	0.20	39.95	45.71	13.29	0.03	0.05	0.32	99.81	86.0
DB-19	0.28	0.21	40.01	45.80	13.38	0.03	0.06	0.32	100.10	85.9
DB-19	0.33	0.21	40.16	45.94	13.49	0.08	0.09	0.30	100.59	85.9
DB-19	0.31	0.21	39.98	45.57	13.54	0.03	0.05	0.30	99.98	85.7
DB-19	0.30	0.20	39.91	45.62	13.57	0.06	0.05	0.30	100.01	85.7
DB-19	0.29	0.19	39.48	45.05	13.44	0.04	0.05	0.29	98.84	85.7
DB-19	0.31	0.20	39.28	44.93	13.66	0.03	0.05	0.31	98.77	85.4
DB-19	0.32	0.22	40.24	45.70	13.90	0.05	0.06	0.30	100.79	85.4
DB-19	0.30	0.20	39.49	44.92	13.68	0.04	0.06	0.30	98.98	85.4
DB-19	0.32	0.22	39.95	45.31	13.91	0.03	0.05	0.29	100.09	85.3

DB-19	0.28	0.20	39.22	45.20	13.91	0.22	1.09	0.14	100.27	85.3
DB-19	0.32	0.22	40.00	45.36	14.05	0.07	0.07	0.31	100.39	85.2
DB-19	0.34	0.23	39.68	44.20	15.17	0.05	0.09	0.30	100.06	83.9
DB-19	0.30	0.22	39.20	43.68	15.34	0.06	0.07	0.29	99.14	83.5
sample ave	0.31	0.20	39.84	45.83	12.89	0.05	0.08	0.30	99.50	86.4
2SD	0.04	0.03	0.63	1.24	1.63	0.06	0.30	0.06	1.43	1.8
PI-10	0.35	0.18	40.31	47.11	11.80	0.04	0.06	0.32	100.18	87.7
PI-10	0.35	0.17	40.47	47.27	11.85	0.06	0.08	0.33	100.58	87.7
PI-10	0.35	0.18	40.22	46.99	11.78	0.07	0.09	0.32	100.00	87.7
PI-10	0.35	0.18	40.39	47.15	11.92	0.07	0.08	0.32	100.46	87.6
PI-10	0.31	0.18	40.11	46.49	11.85	0.10	0.11	0.32	99.48	87.5
PI-10	0.33	0.18	40.29	46.90	11.98	0.04	0.06	0.33	100.12	87.5
PI-10	0.34	0.18	40.42	46.86	11.98	0.04	0.06	0.33	100.21	87.5
PI-10	0.32	0.18	40.06	46.58	11.95	0.05	0.09	0.32	99.55	87.4
PI-10	0.32	0.18	40.33	46.84	12.03	0.05	0.07	0.32	100.14	87.4
PI-10	0.32	0.18	40.17	46.66	12.04	0.05	0.08	0.32	99.82	87.4
PI-10	0.34	0.19	40.22	46.75	12.10	0.05	0.08	0.32	100.04	87.3
PI-10	0.32	0.18	40.27	46.63	12.12	0.05	0.08	0.33	99.99	87.3
PI-10	0.30	0.19	40.28	46.61	12.47	0.05	0.06	0.32	100.28	86.9
PI-10	0.29	0.19	40.28	46.21	12.61	0.05	0.06	0.32	100.01	86.7
PI-10	0.29	0.20	40.05	45.93	12.70	0.05	0.07	0.32	99.60	86.6
PI-10	0.30	0.20	39.88	45.88	12.79	0.05	0.15	0.32	99.57	86.5
PI-10	0.31	0.20	40.12	45.93	13.08	0.05	0.06	0.34	100.09	86.2
PI-10	0.31	0.20	39.96	45.67	13.33	0.04	0.05	0.34	99.90	85.9
sample ave	0.32	0.19	40.21	46.58	12.24	0.05	0.08	0.32	100.00	87.1
2SD	0.04	0.02	0.32	0.95	0.94	0.03	0.05	0.01	0.62	1.1
PI-15	0.43	0.15	41.08	49.50	8.84	0.06	0.12	0.29	100.47	90.9
PI-15	0.40	0.14	40.92	49.09	9.39	0.12	0.16	0.28	100.49	90.3
PI-15	0.40	0.15	40.67	48.45	9.83	0.11	0.16	0.28	100.05	89.8
PI-15	0.38	0.15	40.76	48.33	10.13	0.12	0.13	0.28	100.29	89.5
PI-15	0.40	0.17	40.71	47.97	10.61	0.06	0.09	0.29	100.29	89.0
PI-15	0.38	0.17	40.71	47.84	10.85	0.05	0.08	0.32	100.41	88.7
PI-15	0.37	0.16	40.61	47.83	10.85	0.06	0.10	0.33	100.32	88.7
PI-15	0.39	0.16	40.52	47.74	10.94	0.09	0.13	0.29	100.26	88.6
PI-15	0.38	0.17	40.60	47.64	10.97	0.07	0.10	0.30	100.23	88.6
PI-15	0.37	0.18	40.48	47.43	11.32	0.08	0.09	0.32	100.26	88.2
PI-15	0.37	0.16	40.70	47.57	11.35	0.05	0.07	0.32	100.58	88.2
PI-15	0.36	0.17	40.54	47.38	11.35	0.06	0.08	0.32	100.26	88.2
PI-15	0.36	0.16	40.43	47.24	11.34	0.07	0.08	0.32	100.00	88.1
PI-15	0.36	0.17	40.40	47.43	11.39	0.05	0.17	0.31	100.28	88.1
PI-15	0.35	0.18	40.41	47.22	11.39	0.06	0.08	0.32	100.01	88.1
PI-15	0.35	0.17	40.62	47.29	11.42	0.07	0.09	0.32	100.33	88.1
PI-15	0.37	0.18	40.31	47.32	11.43	0.13	0.12	0.31	100.16	88.1
PI-15	0.35	0.18	40.55	47.34	11.52	0.05	0.06	0.34	100.39	88.0
PI-15	0.35	0.19	40.30	47.00	11.89	0.08	0.08	0.26	100.14	87.6
sample ave	0.38	0.17	40.59	47.77	10.89	0.08	0.10	0.30	100.27	88.7
2SD	0.04	0.03	0.40	1.32	1.60	0.05	0.06	0.04	0.32	1.7
PI-17	0.46	0.11	41.47	50.80	7.06	0.10	0.16	0.29	100.45	92.8
PI-17	0.45	0.11	41.25	50.42	7.10	0.10	0.17	0.28	99.88	92.7
PI-17	0.45	0.12	41.31	50.69	7.22	0.10	0.16	0.28	100.33	92.6
PI-17	0.46	0.12	41.41	50.47	7.21	0.10	0.18	0.28	100.23	92.6
PI-17	0.46	0.11	41.35	50.45	7.30	0.11	0.17	0.28	100.22	92.5
PI-17	0.46	0.12	41.41	50.53	7.37	0.11	0.15	0.28	100.43	92.4

PI-17	0.46	0.11	41.31	50.40	7.35	0.10	0.16	0.28	100.17	92.4
PI-17	0.45	0.11	41.33	50.26	7.60	0.11	0.15	0.28	100.30	92.2
PI-17	0.46	0.13	41.20	50.10	7.77	0.11	0.17	0.29	100.24	92.0
PI-17	0.46	0.12	41.19	49.98	7.96	0.11	0.17	0.28	100.28	91.8
PI-17	0.45	0.13	41.10	49.92	8.10	0.12	0.16	0.28	100.26	91.7
PI-17	0.44	0.13	41.00	49.77	8.18	0.11	0.12	0.29	100.05	91.6
PI-17	0.45	0.13	41.19	49.79	8.31	0.10	0.16	0.28	100.41	91.4
PI-17	0.43	0.14	41.02	49.33	8.94	0.10	0.15	0.28	100.38	90.8
PI-17	0.44	0.14	40.87	48.76	9.48	0.10	0.14	0.29	100.21	90.2
PI-17	0.40	0.15	40.73	48.50	9.83	0.10	0.15	0.28	100.14	89.8
PI-17	0.39	0.16	40.63	47.80	10.64	0.09	0.14	0.29	100.14	88.9
PI-17	0.39	0.16	40.59	47.83	10.69	0.10	0.13	0.28	100.17	88.9
PI-17	0.39	0.17	40.74	47.88	10.71	0.10	0.11	0.29	100.39	88.9
PI-17	0.38	0.16	40.50	47.53	10.86	0.11	0.12	0.29	99.96	88.6
PI-17	0.38	0.17	40.55	47.70	10.98	0.09	0.13	0.29	100.29	88.6
PI-17	0.36	0.17	40.59	47.54	11.11	0.08	0.11	0.29	100.24	88.4
PI-17	0.37	0.17	40.27	46.88	11.50	0.09	0.11	0.29	99.68	87.9
PI-17	0.32	0.19	40.24	46.14	12.74	0.05	0.06	0.33	100.07	86.6
PI-17	0.34	0.19	40.17	46.17	12.79	0.08	0.06	0.33	100.13	86.5
PI-17	0.31	0.19	40.21	46.01	12.93	0.05	0.07	0.32	100.09	86.4
sample ave	0.42	0.14	40.91	48.91	9.30	0.10	0.14	0.29	100.20	90.4
2SD	0.10	0.06	0.84	3.16	3.95	0.03	0.07	0.03	0.35	4.3
PI-18	0.46	0.11	41.51	50.80	7.15	0.11	0.16	0.28	100.58	92.7
PI-18	0.43	0.12	41.25	50.45	7.32	0.09	0.16	0.28	100.11	92.5
PI-18	0.45	0.11	41.35	50.37	7.38	0.10	0.15	0.29	100.20	92.4
PI-18	0.44	0.12	41.19	50.25	7.41	0.10	0.17	0.27	99.95	92.4
PI-18	0.46	0.12	41.21	50.22	7.46	0.10	0.16	0.28	100.01	92.3
PI-18	0.45	0.13	41.12	49.92	7.76	0.10	0.16	0.28	99.93	92.0
PI-18	0.44	0.12	41.25	49.96	7.99	0.11	0.17	0.27	100.30	91.8
PI-18	0.40	0.14	40.90	49.41	8.55	0.08	0.13	0.27	99.87	91.2
PI-18	0.40	0.15	40.73	48.50	9.90	0.09	0.12	0.29	100.17	89.7
PI-18	0.42	0.16	40.42	47.88	10.14	0.10	0.16	0.28	99.56	89.4
PI-18	0.40	0.16	40.70	48.29	10.24	0.09	0.13	0.28	100.29	89.4
PI-18	0.40	0.17	40.50	47.62	10.89	0.10	0.12	0.28	100.09	88.6
PI-18	0.40	0.16	40.48	47.32	11.32	0.10	0.12	0.27	100.18	88.2
PI-18	0.38	0.17	40.36	47.12	11.34	0.08	0.11	0.29	99.85	88.1
PI-18	0.38	0.17	40.41	47.21	11.52	0.07	0.11	0.28	100.16	88.0
PI-18	0.34	0.18	40.42	47.04	11.96	0.03	0.04	0.17	100.19	87.5
PI-18	0.33	0.20	40.07	46.02	12.82	0.05	0.07	0.32	99.87	86.5
PI-18	0.32	0.19	40.14	45.92	13.00	0.05	0.07	0.32	100.00	86.3
sample ave	0.41	0.15	40.78	48.57	9.67	0.09	0.13	0.28	100.07	89.9
2SD	0.09	0.06	0.90	3.24	4.12	0.04	0.08	0.06	0.45	4.5
PI-20	0.46	0.12	41.50	50.85	7.23	0.11	0.16	0.29	100.71	92.6
PI-20	0.45	0.12	41.22	50.43	7.39	0.11	0.17	0.28	100.17	92.4
PI-20	0.45	0.11	41.19	50.44	7.43	0.11	0.17	0.29	100.20	92.4
PI-20	0.41	0.13	41.43	50.52	8.00	0.07	0.12	0.28	100.95	91.8
PI-20	0.44	0.12	41.06	49.92	8.27	0.11	0.16	0.28	100.37	91.5
PI-20	0.41	0.12	41.07	49.92	8.32	0.09	0.14	0.27	100.34	91.5
PI-20	0.45	0.13	40.97	49.50	8.81	0.11	0.15	0.28	100.41	90.9
PI-20	0.41	0.15	40.66	48.45	10.13	0.10	0.14	0.28	100.33	89.5
PI-20	0.35	0.19	40.32	47.01	12.07	0.08	0.05	0.23	100.29	87.4
PI-20	0.34	0.18	40.42	46.75	12.33	0.09	0.09	0.32	100.52	87.1
PI-20	0.32	0.20	40.30	46.60	12.37	0.05	0.06	0.32	100.22	87.0
sample ave	0.41	0.14	40.92	49.13	9.30	0.10	0.13	0.28	100.41	90.4
2SD	0.10	0.06	0.86	3.27	4.12	0.04	0.08	0.05	0.47	4.4

Table S2. Major and trace oxide compositions of olivines measured by electron probe microanalysis.

Supplementary Table 3. Measured, age-corrected, and calculated Baffin "mantle source today" isotopic compositions

	$^{87}Sr/^{86}Sr$ (m)	2 σ	Rb/Sr lava	$^{87}Sr/^{86}Sr$ (60 Ma)	Rb/Sr BSE	$^{87}Sr/^{86}Sr_{\text{calc'd mantle today, BSE traces}}$	Rb/Sr DMM	$^{87}Sr/^{86}Sr_{\text{calc'd mantle today, DMM traces}}$
AK-1	0.703559	0.000006	0.003972	0.70355	0.03015	0.70362	0.00652	0.70357
AK-6	0.703501	0.000006	0.024259	0.70344	0.03015	0.70351	0.00652	0.70346
AK-8b	0.703009	0.000006	0.002496	0.70300	0.03015	0.70307	0.00652	0.70302
AK-9	0.702995	0.000006	0.003064	0.70299	0.03015	0.70306	0.00652	0.70300
AK-12	0.703579	0.000007	0.005039	0.70357	0.03015	0.70364	0.00652	0.70358
AK-13	0.703579	0.000008	0.003193	0.70357	0.03015	0.70364	0.00652	0.70359
AK-14	0.703618	0.000021	0.003829	0.70361	0.03015	0.70368	0.00652	0.70362
AK-18a	0.703635	0.000006	0.006334	0.70362	0.03015	0.70369	0.00652	0.70364
DB-9	0.702997	0.000009	0.013425	0.70297	0.03015	0.70304	0.00652	0.70298
DB-13	0.703021	0.000005	0.001598	0.70302	0.03015	0.70309	0.00652	0.70303
DB-14	0.703021	0.000005	0.002189	0.70302	0.03015	0.70309	0.00652	0.70303
DB-17	0.703228	0.000006	0.003385	0.70322	0.03015	0.70329	0.00652	0.70324
DB-19	0.703946	0.000005	0.017284	0.70390	0.03015	0.70398	0.00652	0.70392
PI-10	0.703401	0.000005	0.002172	0.70340	0.03015	0.70347	0.00652	0.70341
PI-15	0.703008	0.000005	0.002383	0.70300	0.03015	0.70307	0.00652	0.70302
PI-17	0.703845	0.000006	0.003110	0.70384	0.03015	0.70391	0.00652	0.70385
PI-18	0.703848	0.000006	0.004391	0.70384	0.03015	0.70391	0.00652	0.70385
PI-20	0.703846	0.000006	0.006661	0.70383	0.03015	0.70390	0.00652	0.70385

	$^{143}Nd/^{144}Nd$ (m)	2 σ	Sm/Nd lava	$^{143}Nd/^{144}Nd$ (60 Ma)	Sm/Nd BSE	$^{143}Nd/^{144}Nd_{\text{calc'd mantle today, BSE traces}}$	Sm/Nd DMM	$^{143}Nd/^{144}Nd_{\text{calc'd mantle today, DMM traces}}$
AK-1	0.512963	0.000006	0.41328	0.51287	0.32480	0.51294	0.41136	0.51296
AK-6	0.512997	0.000003	0.40242	0.51290	0.32480	0.51298	0.41136	0.51300
AK-8b	0.513128	0.000003	0.36670	0.51304	0.32480	0.51312	0.41136	0.51314
AK-9	0.513174	0.000003	0.45972	0.51306	0.32480	0.51314	0.41136	0.51316
AK-12	0.512954	0.000006	0.41387	0.51286	0.32480	0.51293	0.41136	0.51295
AK-13	0.512957	0.000005	0.41460	0.51286	0.32480	0.51294	0.41136	0.51296
AK-14	0.512956	0.000006	0.41884	0.51286	0.32480	0.51293	0.41136	0.51295
AK-18a	0.512952	0.000006	0.40158	0.51286	0.32480	0.51293	0.41136	0.51295
DB-9	0.513135	0.000003	0.38153	0.51304	0.32480	0.51312	0.41136	0.51314
DB-13	0.513102	0.000003	0.40252	0.51301	0.32480	0.51308	0.41136	0.51310
DB-14	0.513097	0.000003	0.40365	0.51300	0.32480	0.51308	0.41136	0.51310
DB-17	0.513104	0.000003	0.39100	0.51301	0.32480	0.51309	0.41136	0.51311
DB-19	0.512937	0.000003	0.33089	0.51286	0.32480	0.51294	0.41136	0.51296
PI-10	0.513028	0.000003	0.35550	0.51294	0.32480	0.51302	0.41136	0.51304
PI-15	0.513094	0.000003	0.38000	0.51300	0.32480	0.51308	0.41136	0.51310
PI-17	0.512926	0.000003	0.34546	0.51284	0.32480	0.51292	0.41136	0.51294
PI-18	0.512920	0.000003	0.34938	0.51284	0.32480	0.51291	0.41136	0.51293
PI-20	0.512923	0.000003	0.34196	0.51284	0.32480	0.51292	0.41136	0.51294

	$^{176}Hf/^{177}Hf$ (m)	2 σ	Lu/Hf lava	$^{176}Hf/^{177}Hf$ (60 Ma)	Lu/Hf BSE	$^{176}Hf/^{177}Hf_{\text{calc'd mantle today, BSE traces}}$	Lu/Hf DMM	$^{176}Hf/^{177}Hf_{\text{calc'd mantle today, DMM traces}}$
AK-1	0.283231	0.000004	0.26602	0.28319	0.23852	0.28323	0.36943	0.28325
AK-6	0.283222	0.000005	0.24695	0.28318	0.23852	0.28322	0.36943	0.28324
AK-8b	0.283266	0.000003	0.16526	0.28324	0.23852	0.28328	0.36943	0.28330
AK-9	0.283287	0.000005	0.31128	0.28324	0.23852	0.28327	0.36943	0.28330
AK-12	0.283234	0.000004	0.26207	0.28319	0.23852	0.28323	0.36943	0.28325
AK-13	0.283212	0.000005	0.26296	0.28317	0.23852	0.28321	0.36943	0.28323
AK-14	0.283218	0.000005	0.25079	0.28318	0.23852	0.28322	0.36943	0.28324
AK-18a	0.283229	0.000004	0.25946	0.28319	0.23852	0.28323	0.36943	0.28325
DB-9	0.283272	0.000004	0.20941	0.28324	0.23852	0.28328	0.36943	0.28330
DB-13	0.283265	0.000004	0.21648	0.28323	0.23852	0.28327	0.36943	0.28329
DB-14	0.283284	0.000003	0.21828	0.28325	0.23852	0.28329	0.36943	0.28331
DB-17	0.283230	0.000006	0.24412	0.28319	0.23852	0.28323	0.36943	0.28325
DB-19	0.283144	0.000004	0.17326	0.28312	0.23852	0.28315	0.36943	0.28317
PI-10	0.283222	0.000004	0.19009	0.28319	0.23852	0.28323	0.36943	0.28325
PI-15	0.283279	0.000003	0.22461	0.28324	0.23852	0.28328	0.36943	0.28330
PI-17	0.283169	0.000004	0.20710	0.28314	0.23852	0.28317	0.36943	0.28319
PI-18	0.283169	0.000004	0.19899	0.28314	0.23852	0.28318	0.36943	0.28320
PI-20	0.283182	0.000003	0.20296	0.28315	0.23852	0.28319	0.36943	0.28321

	$^{206}Pb/^{204}Pb$ (m)	2 σ	U/Pb lava	$^{206}Pb/^{204}Pb$ (60 Ma)	U/Pb BSE	$^{206}Pb/^{204}Pb$ calc'd mantle today, BSE traces	U/Pb DMM	$^{206}Pb/^{204}Pb$ calc'd mantle today, DMM traces
AK-1	17.6822	0.0013	0.1257	17.609	0.1353	17.688	0.1778	17.712
AK-6	17.6249	0.0009	0.1702	17.527	0.1353	17.605	0.1778	17.629
AK-8b	17.7560	0.0010	0.1233	17.685	0.1353	17.763	0.1778	17.787
AK-9	17.7715	0.0050	0.0818	17.724	0.1353	17.802	0.1778	17.827
AK-12	17.6890	0.0015	0.1327	17.612	0.1353	17.690	0.1778	17.715
AK-13	17.6601	0.0018	0.1202	17.590	0.1353	17.669	0.1778	17.693
AK-14	17.6951	0.0028	0.1271	17.621	0.1353	17.700	0.1778	17.724
AK-18a	17.7029	0.0045	0.1335	17.626	0.1353	17.704	0.1778	17.728
DB-9	17.9507	0.0031	0.1525	17.862	0.1353	17.941	0.1778	17.965
DB-13	17.9317	0.0025	0.0688	17.892	0.1353	17.970	0.1778	17.995
DB-14	17.9297	0.0025	0.0792	17.884	0.1353	17.962	0.1778	17.987
DB-17	17.5114	0.0042	0.1369	17.433	0.1353	17.510	0.1778	17.535
DB-19	18.0095	0.0012	0.1827	17.903	0.1353	17.982	0.1778	18.006
PI-10	17.9607	0.0032	0.1136	17.894	0.1353	17.973	0.1778	17.998
PI-15	17.9375	0.0029	0.0901	17.885	0.1353	17.964	0.1778	17.988
PI-17	17.7551	0.0013	0.1493	17.669	0.1353	17.747	0.1778	17.771
PI-18	17.7542	0.0012	0.1447	17.670	0.1353	17.748	0.1778	17.773
PI-20	17.7540	0.0015	0.1862	17.646	0.1353	17.724	0.1778	17.749

	$^{207}Pb/^{204}Pb$ (m)	2 σ	$^{207}Pb/^{204}Pb$ (60 Ma)	$^{207}Pb/^{204}Pb$ calc'd mantle today, BSE traces	$^{207}Pb/^{204}Pb$ calc'd mantle today, DMM traces
AK-1	15.2945	0.0014	15.291	15.295	15.296
AK-6	15.2887	0.0010	15.284	15.288	15.289
AK-8b	15.3932	0.0009	15.390	15.394	15.395
AK-9	15.3812	0.0045	15.379	15.383	15.384
AK-12	15.2932	0.0015	15.290	15.293	15.294
AK-13	15.2930	0.0018	15.290	15.293	15.295
AK-14	15.3013	0.0025	15.298	15.302	15.303
AK-18a	15.3128	0.0040	15.309	15.313	15.314
DB-9	15.4168	0.0030	15.413	15.416	15.417
DB-13	15.4291	0.0021	15.427	15.431	15.432
DB-14	15.4279	0.0030	15.426	15.429	15.431
DB-17	15.2942	0.0037	15.290	15.294	15.295
DB-19	15.3929	0.0009	15.388	15.392	15.393
PI-10	15.4001	0.0035	15.397	15.401	15.402
PI-15	15.4223	0.0025	15.420	15.424	15.425
PI-17	15.3663	0.0012	15.362	15.366	15.367
PI-18	15.3680	0.0011	15.364	15.368	15.369
PI-20	15.3642	0.0015	15.359	15.363	15.364

	$^{208}Pb/^{204}Pb$ (m)	2 σ	Th/Pb lava	$^{208}Pb/^{204}Pb$ (60 Ma)	Th/Pb BSE	$^{208}Pb/^{204}Pb_{\text{calc'd mantle today, BSE traces}}$	Th/Pb DMM	$^{208}Pb/^{204}Pb_{\text{calc'd mantle today, DMM traces}}$
AK-1	37.751	0.0031	0.555	37.64	0.530	37.75	0.439	37.73
AK-6	37.664	0.0032	0.711	37.53	0.530	37.63	0.439	37.61
AK-8b	37.532	0.0022	0.457	37.45	0.530	37.55	0.439	37.53
AK-9	37.500	0.0115	0.270	37.45	0.530	37.55	0.439	37.53
AK-12	37.738	0.0035	0.583	37.63	0.530	37.73	0.439	37.71
AK-13	37.700	0.0046	0.544	37.60	0.530	37.70	0.439	37.68
AK-14	37.762	0.0060	0.549	37.66	0.530	37.76	0.439	37.74
AK-18a	37.761	0.0105	0.495	37.67	0.530	37.77	0.439	37.75
DB-9	37.717	0.0083	0.576	37.61	0.530	37.71	0.439	37.69
DB-13	37.732	0.0064	0.446	37.65	0.530	37.75	0.439	37.73
DB-14	37.735	0.0066	0.435	37.65	0.530	37.75	0.439	37.74
DB-17	37.455	0.0087	0.539	37.35	0.530	37.45	0.439	37.44
DB-19	37.971	0.0028	0.890	37.80	0.530	37.90	0.439	37.88
PI-10	37.920	0.0108	0.777	37.77	0.530	37.87	0.439	37.85
PI-15	37.723	0.0078	0.505	37.63	0.530	37.73	0.439	37.71
PI-17	37.662	0.0025	1.140	37.45	0.530	37.55	0.439	37.53
PI-18	37.660	0.0025	1.216	37.43	0.530	37.53	0.439	37.51
PI-20	37.659	0.0040	1.151	37.44	0.530	37.54	0.439	37.52

Table S3. Measured, age-corrected, and calculated Baffin "mantle source today" isotopic compositions. 1. Isotopic ratio labels: (m) = measured basalt values; (60 Ma) = age corrected basalt to 60 Ma; "calc'd mantle today, BSE traces" = isotopic composition calculated using parent and daughter elemental concentrations of pyrolite from McDonough and Sun (1995); "calc'd mantle today, DMM traces" = isotopic composition calculated using parent and daughter elemental concentrations from depleted mantle in Workman and Hart (2005).